Journal of Medicinal Chemistry

pubs.acs.org/jmc Article

Discovery of IACS-9779 and IACS-70465 as Potent Inhibitors Targeting Indoleamine 2,3-Dioxygenase 1 (IDO1) Apoenzyme

Matthew M. Hamilton,* Faika Mseeh, Timothy J. McAfoos, Paul G. Leonard, Naphtali J. Reyna, Angela L. Harris, Alan Xu, Michelle Han, Michael J. Soth, Barbara Czako, Jay P. Theroff, Pijus K. Mandal, Jason P. Burke, Brett Virgin-Downey, Alessia Petrocchi, Dana Pfaffinger, Norma E. Rogers, Connor A. Parker, Simon S. Yu, Yongying Jiang, Stephan Krapp, Alfred Lammens, Graham Trevitt, Martin R. Tremblay, Keith Mikule, Keith Wilcoxen, Jason B. Cross, Philip Jones, Joseph R. Marszalek, and Richard T. Lewis

Cite This: https://doi.org/10.1021/acs.jmedchem.1c00679 Read Online

ACCESS | Metrics & More | Article Recommendations | Supporting Information

ABSTRACT: Indoleamine 2,3-dioxygenase 1 (IDO1), a heme-containing enzyme that mediates the rate-limiting step in the metabolism of L-tryptophan to kynurenine, has been widely explored as a potential immunotherapeutic target in oncology. We developed a class of inhibitors with a conformationally constrained bicyclo[3.1.0]hexane core. These potently inhibited IDO1 in a cellular context by binding to the apoenzyme, as elucidated by biochemical characterization and X-ray crystallography. A SKOV3 tumor model was instrumental in differentiating compounds, leading to the identification of IACS-9779 (**62**) and IACS-70465 (**71**). IACS-70465 has excellent cellular potency, a robust pharmacodynamic response, and in a human whole blood assay was more potent than linrodostat (BMS-986205). IACS-9779 with a predicted human efficacious once daily dose below 1 mg/kg to sustain >90% inhibition of IDO1 displayed an acceptable safety margin in rodent toxicology and dog cardiovascular studies to support advancement into preclinical safety evaluation for human development.

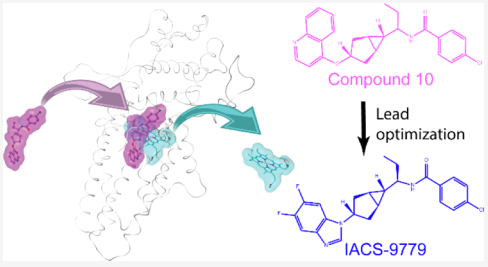

INTRODUCTION

The tryptophan−kynurenine−aryl hydrocarbon receptor (Trp−KYN−AhR) pathway plays a major role in immune regulation by promoting immune tolerance via suppression of local T cell responses under physiological (e.g., maternal−fetal tolerance) and pathophysiological (e.g., tumor immune evasion) conditions.[1−3] L-Tryptophan (Trp) is metabolized in a tissue-specific manner by the rate-limiting heme-containing enzymes indoleamine 2,3-dioxygenase (IDO1 and IDO2) and tryptophan 2,3-dioxygenase (TDO) to generate *N*-formylkynurenine (NFK), which is subsequently hydrolyzed to kynurenine (KYN) and formate.[4] The active site heme is essential for dioxygenase activity and although these enzymes catalyze the same reaction and contain similar heme active sites, IDO and TDO are distinct enzymes sharing only 10% sequence identity.[1] IDO1 has been shown to play an aberrant role in cancer development. It can be expressed by tumor cells and by myeloid cells surrounding the tumor, and IDO1 transcription in vivo is mainly regulated by interferon-γ (IFNγ).[5] IDO1-mediated Trp catabolism and KYN accumulation in the tumor microenvironment exert a profound inhibitory effect on T cells, leading to an immunosuppressive response and tumor immune evasion.[3,6,7] Increased levels of IDO expression in tumors have been shown to correlate with a lower presence of tumor-infiltrating lymphocytes (TILs), a high percentage of T_{reg} cells, and a worse disease outcome.[7,8] The maintenance of an active immune response in the tumor microenvironment is expected to be an effective strategy for disease mitigation.[9] Tumor biology, however, is frequently adapted to exploit the control systems, which keep the immune system under control, and thereby evade surveillance and an appropriate T-cell response to the aberrant cell growth. Recent exploration of the role of IDO1 in this process has suggested activation of IDO1 as a potential means of tumor escape from a variety of cancer immunotherapy agents, including those that seek to control the PD1-PDL1 axis.[10] Based on these results, we and several other groups have invested significant efforts to develop IDO1 inhibitors amenable for cancer treatment.

At the inception of our IDO1 inhibitor program, a survey of the literature revealed several chemical classes of disclosed

Received: April 13, 2021

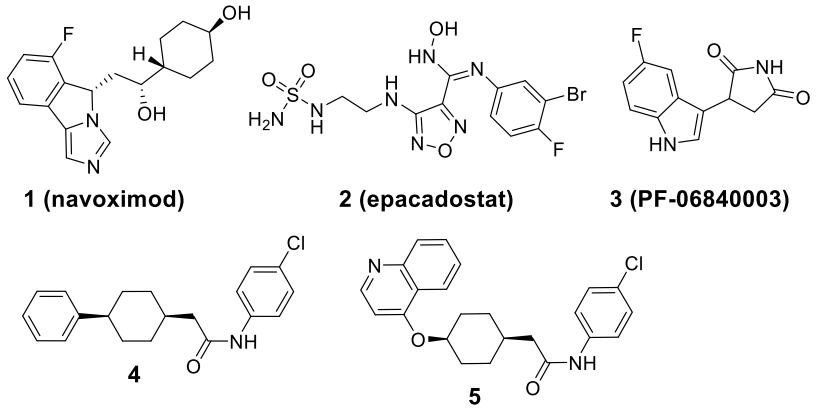

Figure 1. Known inhibitors of hIDO1.

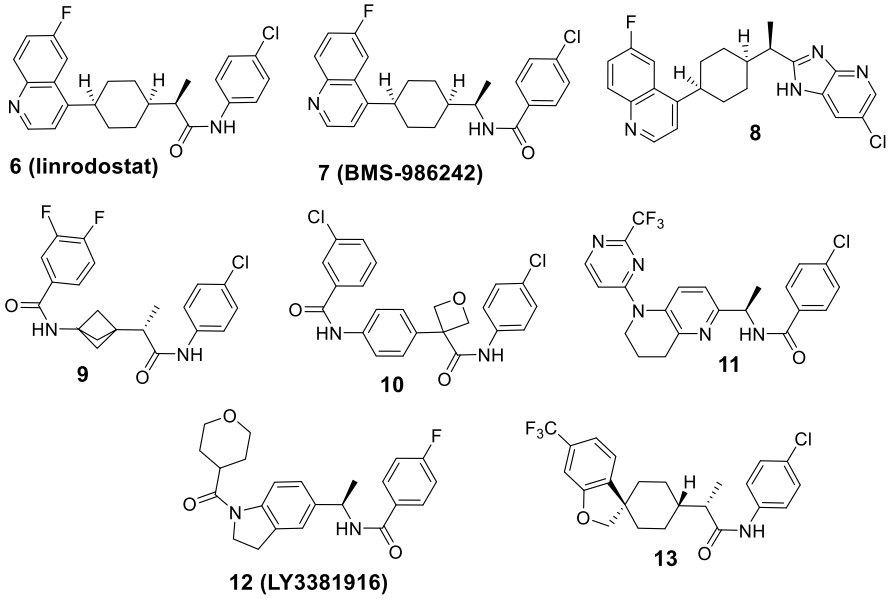

Figure 2. Apo-IDO1 inihibitors.

IDO1 inhibitors (Figure 1 presents a few that were of interest to us).[11−15]

Since then, numerous IDO1 inhibitors have been developed and evaluated preclinically, including those represented in Figures 2 and 3. Eight IDO1 inhibitors have entered clinical trials in combination with chemotherapeutics, checkpoint inhibitors, and vaccines.[16,17] Among the clinical candidates were navoximod **1** (NewLink Genetics),[11,20] epacadostat **2** (Incyte Corp.),[12,18,19] PF-06840003 **3** (iTeos Therapeutics/Pfizer),[13] and linrodostat **6** (BMS-986205; Flexus Biosciences, Inc./Bristol-Myers Squibb, Figure 2).[21,22] Epacadostat, the most advanced compound in clinical development, showed promising anticancer activity in its early phase I/II trials, but disappointingly failed in subsequent pivotal phase III trial due to the lack of efficacy.[19] Consequently, 27 trials including those of the inhibitors mentioned above have been terminated, suspended, or withdrawn.[16,23] Since the second half of 2018, several new phase I/II trials have been initiated; however, it appears that only one agent, linrodostat (BMS-986205), has entered into a phase III trial (bladder cancer).[16]

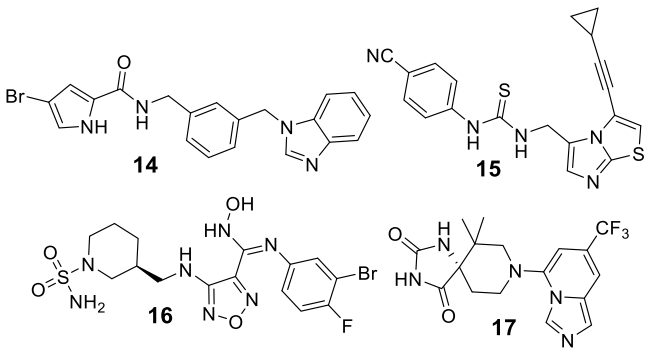

Figure 3. Holo-IDO1 inhibitors.

The mechanism of action of these inhibitors on IDO1 has now been presented in multiple reports, and it has been shown that compounds can display four distinct mechanisms of binding. Type I, II, and III inhibitors bind to the holoenzyme encompassing the substrate pocket (pocket A) and pockets B and C above the heme. Type IV inhibitors bind to the apoenzyme devoid of the heme prosthetic group, still occupying pocket A and filling pocket D exposed by the absence of the heme.[21,24,25] For example, linrodostat **6** (BMS-986205) and similar compounds (Figure 2) have been suggested by either crystal structure, docking, or modeling to bind to the IDO1

https://doi.org/10.1021/acs.jmedchem.1c00679
J. Med. Chem. XXXX, XXX, XXX−XXX

apoenzyme and have been classified as type IV inhibitors.[21,24,26,32−38] These inhibitors all contain a *para*-haloaryl moiety that binds in pocket A, make a crucial hydrogen bond with Ser-167, and have a middle core that spans the space of the absent heme with an attachment to a lipophilic aryl group that binds in pocket D. Linrodostat[21] and the close analogs **7**[32] (reversed amide of linrodostat) and **8**[33] (benzimidazole isostere of linrodostat) were based on a cyclohexyl core with a direct attachment to the fluoroquinoline. Linrodostat **6** is apparently still in clinical trials[16] and the phase 1/2A trial of **7** (BMS-986242) was terminated.[39] Inhibitors **9** to **13** all contain the 4-halo aniline amide similar to linrodostat but with varying cores and lipophilic moieties binding in pocket D. Eli Lilly's inhibitor **12** (LY-3391916) entered the clinic but the trial was terminated.[16,17]

Furthermore, epacadostat, and the inhibitors illustrated in Figure 3 have been suggested to occupy the active site of the holo-IDO1 enzyme and are considered type II or III binders, depending on their preference for ferric or ferrous iron states of the heme. Specifically, compounds **14**−**17** have been implied to coordinate to the iron of the heme: the 3-N nitrogen of the benzimidazole of **14**[27] by docking, 7-N nitrogen of the imidazolothiazole of **15**[28] by a crystal structure, the hydroxyamidine of **16**[24,29] by modeling in epacadostat's crystal structure, and the 1-N nitrogen of the imidazopyridine **17**[30,31] (independently developed by our group and also by Iomet/Merck) by a crystal structure (Figure 4). Imidazopyridine **17** and the other heme-binding IDO1 compounds **1**, **2**, and **3** display inhibition of IDO1 activity in the purified IDO1 holoenzyme and in the cellular context (Table 1).

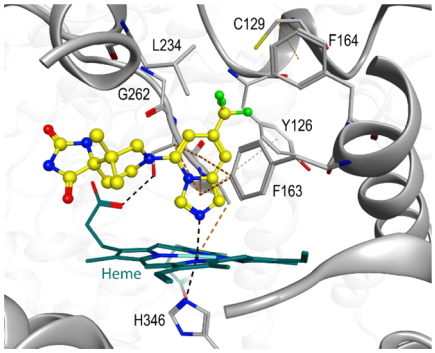

Figure 4. Crystal structure of **17** bound to human IDO1 showing key interactions in the binding pocket (PDB 7M7D).

At the initiation of our program to identify novel IDO1 inhibitors, the unique mechanism of the type IV inhibitors had not yet been reported. Interestingly, we noticed that compounds **4** and **5**, unlike compounds **1**, **2**, and **3** (Figure 1), showed no activity against the purified IDO1 enzyme, but were potent inhibitors of IDO1 activity in the cellular context (Table 1).[40] Herein we describe our mechanistic studies and structural biology confirming their mode of inhibition, and the drug discovery efforts to identify **62** (IACS-9779) and **71** (IACS-70465) as potent and selective inhibitors targeting the IDO1 apoenzyme.

RESULTS AND DISCUSSION

Identification of the [3.1.0] Bicyclic Scaffold. Based on the structures of **4** and **5**, we prepared several concept compounds (Figure 5) and in hindsight they have structural similarity to the subsequently disclosed inhibitors summarized in Figure 2. Table 1 highlights their comparison to the inhibitors in Figure 1. It was evident that **4**, **5**, and **18** suffered from metabolic instability and **19** and **20** had only a modest improvement (Table 1). Interestingly, one stereoisomer of **21** and **22** was significantly more metabolically stable. The cis isomer **22**, where the fused [3.1.0] bicyclic scaffold is forced into a boat conformation, infers that this orientation provides additional stability.

We hypothesized that **21** and **22** (Figure 5, Table 1) with a conformational constraint in the form of a [3.1.0] bicycle might offer a benefit, and potentially also improve the off-target pharmacology profile of these relatively lipophilic molecules by restricting the number of accessible conformations.[41−43] We also proposed in the concept compounds **21** and **22**, two additional changes with respect to compound **5**; reversing the amide and introducing a substituent at the methylene linker. The benzoyl amide was a logical modification to avoid potential metabolic release of 4-chloroaniline and the assessment of the potential for genotoxicity in that event.[44,45] The introduction of an ethyl substituent on the methylene linker was anticipated to minimize the metabolic cleavage of the amide bond by providing additional steric hindrance.[46,47] The single-digit nM hIDO1 cellular potency and low microsomal intrinsic clearance of compound **22** were supportive of our structural modifications.

Table 1. Enzymatic and Cellular IDO1 Inhibition

compound	hIDO1 RFMS IC_{50} (nM)[a,b]	HeLa hIDO1 IC_{50} (nM)[a]	liver microsomal CI_{int} (mL/min/kg)	
			rat	human
1	14	210 ± 60 (3)	39	11
2	3.5 ± 1.1 (58)	11 ± 9 (174)	32	12
3	216 ± 79 (2)		7.2	2.9
4	>50,000 ± 0 (2)	9.1 ± 2.2 (4)	884	681
5	>16,000	108 ± 12 (2)	455	44
17R[c]	68 ± 7(3)	61 ± 32 (16)	37	21
17	24 ± 47 (5)	26 ± 9(34)	42 ± 10 (4)	22 ± 2 (4)
18	>50,000	145	526	227
19	>16,000	32 ± 5 (3)	170	115
20	>16,000	28 ± 4 (3)	137	171
21	>50,000	9.9 ± 2.3 (4)	956	316
22	>50,000	1.6 ± 0.7 (3)	14	23

[a]Average ± standard deviation (number of measurements). [b]Enzymatic assay; RFMS, rapid-fire mass spectrometry.[40] [c]Racemate of 17.

https://doi.org/10.1021/acs.jmedchem.1c00679
J. Med. Chem. XXXX, XXX, XXX−XXX

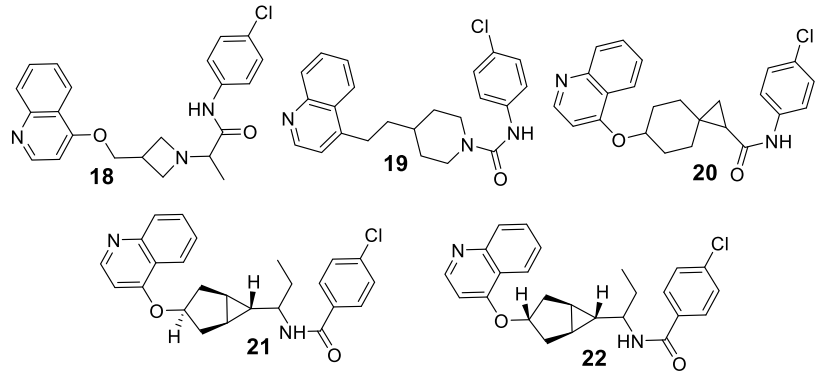

Figure 5. Proposed concept compounds.

This molecule was cell permeable and had a 12.8 h half-life in mouse plasma.[48] Compounds **21** and **22** were used in mechanistic studies and this framework became our starting point for further optimization.

Compounds 21 and 22 Block Heme Incorporation into IDO1 Apoenzyme. The mode of inhibition of IDO1 was characterized in human HeLa cells expressing IDO1 after IFNγ induction using tool compounds **4**, **21**, **22**, and epacadostat **2**. It is well described that IDO1 expression and enzymatic activity are tightly regulated at multiple levels within the cell.[49] At the transcriptional level, IDO1 expression is robustly induced in response to inflammation and infection, with IFNγ representing the most potent stimulus for IDO1 gene expression in vitro and in vivo.[50] In fact, IFN-γ treatment can induce IDO1 expression in many cells.[51] Catabolites of IDO1 products, such as KYN, can also promote IDO1 transcription by binding and activating the aryl hydrocarbon receptor (AhR) in a positive feedback loop. Once transcribed and translated into the IDO1 apoprotein, the heme cofactor must be incorporated to form the heme-containing holoenzyme, and activation of IDO1 requires the reduction of ferric (Fe^{3+}) heme to the active ferrous (Fe^{2+}) heme-IDO1 state, facilitating Trp and O_2 binding.[52] IDO1 can be post-translationally modified by Src family kinases that phosphorylate Tyr115 and Tyr253, ultimately leading to IDO1 proteasomal degradation by associating with the suppressor of cytokine signaling 3 (SOCS3).[49,52,53] In order to assess the effect of **21** and **22** on IDO1 transcription, translation, and degradation, we measured the endogeneous and recombinant human IDO1 activity and the protein level in cells after induction of IDO1 expression in the absence or presence of IDO1 inhibitors. Compounds **21**, **4**, and **2** inhibited IFN-γ-induced IDO1 activity without altering the IDO1 protein levels in HeLa cells (Figure 6). These results indicated these inhibitors did not modulate endogeneous IDO1 gene transcription or IDO1 protein stability.

Next, we evaluated the ability of **22** to block heme incorporation into the newly expressed IDO1 apoenzyme. We hypothesized that if **22** blocked heme incorporation, induction of IDO1 expression in the presence of a compound would lead to newly synthesize IDO1 protein devoid of the heme prosthetic group, and the cell lysates would show IDO1 expression, but no IDO1 activity. In addition, we reasoned that exogeneous addition of hemin to the cell lysate would allow reconstitution of the apoenzyme into the active holoenzyme, and IDO1 activity would be restored in the cell lysate. First, we established a stable recombinant HEK293 cell line expressing tetracycline-inducible human IDO1, then we induced expression of human IDO1 in cells by doxycycline (1 μg/mL) treatment in the absence (Figure 7A) or presence of **22** (Figure 7B) for a period of 24 h. The cell lysates were incubated for 30 min under three different conditions: (1) the absence of hemin, (2) the presence of hemin, and (3) the presence of hemin plus **22**. We observed by Western-blot similar levels of IDO1 expression in lysates of cells induced with doxycycline in the absence or presence of **22** (Figure 7C). The lysates from the cells induced in the absence of **22** (Figure 7A) displayed similar activities under the three described conditions above, (condition 1 vs 2, $p < 0.05$). However, IDO1 activity was significantly lower in lysates of cells induced in the presence of **22** (Figure 7B), but the addition of hemin to the cell lysate completely restored the IDO1 activity (Figure 7B, condition 1 vs 2, $p < 0.01$). However, coaddition of hemin and **22** showed reduced recovery of IDO1 activity (Figure 7B, conditions 2 vs 3, $p < 0.01$), suggesting competition between **22** and hemin for binding to the newly synthesized IDO1 apoenzyme. In summary, these results indicate that the presence of **22** during IDO1 synthesis blocked heme incorporation into the apoenzyme, addition of hemin to cell lysates containing the newly synthesized IDO1 apoenzyme can reconstitute and restore IDO1 activity, and **22** appears to compete with hemin for binding to the IDO1 apoenzyme during the holoenzyme reconstitution.

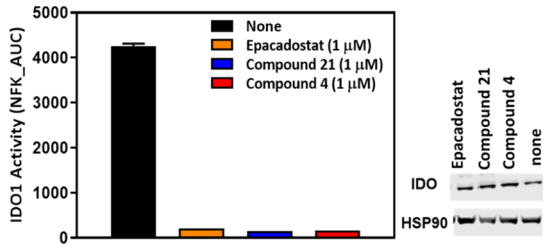

Figure 6. Effect of compound treatment on cellular IDO1 activity and protein level. HeLa cells stimulated with 10 ng/mL of IFN-γ in the absence or the presence of IDO1 inhibitors (1 μM) for 24 h. IDO1 Activity (NFK_AUC) is the cellular production of NFK measured from aliquots of harvested cell conditioned media analyzed via RFMS [NFK_AUC is the area under the curve and is the integration of the total ion count peak intensities from the relative abundance of NFK in the mass spectrometry (MS) signal]. All compounds significantly ($p < 0.01$) inhibited cellular NFK production as compared to their absence. Western-blot analysis of cell lysates for expression levels of IDO1 protein (HSP90 as control). These are representative results from at least two independent test occasions performed in triplicate.

In order to further validate our hypothesis, we first purified a batch of His-tagged human IDO1 protein containing very low levels of heme incorporation (<5% heme content). Next, the activity of the low heme-IDO1 was measured in the absence or

https://doi.org/10.1021/acs.jmedchem.1c00679
J. Med. Chem. XXXX, XXX, XXX−XXX

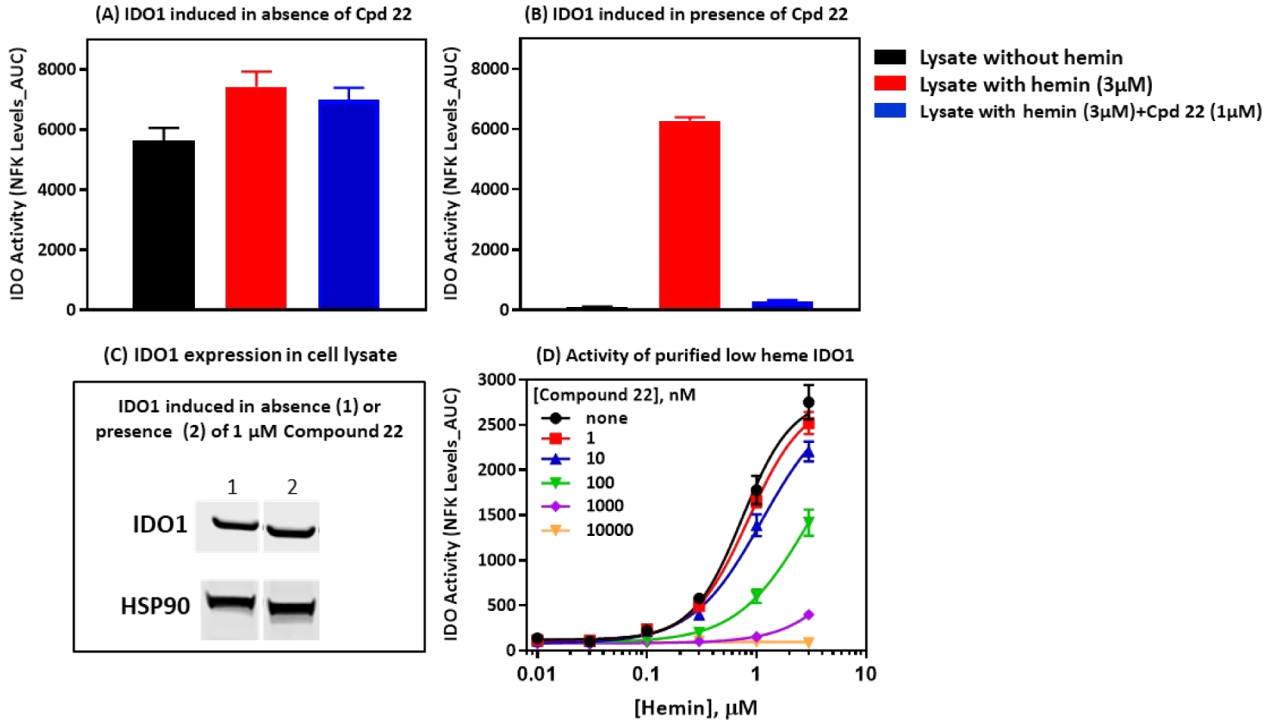

Figure 7. Compound **22** competes against heme incorporation into newly synthesized IDO1 protein. HEK293 cells were stimulated with doxycycline (1 ng/mL) in the absence (**7A**) or presence (**7B**) of **22** (1 μM). IDO1 activity in the cell lysates was assessed in (1) the absence of hemin (black), (2) the presence of hemin (3 μM, red), or (3) the presence of hemin (3 μM) plus **22** (1 μM) (blue). (**7C**) Western-blot analysis for IDO1 protein expression in the absence (1) or presence (2) of **22** (HSP90 as control). (**7D**) Activity of purified low heme-IDO1 in the presence of increasing concentrations of hemin and **22**. These are representative results from at least two independent test occasions performed in triplicates.

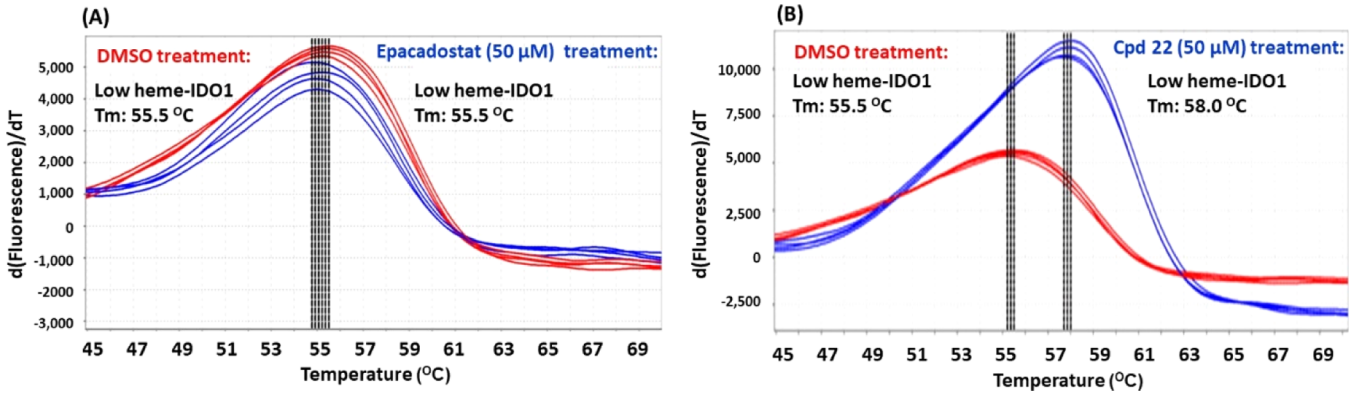

Figure 8. Compound **22** binds and promotes thermal stability of purified low-heme content IDO1 enzyme. (A) DSF profile of purified low heme-IDO1 protein in the presence of DMSO (control, red) or 50 μM of epacadostat (blue), displaying an unchanged T_m value of 55.5 °C under both treatment. (B) DSF profile of purified low heme-IDO1 protein in the presence of DMSO (control, red) or 50 μM of **22** (blue). IDO1 melting temperature (T_m) values showed a significant ($p < 0.01$) shift from 55.5 to 58 °C. T_m values were calculated by averaging the results from at least four independent test occasions.

presence of increasing concentrations of hemin. Addition of hemin promoted a dose-dependent increase in low heme-IDO1 activity (Figure 7D). Finally, we performed competition studies by assessing the hemin-dependent recovery of low heme-IDO1 activity in the presence of increasing concentrations of compound **22** (Figure 7D). Addition of **22** inhibited the hemin-induced IDO1 activation in a dose-dependent manner, further indicating that the hemin and **22** compete for binding to the purified low-heme IDO1 enzyme.

In order to directly assess the binding of **22** to IDO1 apoenzyme, we conducted thermal shift assays using the purified recombinant His-tagged low-heme human IDO1 protein (<5% heme content) in the absence or presence of IDO1 inhibitors. The thermal stability profile of the purified low heme-IDO1 protein was evaluated via differential scanning fluorimetry (DSF) methodology (Figure 8A,B), showing a melting temperature (T_m) of 55.5 °C in the absence of compound. T_m of the low heme-IDO1 protein was significantly increased in the presence of **22** (2.5 °C shift, Figure 8B), and as we expected, epacadostat **2** did not induce a significant increase in the low heme-IDO1 protein thermal stability (Figure 8A). It is well documented that epacadostat binds to the IDO1 holoenzyme via a key interaction with the heme cofactor.[24] These results further indicate that **22**, unlike epacadostat, occupies the heme-binding site of IDO1

https://doi.org/10.1021/acs.jmedchem.1c00679
J. Med. Chem. XXXX, XXX, XXX−XXX

apoenzyme, blocks incorporation of the essential heme cofactor after IDO1 translation, and thereby inhibits IDO1 activity.

X-ray Crystallography Studies Confirmed the Binding Mode of Compound 22 to IDO1 Apoenzyme. In order to elucidate the binding mode of IDO1−inhibitor complexes, the crystal structure was determined by cocrystallization of IDO1 with **22** (Figure 9A). Interestingly, soaking the high-heme enzyme IDO1 crystals (75% heme content) with **22** (4 mM addition of **22** to the hanging drop containing the IDO crystal) promoted a slow loss of the characteristic red coloration of the IDO1 crystals over a 24 h period at 20 °C, indicating a gradual displacement of the heme cofactor from the crystals. Unfortunately, the resulting crystals did not diffract well. Alternatively, high-heme IDO1 protein was mixed with the compound in the protein buffer and incubated overnight to allow for displacement of the heme cofactor, prior to cocrystallization of the protein with the bound inhibitor. X-ray diffraction of the crystals thus obtained showed **22** to be occupying the apoenzyme of IDO1, which implies a favorable trapping of the apoenzyme after in situ loss of the heme cofactor from the holoenzyme.

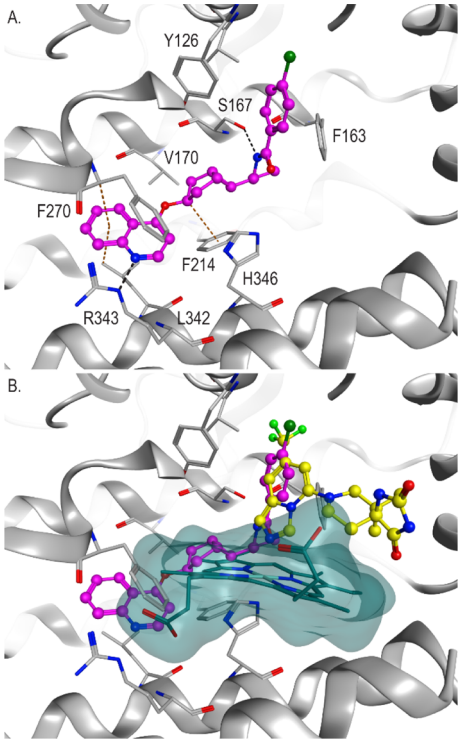

Figure 9. (A) Crystal structure of **22** bound to human IDO1 showing key interactions in the binding pocket (purple, PDB 7B1O). (B) Crystal structure of **22** (light purple) superposed with the crystal structure of the IDO1 holoenzyme with **17** (yellow, PDB 7M7D) with the heme (teal) depicted using a surface representation, to show the volume occupied by heme in the IDO1 holoenzyme.

A superposition of **22** overlaid with the crystal structure of **17** (previously shown to bind to the IDO1 holoenzyme, Figure 4) illustrates how **17** directly engages the iron of the heme, whereas **22** can only bind to the apo form of the protein (Figure 9B), presumably by competing with the incorporation of heme. Overall, the protein fold of the apoprotein is consistent with that observed for the holoenzyme. However, we observe a difference in the conformation of Phe270 side chain, which adopts a distinct rotamer conformation that interacts with the quinoline, with the Cα proton of this phenylalanine making an arene−proton interaction with the quinoline. This quinoline moiety is projected into a largely lipophilic cavity of pocket D exposed by the absence of the heme. On the opposite face of the quinoline group, Leu342 side chain makes an additional arene−proton interaction with **22**.

It is worth noting that the rotamer conformation of Phe270 that allows for this interaction with the quinoline is not accessible in the heme-bound holoenzyme as it would sterically clash with the heme cofactor. The crystal structure revealed a number of additional interactions between **22** and the apoprotein (Figure 9A). The quinoline nitrogen makes a hydrogen bond with the side chain of Arg343 and a second direct hydrogen bond is found between the hydroxyl side chain of Ser167 and the amide N−H of the compound.

The bicyclo[3.1.0]hexane scaffold occupies a hydrophobic region vacated by the displaced heme cofactor between Ala264 and Tyr126 on one side of the core scaffold and Phe214 on the

Table 2. Quinoline Ether Exploration

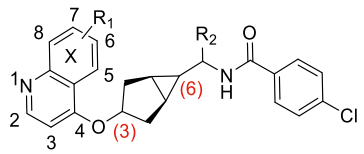

compound	(3)[a]	(6)[a]	X	R_1	R_2	HeLa hIDO1 IC_{50} (nM)[b]	HLM[c] CLint (mL/min/kg)	CYP $3A4_m$[d]; IC_{50} (μM)[b]	clog *P*	hPPB (%)[b,e]
21	e	e	C	H	Et	9.9 ± 2.3 (4)	316	1.1 ± 0.4 (2)	5.03	99.8
22	a	e	C	H	Et	1.6 ± 0.7 (3)	23	3.3 ± 0.02 (2)	5.03	99.7 ± 0.2 (3)
23	e	e	C	6-F	Et	6.1 ± 1.1 (4)	493	1.4	5.17	99.8
24	a	e	C	6-F	Et	1 ± 0.3 (3)	0	>5 ± 0 (2)	5.17	100
25	e	e	C	6-F	H	334 ± 0 (1)	227	2.1	4.24	99.7
26	a	a	C	6-F	H	14 ± 3 (2)	38	1.9	4.24	99.5
27	a	e	C	6-F	H	4.2 ± 1.1 (3)	39	6.7 ± 0.8 (2)	4.24	100
28	a	e	C	7-F	Et	1.4	32	5.4	5.17	100
29	a	e	5-N	H	Et	18 ± 6 (5)	14	13	4.20	95
30	a	e	6-N	H	Et	23	54	18	3.81	98.9

[a]The orientation [equatorial (e) or axial (a)] of the substituents at the 3- and 6-positions of the bicycle core. [b]Average ± standard deviation (number of measurements). [c]HLM, human liver microsomes. [d]Midazolam was the probe substrate for this assay. [e]Human plasma protein binding.

https://doi.org/10.1021/acs.jmedchem.1c00679
J. Med. Chem. XXXX, XXX, XXX−XXX

Table 3. Diverse Set of IDO1 Inhibitors and Their Species Shift

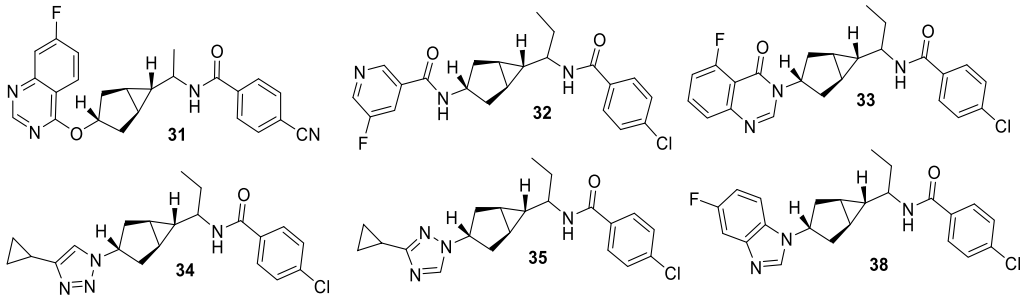

compound	HeLa hIDO1 IC_{50} (nM)[a]	$PANCO_2$ mIDO1 IC_{50} (nM)[a]	species shift[b]	HLM[c] CLint (mL/min/kg)	CYP $3A4_m$[d]; IC_{50}(μM)[a]	clog *P*	hPPB (%)[a,e]
2	11 ± 9 (174)	74 ± 30 (56)	7	12	28 ± 5 (6)	0.02	97.2 ± 0.1 (3)
23	6.1 ± 1.1 (4)	76	12	490	1.4	5.17	99.8
29	18 ± 6 (5)	1200	69	14	13	4.20	95
31	6.9 ± 2.2 (6)	2200	320	17	>17	3.79	98.3
32	6.2 ± 2 (3)	1300	210	13	>50	3.03	95.3
33	8.4 ± 1.5 (6)	570 ± 48 (2)	68	0.7	>17	4.15	96.8
34	19 ± 8 (8)	106 ± 18 (2)	6	6.5	>50	3.99	95.4 ± 2.8 (1)
35	69 ± 12 (2)	230	3	2.0	31	3.81	91.7
38	2.6 ± 2.2 (10)	23 ± 21 (3)	9	8.3	1.3	4.68	99.4

[a]Average ± standard deviation (number of measurements). [b]Ratio of PANCO IC_{50}/HeLa IC_{50}. [c]HLM, human liver microsomes. [d]Midazolam was the probe substrate for this assay. [e]Human plasma protein binding.

other side. The axially disposed equatorial hydrogen of the 3-carbon of the bicyclo[3.1.0]hexane scaffold in a boat conformation is directed at the center of Phe214 phenyl ring, making a further arene−proton interaction between the compound and the protein. The amide linker extends into the bottom of the substrate pocket of the enzyme, with the chlorobenzene group occupying the tryptophan-binding pocket (pocket A).

The binding mode for **22** is most similar to the crystal structures reported for other type IV inhibitors: analog of linrodostat **6** (FXB-001116, BMS-116, PDB 6AZW),[21] analog of Merck compound **10** (3-chloro-*N*-(3-{(2*S*)-1-[(4-fluorophenyl)amino]-1-oxopropan-2-yl}bicyclo[1.1.1]pentan-1-yl)benzamide, PDB 6V52),[34] and analog of Merck compound **9** (3-chloro-*N*-{4-[1-(propylcarbamoyl)cyclobutyl]phenyl}-benzamide PDB 6WJY).[35] These molecules span between pocket A and pocket D of the IDO1 protein. The BMS-116 inhibitor in particular also has a quinoline group occupying pocket D and makes the same direct hydrogen bond interaction with Arg343 as we observed for **22**. BMS-116 has a cyclohexane core with a nitrogen linkage to the quinoline that occupies a similar part of the pocket to our bicyclo[3.1.0]hexane core. In pocket A, BMS-116 has a 4-cyanophenyl group, which overlaps with the chlorobenzene in **22** and although the amide in the linker is reversed, the amide still makes a hydrogen bond interaction with Ser167. The X-ray structure confirms that **22** binds to the apoenzyme form of IDO1.

Metabolic Stability of 22. The metabolic profile of **22**, characterized in mouse, rat, and human liver microsomes, indicated that the main metabolite observed was N-oxidation of the quinoline moiety. The crystal structure of **22** reveals potential space in the pocket D region of the protein, available in the vicinity of the quinoline moiety to accommodate substituents on the benzo-fused ring. Table 2 summarizes the SAR investigated to improve the metabolic stability. The fluoro substituent at the 6-position **24** resulted in an unmeasurably low-intrinsic liver microsomal clearance, ameliorating the susceptibility of the quinoline nitrogen toward N-oxidation. Interestingly, placement of fluorine at the 7 position, of the quinoline, **28**, was somewhat less impactful on metabolic stability. As with compounds **21** and **22**, there was a distinct difference between the diastereoisomers with respect to their potency and microsomal stability.

Apparent from the crystal structure of **22**, the bicyclo[3.1.0]-hexane system is constrained in a pseudoboat conformation. The placement of the quinolinoxy substituent in the axial position appears to be the preferred binding geometry for the apoenzyme. The diastereoisomers represented by **21** and **23** with the quinolinoxy disposed pseudoequatorially are still accommodated, albeit with a 5-fold loss of potency. Fortunately, the more potent isomer is also the more metabolically stable. Removal of the ethyl substituent resulted in a loss of metabolic stability (**27** vs **24** and **25** vs **23**, Table 2). Despite the lower clog *P*, the removal did not afford a measurable change in plasma protein binding and also resulted in a reduction in potency. Compound **24** was well absorbed with a long half-life and good bioavailability when orally dosed to mice at 10 mg/kg (Table 4), but the clog *P* and plasma-protein binding were very high. The protein binding was modulated by lowering the clog *P* via the incorporation of an additional nitrogen (**29** or **30**, Table 2), but the cost was a 10-fold loss in potency compared to **22**.

Species Differences within the IDO1 Binding Pocket. Despite the good pharmacokinetic (PK) and human IDO1 potency of **24**, the physical properties of the quinoline series were less than desirable (hPPB 100% and clog *P* 5.17). To evaluate other promising compounds in vivo, we initially used the murine CT26 syngeneic mouse model similar to that used for the evaluation of epacadostat **2**.[54,55] When comparing **2**, our type III inhibitor **17** and a representative type IV inhibitor **31** (analog with improved hPPB, Table 3, PK Table 4) in the model, we obtained the expected results with **2** and **17** [10% ± 7% (n = 10) KYN % of vehicle control, for both compounds]; however, we observed not only a significant variation in KYN levels in the vehicle-treated cohort [11 ± 7 μM (n = 65)] but **31**

https://doi.org/10.1021/acs.jmedchem.1c00679
J. Med. Chem. XXXX, XXX, XXX−XXX

Table 4. Mouse PK Profile of the Selected Compounds

PK parameter[a]	24	31	34	38
CI (L/h/kg)[b]	0.014 ± 0.002	0.007 ± 0.001	0.28 ± 0.05	0.15 ± 0.01
V_{ss}[b]	0.27 ± 001	0.31 ± 0.04	1.04 ± 0.10	0.8 ± 0.2
$T_{1/2}$ (terminal h)[b]	15 ± 3	33 ± 12	2.7 ± 0.7	3.9 ± 1.0
AUC_{Inf} (h·μM)[b]	51 ± 7	106 ± 25	2.8 ± 0.5	4.9 ± 0.4
C_{max} (μM)[c]	51 ± 4	44 ± 3	1.5 ± 0.5	19.0 ± 0.9
F (%)	146 ± 81	62 ± 4	22 ± 17	127 ± 10

[a]Each dose done in triplicate. [b]IV (0.3mpk). [c]po (10 mpk).

Table 5. Initial Benzimidazole Series SAR

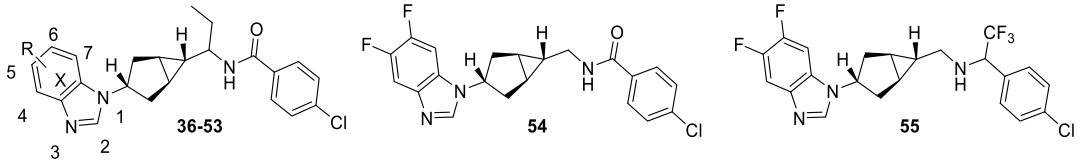

compound	R	X	HeLa hIDO1 IC_{50} (nM)[a]	$PANCO_2$ mIDO1 IC_{50} (nM)[b]	HLM[c] CLint (mL/min/kg)	CYP 2C9 IC_{50} (μM)[a]	hERG (FP)[c] IC_{50} (μM)[a]	hERG safety margin[d]	clog *P*	hPPB (%)[e]
36	H	C	6.3 ± 2 (4)	108	13.5	7.8	0.78	120	4.54	98
37	4-F	C	7.0 ± 1 (5)	134 ± 31 (2)	19	3.9	1	140	4.68	99
38	5-F	C	2.6 ± 2.2 (10)	23 ± 21 (3)	8.3	0.71	0.18	69	4.68	99.4
39	6-F	C	3.8 ± 0.4 (8)	23 ± 4 (4)	11.8	4.2	5.4	1400	4.68	98.9
40	7-F	C	5.2 ± 0.6 (3)	97	16.3	2.1	2.1	400	4.68	99.1
41	5-CN	C	73 ± 14 (2)		5.5	4.6	0.15	2.1	4.4	99.4
42	4,6-F_2	C	7 ± 0.9 (4)	65	6.6	3.06 ± 0.01 (2)	1.9	270	4.83	99.4
43	5,7-F_2	C	6.2 ± 2.4 (2)	67	5.5	1.6 ± 0.2 (2)	0.57	92	4.83	99.6
44	6,7-F_2	C	4 ± 0.8 (4)	45 ± 20 (2)	18	1.9 ± 0.1 (2)	5.4	1400	4.83	99.7
45	5,6-F_2	C	4.6 ± 2.9 (4)	20 ± 8 (2)	15	2.2 ± 0.2 (2)	5.0	110	4.83	99.9
46	5,6-CI_2	C	12 ± 4.8 (9)	72 ± 24 (4)	3.8	2.1 ± 0.3 (2)	9.6	800	5.75	100
47	H	4-N	68	1024	0	8.0[f]			3.65	91.8
48	H	5-N	22 ± 2.8 (5)	240		0.18	0.059	2.7	3.32	
49	H	6-N	30 ± 3.1 (3)	1824	8.8	16	1.2	40	3.32	96.6
50	H	7-N	33	236	16	5.1	11	330	3.69	96.2
51	5-F	7-N	19 ± 11 (4)	194 ± 5 (2)	0.46	2.7 ± 0.2 (2)	2.1	110	3.83	65.9
52	5-CN	7-N	343 ± 52 (2)	1573	10	>30 ± 0 (2)	0.69	2	3.55	99.2
53	6-CN	4-N	357 ± 13 (2)	1837	4.5	>10	5.2	15	3.51	96.3
54	5,6-F_2	C	19 ± 3 (2)	33 ± 2 (2)	100	6.2	4.8	250	3.89	99.6
55	5,6-F_2	C	471		100	4.3	0.46	1	5.39	99.8

[a]Average ± standard deviation (number of measurements). [b]HLM, human liver microsomes. [c](FP), hERG florescence polarization assay. [d]Safety margin is the ratio of hERG (FP) IC_{50}/HeLa IC_{50}. [e]Human plasma protein binding. [f]Compound 35 also had CYP 2d6 = 0.20 μM.

[53% ± 31% (*n* = 8) KYN % of vehicle control] and other compounds did not perform nearly as well as **2** and **17**. Our concern was the challenge to deliver a sufficient concentration of unbound drug to the tumor tissue to cover the murine IC_{90} due to not only the high protein binding of this class of compounds but also the significant shift in IDO1 potency we observed between our murine PANC02 (Table 3) and human HeLa cellular assays.[56] In our effort to find an alternative replacement for the quinoline or quinazoline, we also considered moieties that possessed a lower species shift in potency.

Sequence comparison between human and mouse IDO1 proteins identified several amino acid differences in the compound binding site. In order to understand and potentially predict shifts of compound potency across species, the amino acid sequence of the human IDO1 protein was aligned with those of other species (see Supporting Information, Table S6) and a homology model was constructed. The residues (Y126, V130, S167, and F163; key interactions from the X-ray crystal structure) that line the indole-binding pocket of the natural substrate, tryptophan, are conserved across species, including S167, which forms a hydrogen bond with the amide NH of **22**. However, we observed side chain variations across species in the vicinity of the heme-binding pocket, where the quinoline moiety of **22** binds (pocket D). The human to mouse sequence changes were: V269I, F273L, and L342V resulting in a distinct binding pocket in the murine enzyme.

To assess the impact of IDO1 amino acid sequence differences across species on inhibitor potency, we screened compounds against the PANC02 murine cell line in comparison to the HeLa human cell line assay. The results for a representative group of molecules are presented in Table 3. These hydrophobic steric changes in the vicinity of the compound-binding site resulted in sensitivity to the substitution pattern of the moiety occupying pocket D. The human IDO1 tolerated a diversity of substituents; however, the mouse protein was significantly more sensitive. From this exploration, **38** (benzimidazole) and **34** (triazole) had the best overall balance of potency, ancillary pharmacology, and species shifts that were deemed manageable from a translational perspective. Of the two

https://doi.org/10.1021/acs.jmedchem.1c00679
J. Med. Chem. XXXX, XXX, XXX−XXX

Table 6. Benzimidazole Selection

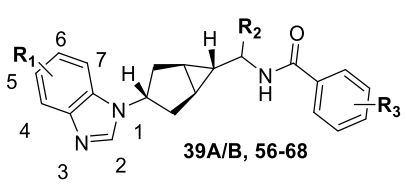

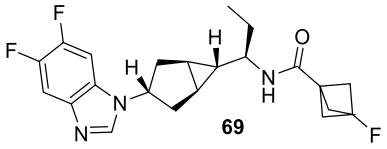

compound	R_1	R_2[a]	R_3	HeLa hIDO1 IC_{50} (nM)[b]	hERG (FP) IC_{50} (μM)[b,c]	hERG (QP) IC_{50} (μM)[b,d]	hERG (MP) IC_{50} (μM)[b,e]	hERG safety margin[f]	hPPB (%)[b,g]
56	6-F	Et	4-CI	2.8 ± 1.1 (2)		9.9			99.5
39A	6-F	Et(R)	4-CI	2.2					
39B	6-F	Et(S)	4-CI	8.4 ± 1.9 (8)		14			99.2 ± 0.1 (2)
57	6-F, 2-Me	Et	4-CI	9.2 ± 2.8 (4)	2.05 ± 0.01 (2)	21	1.1[h]	120	99.1
58	6-CI	Et	4-CI	3.4 ± 0.3 (2)	2.3	>30 ± 0 (2)			99.0
59	6-CN	Et	4-CI	8.8 ± 1.9 (4)	5.3	5.6	1.1[h]	120	98.4
60	6-CI	Et	4-CN	52 ± 13 (2)	0.5	2.1			98.5
61	6-CN	Et	4-CN	35 ± 5.8 (2)	1.2				96.9
62	5,6 F_2	Et	4-CI	1.7 ± 0.6 (20)	2.4 ± 0.3 (3)	11	0.79 ± 0.22 (3)[i]	470	99.4
63	5,6 F_2	Et	3-F, 4-CI	3.9 ± 1.6 (4)	2.5		0.95	240	99.0
64	5,6 F_2	Et	4-CN	4.4 ± 1.2 (10)	1.1	1.4	0.43[g]	100	96.6 ± 0.2 (2)
65	5,6 F_2	Me	4-CI	5.3 ± 1.2 (8)	0.52 ± 0.03 (2)	>30	0.53 ± 0.29 (2)[h,i]	100	99.3
66	5,6 F_2	Me_2[j]	4-CI	8.3 ± 0.89 (4)	1.6 ± 0.6 (2)	12	1.4[h]	260	99.6
67	5,6 F_2	cProp	4-CI	3.6 ± 0.72 (4)	0.56				99.2 ± 0.2 (2)
68	5,6 F_2	Me	4-CN	33 ± 6.2 (6)	1.3	0.74			94.0
69	5,6 F_2	Et		426 ± 144 (2)	48				86.1

[a]R_2 enantiomer chirally synthesized, (R) (S) designation assigned from potency. [b]Average ± standard deviation (number of measurements). [c](FP) fluorescence polarization. hERG-binding assay. [d](QP) Q-patch electrophysiology hERG assay. [e](MP) manual patch clamp hERG assay. [f]Safety margin is the ratio of hERG (MP)/HeLa. [g]Human plasma protein binding. [h]Precipitation at 30 μM. [i]Precipitation at 10 and 30 μM. [j]Gem dimethyl.

compounds, **38** had better mouse PK (Table 4). Initial SAR of the benzimidazole series is presented in Table 5.

Initial SAR of the Benzimidazole Series. The benzimidazole series was further optimized for metabolic stability and its ancillary pharmacology profile, in particular the safety margin between hERG and HeLa potencies. The inhibition of the hERG (human ether-a-go-go gene) potassium channel is associated with QT interval prolongation (measured on an electrocardiogram, ECG) and the potentially lethal ventricular tachycardia torsades de pointes (TdP).[57,58] The safety margin determined by the ratio of the hERG IC_{50} to the Hela IC_{50} was used as a comparator to rank order compounds for further evaluation.[59−61] Initially, activity against hERG was assessed using a fluorescence polarization-binding assay (Table 5), and subsequent electrophysiological readouts of hERG channel function were measured for key compounds via Q-Patch and Manual Patch clamp assays (Table 6).

The unsubstituted benzimidazole **36** with a hERG safety margin of 120 was the starting point for this series (Table 5). Of the single substituents, a fluorine at the 6 position **39** had the best hERG safety margin and also conferred an improved CYP 2C9 inhibition profile (CYP 3A4 midazolam and testosterone substrates and 2D6 were also monitored but 2C9 was usually the most sensitive unless noted). Furthermore, the 6,7 and the 5,6 difluoro substitutions (**44** and **45**) significantly improved the hERG safety margin. Plasma protein binding was reduced by lowering the clog *P* via the incorporation of an additional nitrogen into the ring between the 4−7 positions to afford the corresponding imidazopyridines. However, those substitutions also reduced the hIDO1 potency. A range of additional analogs were explored but offered no substantial improvements. The ethyl substitution was removed in **54**, which reduced the clog *P* an order of magnitude but did not lower the PPB nor the hERG and also resulted in a 4-fold reduction of the hIDO1potency.

Benzimidazole Selection by SKOV3. In order to progress the benzimidazole series, it was necessary to confirm target engagement (TE) in vivo. The CT26 syngeneic tumor model described earlier was replaced with the SKOV3 model (a human tumor xenograft, which naturally expresses high levels of hIDO1 endogenously). This model offered a better signal to noise ratio with less interanimal variability, and allowed the measurement of TE against the more therapeutically relevant human IDO1 sequence. The in vivo experiments were designed to measure only TE and not inhibition of tumor growth, due to the absence of an innate immune system.[62,63] This model, of necessity, does not have an intact immune system, which mechanistically, is absolutely required in order to observe an immune-mediated antitumor response. Hence tumor growth inhibition or regression was not an expected outcome in this model following intervention via the IDO mechanism. Tumor TE was assessed by measuring KYN concentrations in tumor samples collected after oral compound administration [per os (po)] to mice. The percent of vehicle control of tumor KYN production was used as a pharmacodynamic (PD) biomarker of IDO1 inhibition, and epacadostat **2** was used as a benchmark. TE was assessed after compound treatment (po, 125 mg/kg, QD 5 days, tumor collected 24 h after last dose) relative to a vehicle-dosed control cohort (Figure 10).

From the initial benzimidazole SAR (Table 5), monosubstitutions at the 6 position and disubstitutions at the 5,6 position were chosen for further exploration. The racemic 6-fluoro **39** was separated by chiral SFC. The more potent enantiomer (**39A**, Table 6) was confirmed as the R configuration based on its chiral synthesis (**56**, described in the chemistry section).

https://doi.org/10.1021/acs.jmedchem.1c00679
J. Med. Chem. XXXX, XXX, XXX−XXX

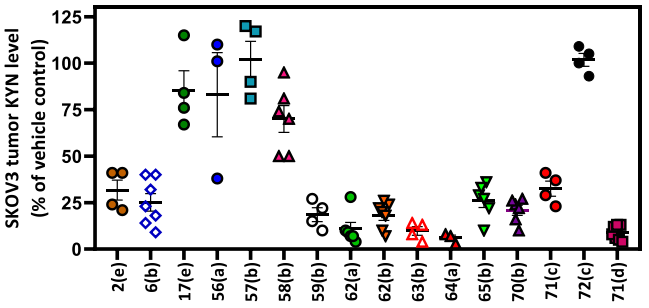

Figure 10. In vivo modulation of tumor KYN production after compound administration (po) using SKOV3 xenograft mouse model. Compounds were dosed as follows: (a) 125 mg/kg, po, QD, 5 days, tumor collected 4 h after last dose; (b) 125 mg/kg, po, QD, 5 days, tumor collected 24 h after last dose; (c) 3 mg/kg, po, tumor collected 24 h after single dose; (d) 50 mg/kg, po, tumor collected 24 h after single dose; (e) 125 mg/kg, po, BID, 5 days, tumor collected 24 h after last dose. Each symbol represents an individual animal, and at least five vehicle-treated animals per study was used as control. Tumor samples were harvested at 4 or 24 h after last dose for KYN quantification. For each study, the average of tumor KYN concentration in the vehicle control was used to calculate the percent inhibition of IDO1 in treated animals. Means ± standard error of the mean (SEM) are represented. po (oral administration); QD (once daily dose). Statistical *t*-test was performed and there was no statistical difference between **6(b)** and **62(a)**, **62(b)** and **71(c)** but there was between **6(b)** and **71(d)**, $p = 0.012$.

Additional compounds were resynthesized homochirally as the R enantiomer. The hERG safety margin was also calculated using the hERG manual patch clamp data. Within the monofluoro- and cyano-substituted benzimidazoles (**56**–**61**), 6-CN **59** was the only compound that exhibited good TE but the hERG safety margin was low compared to the disubstituted benzimidazoles (Tables 6 and 7, Figure 10).

The 5,6-difluorobenzimidazole **45** (Table 5) was synthesized homochirally (**62**) (Table 6), had the best safety margin, and in the SKOV3 model, it displayed robust TE from good tumor exposure (Figure 10, Table 7). However, the hERG activity was still a potential concern and other modifications were explored. Addition of a 3-fluoro (**63**), replacement of the 4-chloro with a 4-nitrile (**64**), and the ethyl (R_2) truncated to a methyl (**65**) resulted in molecules with excellent TE (Figure 10, Table 7), but none of these molecules offered any advantage or an increase in the safety margin over **62** (Table 6). Other modifications including the R_2 gem-dimethyl (**66**), R_2 cyclopropyl (**67**), combination of the R_2 methyl with the 4-nitrile (**68**), and the phenyl replaced with a propellane (**69**) lack optimal safety margins or the potency (Table 6).

Considering our crystal structures of **22** and **17**, it was apparent that the hydrogen bond to the Ser-167 was significant. We postulated that the difference in the HeLa potency between **62** and **6** might be due to our reversal of the amide bond and by switching it back we may improve the potency and the hERG safety margin. To do this, we considered the very close analog **65**. Q-patch hERG data for **65** indicated an apparently improved margin. Hence, the reverse amide of **65** was synthesized, compound **70** (Table 8). After the fact, we received the manual patch clamp data for **62** and **65** and the compounds were actually very similar. Compound **70** (IACS-70099) had improved PK exposure over **62** (Table 9), robust TE (Figure 10), potency less than 1 nM (*n* of 11), and despite the similar hERG potencies, the improved HeLa potency increased the safety margin (Table 8) compared to **62**. It is interesting to note that the decrease in potency of the amide-reversed **65** compared to **70** was not observed for **7** (BMS-986242), the corresponding matched analog of linrodostat **6**, both of which were reported as equipotent (2 nM).[32]

A crystal structure was also obtained for **70** showing binding of the inhibitor spanning between pockets A and D of IDO1, similar to the previously described compound **22**. Reversing the amide, the N–H of compound **70** maintains the hydrogen bond with Ser167 with the chlorophenyl group in the tryptophan pocket (pocket A) and the bicyclo[3.1.0]hexane core occupying the hydrophobic region between Phe214, Phe270 and His346. The direct link from the bicyclo[3.1.0]hexane core to the benzimidazole in **70**, instead of an oxygen-linked quinoline, allows the benzimidazole to orient 90° relative to the quinoline of **22** (Figure 11). This orientation of the benzimidazole group

Table 7. Benzimidazole Selection, SKOV3 TE

compound[a]	tumor [compound] (μM)[b]	plasma [compound] (μM)[c]	mPPB (%)[d]	HeLa hIDO1 IC_{50} (nM)[e]	tumor TE (%)[f]
2	3.2 ± 0.7 (4)	0.1 ± 0.1 (4)	96.4	11 ± 9 (174)	32 ± 5 (4)
6	0.9 ± 0.5 (8)	0.02 ± 0.01 (8)	99.1	0.42 ± 0.11 (19)	25 ± 5 (7)
17	0.7 ± 0.1 (4)	0.1 ± 0 (4)	93.8 ± 1.9 (3)	26 ± 8 (34)	86 ± 10 (4)
56(a)	2.3 ± 0.7 (3)	0.6 ± 0.4 (3)	99.5	2.8 ± 1.1 (2)	83 ± 23 (3)
57(b)	0.1 ± 0.1 (4)	0.01 ± 0 (1)	99.2	9.2 ± 2.8 (4)	102 ± 10 (4)
58(b)	0.6 ± 0.5 (6)	0.5 ± 0.2 (6)	99.2	3.4 ± 0.3 (2)	70 ± 7 (6)
59(b)	12 ± 3 (4)	10.1 ± 3 (4)	98.7	8.8 ± 1.9 (4)	19 ± 4 (4)
62(a)	32 ± 12 (6)	35 ± 9.2 (6)	99.3	1.7 ± 0.6 (20)	11 ± 4 (6)
62(b)	3.4 ± 3 (9)	1.4 ± 1.5 (9)	99.3	1.7 ± 0.6 (20)	18 ± 3 (7)
63(b)	11 ± 6 (4)	4.1 ± 1.2 (4)	99	3.9 ± 1.6 (4)	10 ± 2 (4)
64(a)	52 ± 16 (3)	49.3 ± 6.6 (3)	97.1	4.4 ± 1.2 (10)	6 ± 2 (3)
65(b)	5.1 ± 2.5 (6)	2.8 ± 1.6 (6)	98.9	5.3 ± 1.2 (8)	26 ± 4 (6)
70(b)	2.1 ± 2.3 (6)	0.3 ± 0.1 (6)	99.01	0.69 ± 0.16 (11)	21 ± 3 (6)
71(c)	0.5 ± 0 (4)	0.06 ± 0.02 (4)	99.01	0.60 ± 0.06 (6)	33 ± 4 (4)
71(d)	0.7 ± 0.2 (7)	1.9 ± 1.1 (7)	99.01	0.60 ± 0.06 (6)	9 ± 1 (7)
72(c)	0.5 ± 0.1 (4)	0.01 ± 0.004 (4)		0.92 ± 0.24 (6)	102 ± 3 (4)

[a]Description (a–e) in Figure 11. [b]Compound concentration in tumor [average ± standard deviation (*n*)]. [c]Compound concentration in plasma [average ±standard deviation (*n*)]. [d]Mouse plasma protein binding [average ±standard deviation (*n*)]. [e]Average ± standard deviation (*n*). [f]TE in tumor [% of vehicle control ± SEM, (*n*)].

https://doi.org/10.1021/acs.jmedchem.1c00679
J. Med. Chem. XXXX, XXX, XXX–XXX

Table 8. Lead-Optimized Compounds

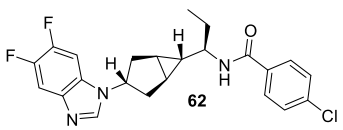

62

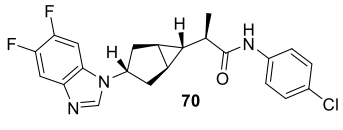

70

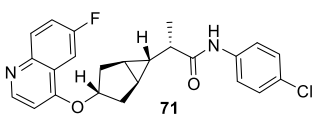

71

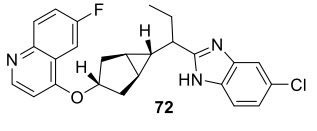

72

compound	HeLa hIDO1 IC_{50} (nM)[a]	$PANCO_2$ mIDO1 IC_{50} (nM)[a]	HLM[b] CI_{int} (mL/min/kg)	CYP 2C9 IC_{50} (μM)	hERG (FP) IC_{50} (μM)[a,c]	hERG (QP) IC_{50} (μM)[a,d]	hERG (MP) IC_{50} (μM)[a,e]	hERG safety margin[f]	hPPB (%)[a,g]	whole blood[l] IC_{50}	whole blood[l] IC_{90}	SKOV3 PK/PD[m] IC_{50}	SKOV3 PK/PD[m] IC_{90}
2	11 ± 9 (174)	74 ± 30 (56)	12	7.8 ± 2 (5)	>36 ± 0 (4)[k]			3300	97.2 ± 0.1 (3)				
6	0.42 ± 0.11 (19)	1.6 ± 0.5 (13)	28	1.4	4.2 ± 1.3 (3)		2.4[h]	6400	100.0	26	260	5.8	52
17	26 ± 8 (34)	23 ± 7 (20)	22	23 ± 6 (6)		>30 ± 0 (2)		>1200	91.6 ± 0.7 (4)				
62	1.7 ± 0.6 (20)	14 ± 5 (11)	8.5	1.8 ± 0.6 (2)	2.4 ± 0.3 (3)	11	0.79 ± 0.22 (3)[h]	465	99.4	116	1047	166	1497
70	0.69 ± 0.16 (11)	1.0 ± 0.2 (11)	19	1.9	3.6 ± 0.8 (2)		1.0[i]	1400	99.0	46	411	85	762
71	0.60 ± 0.06 (6)	2.0 ± 0.2 (2)	15	6.2	>44 ± 0 (4)[j]		>3[h]	>5000	99.0	14	124	25	228
72	0.92 ± 0.24 (6)		17	0.91	1.0			1100	99.97				

[a]Average ± standard deviation (number of measurements). [b]Human liver microsomes. [c](FP) fluorescence polarization hERG-binding assay. [d](QP) Q-patch electrophysiology hERG assay. [e](MP) manual patch clamp hERG assay, each dose $n \geq 2$ current measurements. [f]Safety margin is the ratio of hERG (MP) or available hERG data/HeLa IC_{50}. [g]Human plasma protein binding. [h]Precipitation observed at 10 and 30 μM. [i]Precipitation observed at 30 μM. [j]Four measurements, two at 44 and two at >44 μM. [k]Four measurements, two at 36 and two at >36 μM. [l]Human whole blood assay data from Figure 12. [m]SKOV3 PK/PD data from Figure 13.

https://doi.org/10.1021/acs.jmedchem.1c00679
J. Med. Chem. XXXX, XXX, XXX−XXX

Table 9. Mouse PK Profile of the Selected Compounds

PK parameter[a]	2	6	17	62	70	71
Cl (L/h/Kg)[b]	3.2 ± 0.2	2.0 ± 0.2	1.4 ± 0.4	1.04 ± 0.09	0.45 ± 0.02	0.21 ± 0.01
V_{ss}[b]	7.5 ± 0.9	4.5 ± 0.3	2.1 ± 0.4	3.1 ± 0.2	1.61 ± 0.07	1.55 ± 0.02
$T_{1/2}$ (terminal h)[b]	1.6 ± 0.3	1.57 ± 0.05	0.848 ± 0.05	2.1 ± 0.2	2.49 ± 0.07	5.3 ± 0.3
AUC_{Inf} (h·μM)[b]	0.21 ± 0.01	0.37 ± 0.03	0.45 ± 0..07	0.67 ± 0.06	1.61 ± 0.09	3.3 ± 0.2
C_{max} (μM)[c]	2 ± 2	4.1 ± 0.1	7 ± 2	1.5 ± 0.1	8.6 ± 0.9	5.2 ± 2.1
F (%)	50 ± 13	39 ± 5	132 ± 20	89 ± 38	82 ± 11	48 ± 6

[a]Each dose done in triplicate. [b]IV (0.3 mpk). [c]po (10 mpk).

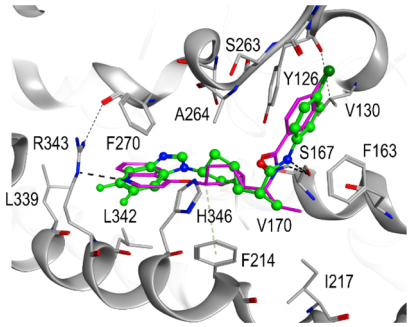

Figure 11. Crystal structure of **70** (light purple, PDB 7M63) superposed with the crystal structure of **22** (green).

appears to be better tolerated by mouse IDO1 resulting in only a small, 1.4-fold, species shift between human and mouse IDO1 (Table 8).

In addition, we wanted to advance a compound without a hERG liability. We revisited the quinoline series and considered reversing the amide of compound **24** (Table 2, mouse PK Table 4). However, to have a direct comparison to **70** and the use of a common intermediate, the R_2 methyl substitution analog was synthesized, compound **71** (IACS-70465). The absolute configuration of the eutomer was not confirmed (assigned based on the SFC elution order). The potency of **71**, was consistently less than 1 nM (*n* of 6, Table 8), had excellent PK (Table 9), robust TE even at 3 mg/kg (Figure 10, Table 7), and did not have a measurable hERG signal in the fluorescence polarization nor the manual patch clamp assays (Table 8).

As mentioned earlier, we were still concerned with the stability of the aniline amides and considered the isostere similar to Merck's series, compound **8**. We synthesized a series of benzimidazole isosteres with the ether-linked 6-fluoroquinoline moiety.[64] Compound **72**, (Table 8), is a representative molecule that was taken into the SKOV3 model but did not show TE as compared to **71** at 3 mg/kg (Table 7 and Figure 10).

The TE of the compounds from Table 6, and compound **8** are compared with linrodostat **6** and two type III inhibitors, epacadostat **2** and imidazopyridine **17** (data in Table 7, Figure 10). The heme-binding inhibitor-dosed BID were not as efficacious as the apoenzyme inhibitor-dosed QD. These two compounds have higher clearances and shorter half lives in mice (Table 9) but they are also less potent in our HeLa cellular assay (Table 8).

The SKOV3 tumor xenograft model in a mouse lacking an intact immune system may not be clinically predictive[16,62,63] and a comparison between different structural classes of inhibitors with this model may not be informative (catalytic and signaling activity and inadvertent AhR agonism).[16,17] However, within our class of type IV inhibitors, differentiation using this model proved beneficial. Most of the compounds exhibited tumor TE, except for **56**, **57**, and **72** (Figure 10, Table 7). Of interest was **64**; dosed QD, it exhibited the best TE, but was not advanced because of its poor hERG safety margin. The more potent **71** was dosed only once at 50 mg/kg with the same resulting efficacy as linrodostat **6** at half the dose (QD 5 days), and TE was observed even at 3 mg/kg. Considering this, the isostere **72** was dosed at only 3 mg/kg but no TE was observed.

Finally, **62** (**IACS-9779**), its close analog **70** (**IACS-70099**), and **71** (**IACS-70465**) displayed the best hIDO1 potencies and hERG safety margin among all the permutations that we profiled, had good PK and bioavailability (Table 9), and consistently showed robust TE and good tumor exposure (Figure 10, Tables 7 and 8). These were advanced to additional studies.

Whole Blood Assay of 62 (IACS-9779), 70 (IACS-70099), 71 (IACS-70465), and 6 (Linrodostat). To assess the impact of the high level of plasma protein binding on compound potency under physiological conditions, we profiled the leading compounds using a human whole blood assay (Figure 12). We observed a decrease in potency for all of the inhibitors as compared to their HeLa potencies (Table 8). The potency differential between linrodostat and IACS-9779 was maintained, IACS-70099 was comparable, but IACS-70465 appeared to be the most potent.

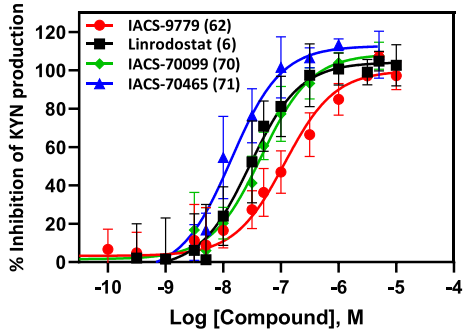

Figure 12. Human whole blood assay. Fresh human peripheral blood was collected from volunteers, treated with DMSO control or increasing concentration of compounds, and stimulated with LPS/IFNγ for 24 h. Plasma samples were then collected for KYN quantification. The percent inhibition of KYN production was determined relative to the DMSO control, and compound potency was calculated: IC_{50}: and IC_{90}: values reported in Table 8. The results are representative of three independent test occasions performed in duplicate.

SKOV3 Comparison of 62 (IACS-9779), 70 (IACS-70099), 71 (IACS-70465), and 6 (Linrodostat). Next, we used the SKOV3 xenograft model to establish a PK and PD relationship between our molecules and **6** (Figure 13, Table 8). Animals were treated for 5 days with each compound at doses ranging from 10 to 125 mg/kg via oral administration (po).

https://doi.org/10.1021/acs.jmedchem.1c00679
J. Med. Chem. XXXX, XXX, XXX−XXX

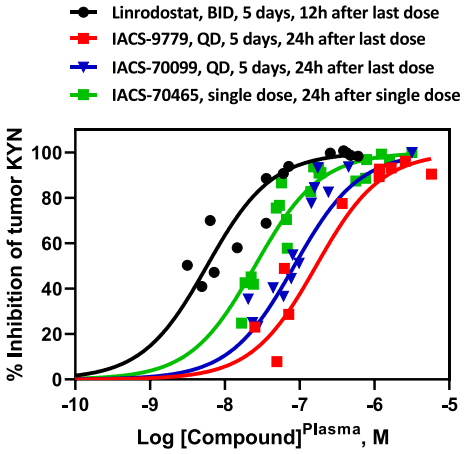

Figure 13. Compound PK/PD relationship. The concentrations of KYN in tumor and compound in plasma samples were derived from in vivo studies using a human SKOV3 xenograft model after administration of compounds at doses ranging from 10 to 125 mg/kg: IACS-9779 (po, QD, 5 days) and linrodostat (po, BID, 5 days), IACS-70099 (po, QD, 5 days), and IACS-70465 (po, single dose). Plasma and tumor samples were collected at 12 h after the last dose for linrodostat, or 24 h after the last dose for IACS-9779, IACS-70099, and IACS-70465. Compound-mediated inhibition of tumor KYN was calculated relative to vehicle-treated animals (vehicle tumor [KYN] = 96 ± 36 μM). Each symbol represents a treated mouse. Estimated tumor PD: IC_{50}: and IC_{90}: values reported in Table 8.

Once daily (QD) for the IACS compounds, and twice daily (BID) for linrodostat (BID to compensate for its higher clearance and shorter half-life in the mouse). Plasma and tumor samples were collected after the last dose. The PK/PD relationship was established by correlating compound plasma exposure against the percent inhibition of tumor KYN relative to vehicle control animals. The relationship for IACS-9779 was consistent with the ex vivo human blood assay (IC_{90}: 1047 nM), giving an estimated IC_{90} of 1497 nM. In this SKOV3 study, IACS-70099 was less potent than linrodostat but was similar to IACS-9779. Due to its improved potency and PK, IACS-70465 was only dosed for a single day unlike the 5 days of dosing with the other compounds and still out performed IACS-9779 and IACS-70099 (Figure 13, Table 8). However, due to its single QD dose, it did not achieve the same response as linrodostat dosed BID for 5 days.

For a direct comparison to linrodostat and epacadostat in an identical dosing experiment, we performed an additional PKPD study in the SKOV-3 model with IACS-9779-dosed BID (Table 10). A 75 mg/kg BID dose of IACS-9779 gave equivalent (>90%) suppression of KYN to either a 125 mg/kg BID dose of linrodostat, or a high dose of 200 mg/kg of epacadostat 12 h after the second dose. It is worth noting that the recent clinical candidate BMS-986242(7),[32] which is more structurally similar to IACS-9779 than to linrodostat **6**, also had an observed improvement of its PD effect.[32]

There is an apparent shift in the IC_{90} of IACS-9779 as compared to linrodostat; however, there is a caveat with this comparison because of the differences in QD and BID dosing (Figure 13). Despite this, the PK profile of IACS-9779 in the mouse allowed for a similar TE in tumors at almost half the dose. The PK of IACS-9779 in other preclinical species was superior to the mouse, and resulted in excellent human PK projections using allometric scaling or IVIVE (in vitro−in vivo extrapolation) methods (Table 11). Modeling of these parameters predicts that the compound should achieve a steady state concentration with a low C_{max}/C_{min} ratio, and permit constant coverage of the IC_{90} from a predicted QD human dose of 50 mg (Figure 14); half of the tolerated dose reportedly used in the clinic for the BMS compound.[65] The IC_{90} values were used to evaluate the therapeutic margin with respect to findings in ancillary pharmacological profiling in vitro and subsequent in vivo tolerability studies.

Safety Studies. Dose range finding toxicity characterization of IACS-9779 and IACS-70099 was performed in a 7-day (po, QD) rat study (Table 12). A low dose (20 mg/kg) of IACS-9779 achieved a C_{max} in plasma above 25 μM [area under the curve (AUC) > 400 μM·h (NOAEL)], which is 16× that of the predicted IDO1 IC_{90} coverage (Figure 14). At a high dose (200 mg/kg), IACS-9779 achieved a coverage in plasma at 87 μM (AUC > 1700 μM·h) with minimal events (Table 12). IACS-70099 at a high dose (500 mg/kg), more than twice that of IACS-9779, achieved only a tenth of the exposure, resulted in serious toxicological events, was significantly worse than IACS-9779 and linrodostat, and was discontinued. In a separate safety pharmacology cardiovascular (CV) dog study, a 10 mg/kg dose of IACS-9779 achieving a C_{max} of 23 μM in plasma was well tolerated, without measurable QTc prolongation, and 15× margin above the predicted IDO1 IC_{90} coverage. A 20 mg/kg dose with a plasma concentration at 43 μM C_{max} was associated with ≤16% prolongation of QT/QTc interval and with transient emesis that resolved. All other CV parameters were within normal ranges. IACS-70099 displayed normal responses up to 30 mg/kg.

The late identification of IACS-70465 resulted in it not being profiled in any safety studies prior to the termination of the program. Its performance appears to be superior to IACS-9779 in the HeLa cellular and whole blood assays as well as in in vivo studies. However, a dose range finding toxicological study would be necessary to clearly differentiate it from IACS-9779.

IACS-9779 has a clog *D* of 4.82 based on a calculated pK_a of 5.6, and low thermodynamic solubility in buffered aqueous media (7 ng/mL at pH 6.7 and 28 ng/mL at pH 5.1). It has excellent passive cell permeability; P_{app} 21 × 10^6/cm·s^{-1} as measured in a confluent monolayer of MDCK MDR1 expressing cells, and it is not a P-gp substrate. The compound was also selective with no measured activity against TDO (IC_{50} > 10 μM, at least three independent test occasions). These physical properties are similar to linrodostat. It is well absorbed upon oral administration to mice, rats, or dogs, and has excellent PK (Table 11).

Table 10. PKPD Comparison

compound	BID Dose (mpk)	tumor [compound] μM	tumor target inhibition (%)	plasma [compound] μM	plasma target inhibition (%)
epacodostat	200	5.0 ± 2.6	82.9	0.69 ± 0.77	57.5
BMS-986205	125	0.61 ± 0.21	88	0.06 ± 0.06	62
IACS-9779	75	17 ± 5.3	95.4	33 ± 2.1	61

https://doi.org/10.1021/acs.jmedchem.1c00679
J. Med. Chem. XXXX, XXX, XXX−XXX

Table 11. Species PK of IACS-9779

	species					
					human[a]	
PK parameters	mouse	rat	dog	monkey	prediction A	prediction B
Cl (L/h/kg)	1.04	0.025	0.075	NA	*0.018*	*0.012*
Vd_{ss} (L/kg)	3.1	1.48	1.42	NA	*1.03*	*0.87*
$T_{1/2}$ (h)	2.1	53.8	12.9	NA	*40*	*50*
F (%)	89	77	68	NA	*>50*	*99*
microsomal Clint (mL/min/kg)	37.8	9.7	13.3	61.4	8.5	
$T_{1/2}$ (h)	2.41	4.28	4.33	0.55	3.39	
hepatocyte CLint (mL/min/kg)	231	0	36.7	24	4.78	
$T_{1/2}$ (h)	1.18	>24	4.33	3.75	12.3	
plasma protein binding (%)	>99	>99			>99	

[a]A: Based on allometric scaling from mouse, rat, and dog (IV) data. B: IVIVE method by XenoGesis.

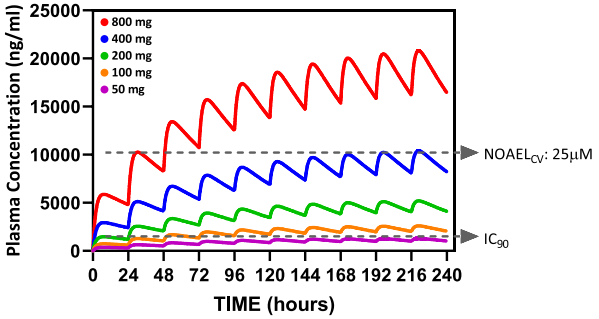

Figure 14. IACS-9779 human prediction of dose escalation over 10 half lives.

Table 12. Rat Dose Range Finding Toxicity of IACS-9779

	compound		
parameters	IACS-9779	IACS-70099[a]	linrodostat
high-dose mpk	200	500	250
AUC projection μM·h	6600	277−689	95−245
ALT	↑	↑↑	↑
bilirubin	no change	↑↑	↑
RBC, HGB, HCT	no change	↓↓, ↓↓, ↓↓	↓RBC only
reticulocytes	↓↓	↓↓	↑
bone marrow smear	50% ↓ erythroid cell	50% ↓ myeloid cell; 70% ↓ erythroid cells; 2.5-fold ↑ lymphoid cell	no change
gross lesion	none visible	bilateral enlarged adrenal gland in 3/5 animals; dark red diffuse ovary noted 3/5 animals	none visible
body weight (high dose)	decrease	decrease	decrease
high-dose mortality	1 death	2 deaths	2 deaths

[a]Strong inhibition for OATP1B1/OATP1B3/BRCP; modest rate inhibition for BSEP.

CONCLUSIONS

The bicyclo[3.1.0]hexane core provided a conformationally constrained scaffold with axial and equatorial substitutions (at the 3 and 6 carbons, respectively) that offer a preferred geometry for optimal IDO1 inhibition as measured by the reduction of KYN with a RFMS technique in lysates from a human HeLa cell line. The crystal structures of compounds **17**, **22**, and **70** revealed that **17** was a type III inhibitor and **22** and **70** were type IV inhibitors of IDO1. Biochemistry experiments elucidated the mechanism of IDO1 inhibition by **22** to be via engagement with the apoenzyme. A protein sequence homology study across species showed the conservation of pocket A and modest changes in the vicinity of the pocket D. Variations in the substitution pattern of the inhibitor in the vicinity of this region resulted in significant shifts in potency between the human and mouse enzyme; the human receptor being more tolerant to a diversity of modifications than the mouse. The benzimidazole moiety provided potency in both mouse and human enzymes with a minimal species shift. Extensive SAR produced potent molecules with excellent PK and tumor TE. Compounds **62** (IACS-9779), **70** (IACS70099), and **71** (IACS-70465) displayed the best combinations of potency and hERG safety margin and had consistent TE with good tumor exposure. IACS-70099 did not progress due to toxicology and the profiling of IACS-70465 was not completed due to termination of the program. IACS-9779 had a better safety profile in a preliminary rat toxicology study than did IACS-70099. From human PK projections of IACS-9779 based on allometric scaling and IVIVE methods, a calculated QD dose of below 1 mg/kg was postulated to be efficacious, sustain exposure at the IDO1 IC_{90}, and provide an adequate safety margin based on rat toxicology. In a CV dog study, IACS-9779 was tolerated without QTc prolongation up to 20 mg/kg offering a 15× therapeutic index with respect to the hIDO1 IC_{90}. The predicted human PK of IACS-9779 indicates suitability for a QD dosing regimen with a low plasma peak-trough ratio. We independently elucidated the mechanism of action of a series of type IV IDO1 inhibitors, and upon recognizing the potential of this mode of action, optimized our leads to culminate in the identification of IACS-9779, a potent and selective IDO inhibitor suitable for human evaluation. In light of the current state of stalled and terminated clinical trials, the utility of IDO1 inhibition in the oncology setting is in question. Linrodostat's phase III trial appears to be still active, as is recruiting for a phase I trial of KHK-2455 (structure undisclosed). Perhaps, when the results of these trials are disclosed, the clinical utility of an IDO1 inhibitor will be better defined.[16,17]

CHEMISTRY

The starting bicyclo[3.1.0]hexane core **73** was synthesized according to known procedures.[66] Briefly, 3-cyclopentene-1-ol protected with TBDPS-Cl is cyclopropanated with ethyl 2-diazoacetate, and then hydrolyzed to give the starting acid.

https://doi.org/10.1021/acs.jmedchem.1c00679
J. Med. Chem. XXXX, XXX, XXX−XXX

Acid **73** was converted to aldehyde **74** via the Weinreb Amide and reduction with DIBAL-H. Condensation with *tert*-butyl sulfinamide formed the intermediate imine **75**, which was either alkylated with a Grignard reagent or reduced with lithium aluminum hydride (LAH). Sulfinamide **76R$_1$** was globally deprotected to give the amino alkyl bicyclo[3.1.0]hexane alcohol, which was amidated without purification. Standard amide-coupling conditions using EDCI or HATU work but some esterification occurs as a side product, the yield can be increased by coupling with the NHS ester of the benzoic acid. The crude amide alcohol was subjected to flash silica gel chromatography to isolate the two major diastereomers, **77R$_1$** and **78R$_1$**, which can be differentially identified by NOSEY NMR experiments that display the interaction or the absence thereof between the protons on the 3 and 6 carbons of the bicyclo[3.1.0]hexane system (Scheme 1).

Scheme 1. Synthesis of Hydroxy Bicyclo[3.1.0]hexane Diastereomers[a]

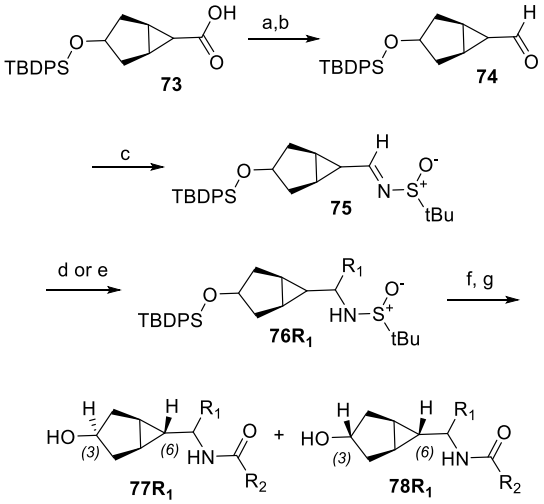

[a]Regents and conditions: (a) MeNHOMe·HCl, DMAP, DIEA, EDCI, DCM; (b) DIBAL-H, PhMe; (c) 2-methylpropane-2-sulfinamide, $CuSO_4$, DCM; (d) R_1MgBr, THF; (e) LAH, THF; (f) HCl/Dioxane, MeOH; (g) R_2COOH, DIEA, HATU, DMF or EDCI, HOBT, DIEA, DCM.

Initially, the preferred diastereomer was undetermined and both isomers were taken forward to make final compounds (Scheme 2). Depending on availability of reagents, the final compounds were synthesized by several methods. The quinolines were synthesized through nucleophilic aromatic substitutions (S_NAr) with retention of configuration (**21−23, 25−30**) or through a Mitsunobu reaction with inversion (**24**). In the synthesis of the benzimidazoles, alcohol **77R$_1$** was activated with mesyl chloride (**79R$_1$**) and displaced inverting the carbon center to produce a more potent isomer (**36−70**).

In the synthesis of benzimidazoles with unsymmetrical substitutions, the two products could usually be separated by prep-HPLC and identified by NOESY experiments. For inseparable products, the benzimidazoles were synthesized by azide nucleophilic displacement (**80R$_1$**) of the mesylate **79R$_1$**, reduction to the amine **81R$_1$**, S_NAr with the appropriate fluoro-nitro-aryl/heteroaryl compound **82R$_1$(R$_3$)**, reduction, and cyclization to the benzimidazole in one pot with iron and formic acid (Scheme 3).[67]

Scheme 2. Synthesis of Quinolines and Symmetric Benzimidazoles[a]

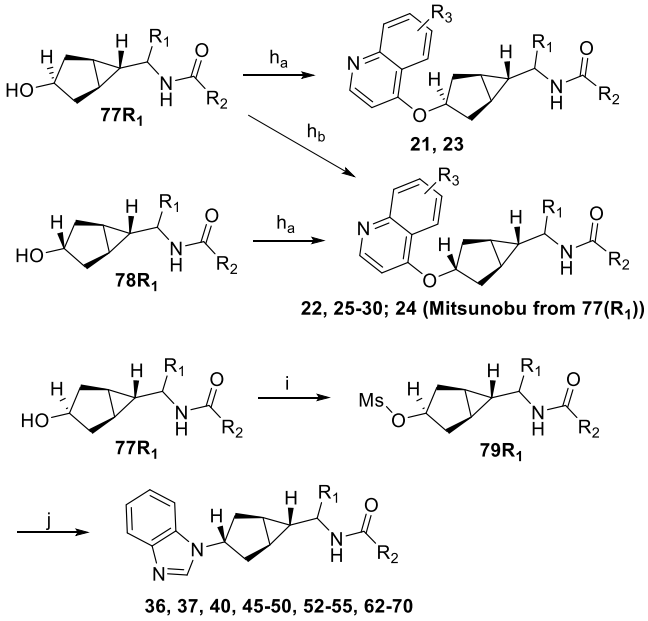

[a]Reagents and conditions: (h_a) 4-bromoquinoline, NaH, DMSO or KOtBu, THF; (h_b) polymer-TPP, quinolin-4-ol, DTAB, THF; (i) MsCl, TEA DCM; (j) Benzimidazole, K_2CO_3, DMF.

Scheme 3. Synthesis of Unsymmetrical Benzimidazoles[a]

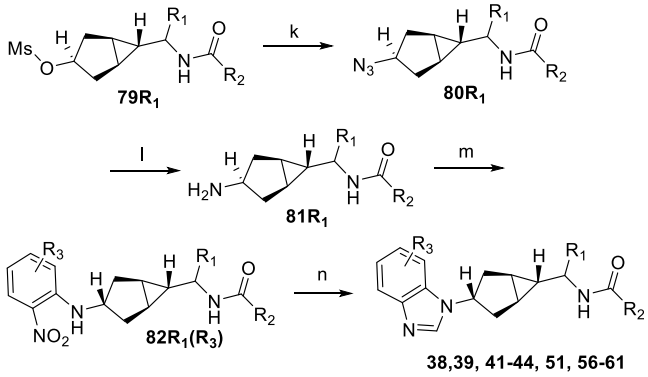

[a]Reagents and conditions: (k) NaN_3, DMF; (l) polymer-TPP, THF, H_2O; (m) 2-fluoronitrobenzene, K_2CO_3, THF, (n) Fe, HCOOH, IPA.

Based on the crystal structure of **22**, it was determined that the R enantiomeric center of **83** should be the more potent isomer. The diastereomeric chiral amine **83**, as illustrated in Scheme 4, was synthesized from an asymmetric Grignard addition to chiral *t*-Bu-sulfinimine **75(S)** as developed by Ellman and co-workers.[68] Following literature examples, condensation of aldehyde **74** with (*S*)-*t*-Bu-sulfinamide in the presence of anhydrous copper sulfate gave imine **75(S)** in moderate yield. Grignard addition to imine **75(S)** gave sulfinamide **76R$_1$(R)**, which upon further removal of the *t*-Bu-sulfinyl auxiliary under mild acid conditions provided chiral amine **83R$_1$(R)**.

Intermediate **83R$_1$(R)** was used in the synthesis of compound **56**, which proved to be equipotent to **39A**, the more potent isomer obtained from SFC separation of racemic **39**, in a human IDO1 HeLa cellular assay (Table 5). This synthesis proved to be very robust for gaining access to the chiral amine **83R$_1$(R)**.

https://doi.org/10.1021/acs.jmedchem.1c00679
J. Med. Chem. XXXX, XXX, XXX−XXX

Scheme 4. Synthesis of Diastereomeric Chiral Bicyclo[3.1.0]hexane Amine[a]

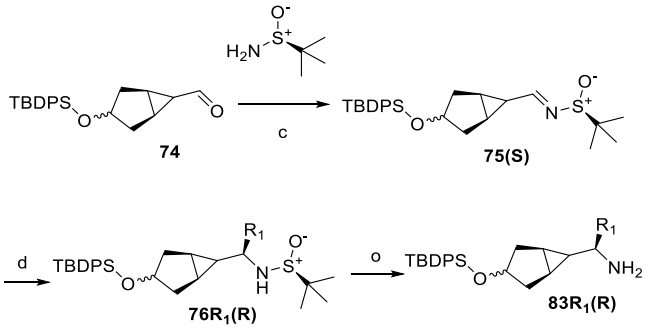

[a]Reagents and conditions: (a) (*S*)-2-methylpropane-2-sulfinamide, $CuSO_4$, DCM; (b) R_1MgBr, THF; (o) HCl/Dioxane, MeOH.

To confirm the chirality of the newly formed (R) stereocenter, a Mosher's amide analysis was utilized (Scheme 5).[69] Comparing the NMRs of the resulting (S) and (R) Mosher amides **84** and **85** showed a nice correlation of the shielding effect of the phenyl group from the Mosher's amide. Calculating the $\Delta\delta SR$ of key NMR proton shifts established chemically that starting from the (*S*)-sulfinamide gave the desired (*R*) stereoisomer.

The reversed amides **70** and **71** were initially synthesized from the same common intermediate **88** (Scheme 6). The starting aldehyde **74** was converted to the methyl ketone **86** via the Grignard and Dess−Martin oxidation. The ketone was homologated to the corresponding carboxylic acid **88** through the Wittig, acid hydrolysis, and Pinnick oxidation. Then, through chemistry previously described, the racemic versions of **70** and **71** were synthesized. The enantiomers were separated by SFC and the assignment of stereo chemistry was based on the order of elution precedently set by the SFC separation of **39**, and were not absolutely confirmed. The synthesis of the benzimidazole isostere **72** (Scheme 7) used the carboxylic acid **72(Et)H** (prepared through an analogous scheme, Supporting Information) that was coupled with the diamine and cyclized using tosic acid.

EXPERIMENTAL SECTION

Synthesis Methods. The inhibitors described were synthesized by employing standard chemical transformations. Starting materials and reagents were purchased from commercial suppliers such as Sigma-Aldrich, Alfa Aesar, TCI, Combi-Block, Enamine, or Acros and were used without further purification unless otherwise indicated. Anhydrous solvents [e.g., tetrahydrofuran (THF), dimethylformamide (DMF), DMA, dimethyl sulfoxide (DMSO), MeOH, dichloromethane (DCM), and toluene] were purchased from Sigma-Aldrich and used directly. Purification of final compounds was performed by column chromatography utilizing a Biotage system applying Biotage SNAP

Scheme 5. Mosher Amide Analysis[a]

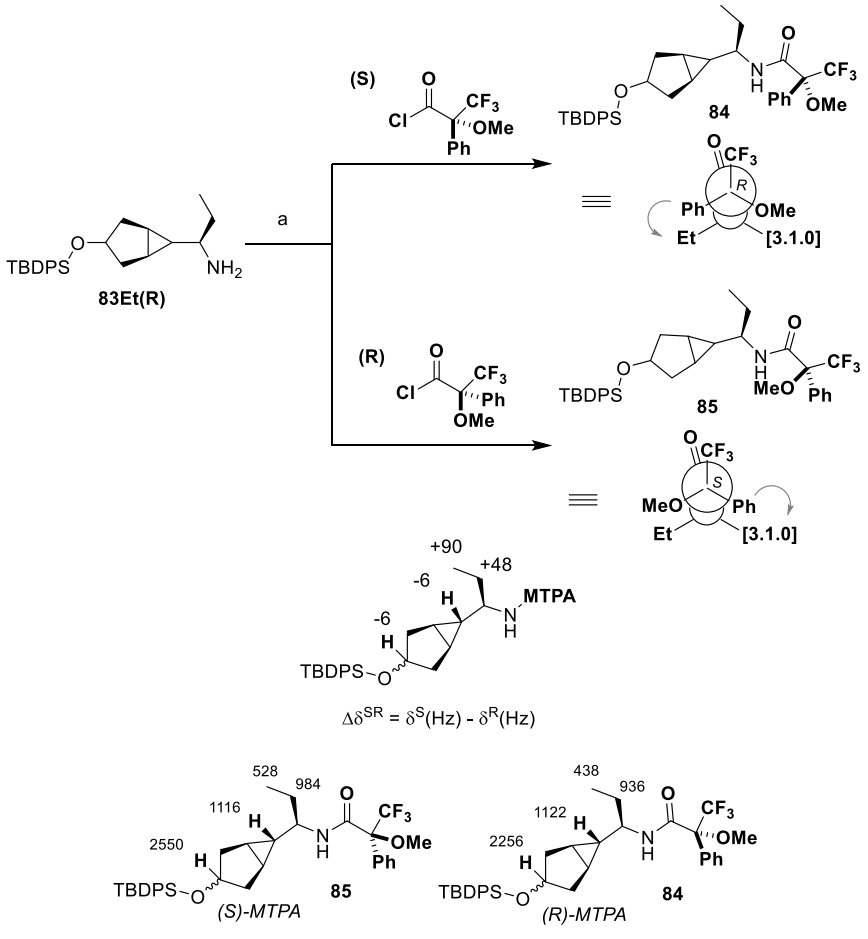

[a]Regents and conditions: (a) DIEA, ClCOMTPA, DCM.

https://doi.org/10.1021/acs.jmedchem.1c00679
J. Med. Chem. XXXX, XXX, XXX−XXX

Scheme 6. Common Intermediate, Reversed Amides[a]

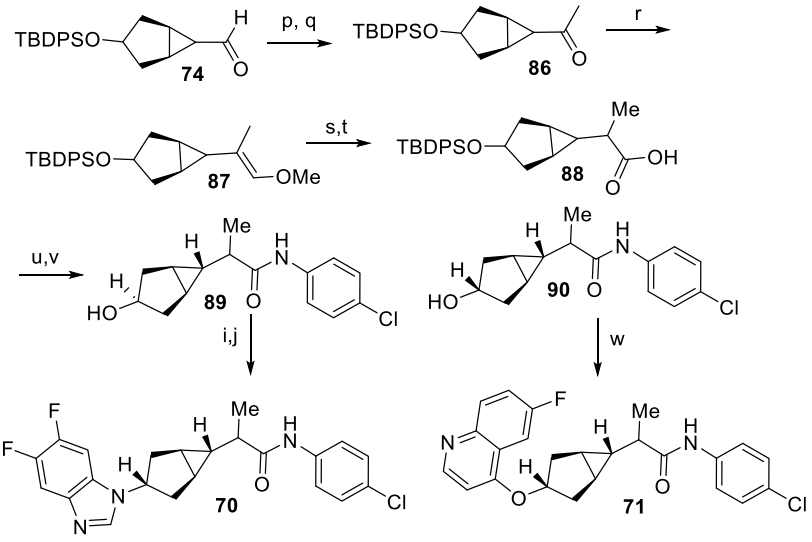

[a]Reagents and conditions: (p) 0 °C, THF, MeMgBr; (q) 0 °C, DCM(wet) DMP; (r) −13 °C Ph_3PCH_2OMe·Cl, THF, LHMDS; (s) PPTS, dioxane, H_2O, 70 °C; (t) 0 °C, tBuOH, $CH_3(CH_3)C{=}CHCH_3$, $NaClO_2$, KH_2PO_4, H_2O; (u) Pyridine, EtOAc, T3P; (v) THF, TBAF, 50 °C. (w) 0 °C, NaH, DMF.

Scheme 7. Benzimidazole Synthesis[a]

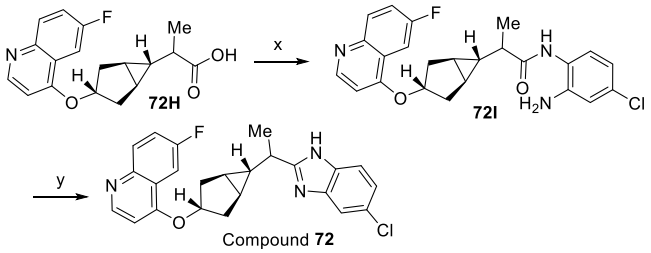

[a]Reagents and conditions: (x) pyridine, EtOAc, T3P, 65 °C; (y) PhMe, pTsOH, 110 °C.

columns with Biotage KP-Sil silica or Biotage Zip Si columns with Biotage KP-Sil silica or a Teledyne ISCO system with RediSep Rf normal phase silica cartridges. Some compounds were purified by preparative HPLC using a Waters Autopurify system with a Waters Xbridge Prep C18 5 μm OBD, 19 mm × 150 mm or 50 mm × 100 mm column, and a SQ detector mass spectrometer with electrospray ionization (ESI) ionization. The identity of all compounds with reported biological activity was confirmed by NMR spectroscopy and low-resolution mass spectrometry, and for selected analogs, high-resolution mass spectrometry (HRMS). Purity of all compounds with reported biological activity was >95% and was determined by ultraperformance liquid chromatography (UPLC). HRMS data were collected for leading compounds **22** and **62** (as well as **24**, **31**, **34**, **38**, **39**, **39A**, **39B**, **46**, **56**, **59**, **62**, and **64**; Supporting Information). NMR spectra were recorded on Bruker instruments operating at 300, 500, or 600 MHz. NMR spectra were obtained as $CDCl_3$, CD_3OD, D_2O, $(CD_3)_2SO$, $(CD_3)_2CO$, C_6D_6, or CD_3CN solutions (reported in ppm), using tetramethylsilane (0.00 ppm) or residual solvent ($CDCl_3$, 7.26 ppm; CD_3OD, 3.31 ppm; D_2O, 4.79 ppm; $(CD_3)_2SO$, 2.50 ppm; $(CD_3)_2CO$, 2.05 ppm; C_6D_6, 7.16 ppm; and CD_3CN, 1.94 ppm) as the reference standard. Low-resolution mass spectra were obtained on either a Waters H class UPLC with a Waters Acquity UPLC BEH C18 1.7 μm, 2.1 mm × 50 mm column, UV detection between 200 and 400 nm, evaporating light scattering detection, and a SQ detector mass spectrometer with ESI ionization or a Water I class UPLC with a Waters Acquity UPLC CSH C18 1.7 μm, 2.1 mm × 50 mm column, UV detection at 254 and 290 nm, evaporating light scattering detection, and a SQ detector 2 mass spectrometer with ESI. HRMS were obtained on a Waters Acquity I-Class UPLC coupled to a LTQ-Orbitrap Elite mass spectrometer. The injection volume was 5 μL. Chromatographic separation was performed on a Waters Acquity UPLC BEH C18 1.7 μm, 2.1 mm × 50 mm column, at a flow rate of 0.5 mL/min. The mobile phases were 0.1% acetic acid in water (solvent A) and 0.1% acetic acid in acetonitrile (solvent B). The gradient had a total run time of 18 min and was as follows: 0−2 min 5% B; 2−12 min from 5 to 65% B; 12−14 min from 65 to 95% B; 14−16 min at 95% B; 16−16.1 min from 95 to 5% B; and 16.1−18 min at 5% B. The column temperature was kept at 40 °C. The samples were analyzed using the positive ESI mode. The ESI source temperature was set at 375 °C, the capillary temperature at 320 °C, and the electrospray voltage at 4.1 kV. Sheath and auxiliary gases were of 45 arbitrary unit and 10 arbitrary unit, respectively. Calculator Plugins were used for structure property prediction and calculation (clog *P*), Marvin 16.8.15, 2016, ChemAxon (http://www.chemaxon.com), and used in ChemCart, version 6.0.1, http://www.deltasoftinc.com.

*4-Chloro-N-(1-((1R,3r,5S,6r)-3-(Quinolin-4-yloxy)bicyclo[3.1.0]-hexan-6-yl)propyl)benzamide (**21**). (1R,5S)-3-((tert-Butyldiphenylsilyl)oxy)-N-methoxy-N-methylbicyclo[3.1.0]hexane-6-carboxamide (Step a).* To a solution of (1*R*,5*S*)-3-((*tert*-butyldiphenylsilyl)oxy)bicyclo[3.1.0]hexane-6-carboxylic acid **74a** (20 g, 53 mmol) in DCM (200 mL) were added DMAP (*N*,*N*-dimethylpyridin-4-amine) (1.3 g, 11 mmol) and *N*,*O*-dimethylhydroxylamine hydrochloride (7.7 g, 79 mmol), and the partially dissolved mixture was chilled in an ice/water bath for 5 min. To the mixture was added *N*,*N*-diisopropylethylamine, Hunig's base (DIEA) (10 g, 79 mmol), stirred for 5 min and then EDC (N1-((ethylimino)methylene)-N3,N3-dimethylpropane-1,3-diamine hydrochloride) (15 g, 79 mmol) was added and the mixture was allowed to warm to room temperature (RT) overnight. The slightly cloudy solution was diluted with a mixture of DCM and hexane (10%) and washed with HCl (0.1 M, 200 mL), NaOH (0.1 M, 200 mL), water (200 mL), and brine (200 mL). The aqueous layers were extracted with DCM (1 × 30 mL). The DCM layers were combined, dried over $MgSO_4$, filtered, and concentrated as a colorless slightly cloudy oil. The residue was dissolved in minimal DCM and purified via silica gel chromatography (0−30% EtOAc in hexanes) to give the title compound **74a** (22.4 g, 50 mmol, 96% yield) as a colorless semisolid/viscous. MS (ES^+) $C_{25}H_{33}NO_3Si$ calculated 423; found 424 $[M + H]^+$. ^1H NMR (600 MHz, $CDCl_3$): δ 7.69−7.60 (m, 4H), 7.45−7.40 (m, 2H), 7.40−7.32 (m, 4H), 4.40−3.90 (m, 1H), 3.79−3.50 (m, 3H), 3.29−3.07 (m, 3H), 2.86−1.42 (m, 7H), 1.10−1.00 (m, 9H).

https://doi.org/10.1021/acs.jmedchem.1c00679
J. Med. Chem. XXXX, XXX, XXX−XXX

*(1R,5S)-3-((tert-Butyldiphenylsilyl)oxy)bicyclo[3.1.0]hexane-6-carbaldehyde (Step b, **74**).* To a solution of (1*R*,5*S*)-3-((*tert*-butyldiphenylsilyl)oxy)-*N*-methoxy-*N*-methylbicyclo[3.1.0] hexane-6-carboxamide **74a** (22.4 g, 52.9 mmol) in dry toluene (260 mL) at −78 °C was added DIBAL-H (1 M in toluene, 58 mL, 58 mmol) dropwise over 17 min, and the resulting colorless solution was stirred at −78 °C for 3.5 h. To the reaction at −78 °C was added EtOAc (135 mL) and allowed to warm in an ice bath for 15 min. To the reaction was added water (2.4 mL) and stirred for 5 min, 15% aqueous NaOH (2.6 mL) and stirred for 5 min, and then water (6 mL), and the reaction was allowed to warm to RT for 30 min. To the stirring reaction was added $MgSO_4$ and allowed stir at RT overnight. The reaction was filtered and the filtrate was washed with (150 mL/each) saturated NH_4Cl, water, and saturated NaCl, dried over $MgSO_4$, filtered, and concentrated. The residue was purified via flash chromatography (0−30% EtOAc in hexanes) to give **74** (17.6 g, 48.4 mmol, 92% yield). MS (ES^+) $C_{23}H_{28}O_2Si$ calculated 364; found 387 $[M + Na]^+$. ^1H NMR (600 MHz, $CDCl_3$): δ 9.31−8.88 (m, 1H), 7.65−7.59 (m, 4H), 7.46−7.40 (m, 2H), 7.39−7.34 (m, 4H), 4.41−3.79 (m, 1H), 2.54−2.20 (m, 1H), 2.09−1.97 (m, 3H), 1.96−1.86 (m, 3H), 1.11−0.98 (m, 9H).

*N-((E)-((1R,5S)-3-((tert-Butyldiphenylsilyl)oxy)bicyclo[3.1.0]hexan-6-yl)methylene)-2-methylpropane-2-sulfinamide (Step c, **75**).* To a solution of (1*R*,5*S*)-3-((*tert*-butyldiphenylsilyl)oxy)bicyclo-[3.1.0]hexane-6-carbaldehyde **74** (13 g, 36 mmol) in DCM (72 mL) were added 2-methylpropane-2-sulfinamide (8.7 g, 72 mmol) and anhydrous copper(II) sulfate (5.7 g, 36 mmol) and the resulting mixture was stirred at RT overnight. The reaction was filtered through Celite, concentrated, and purified via flash chromatography (0−15% EtOAc in hexanes) to give **75** (14.5 g, 31 mmol, 86% yield). MS (ES^+) $C_{27}H_{37}NO_2SSi$ calculated 467; found 468 $[M + H]^+$. ^1H NMR (600 MHz, $CDCl_3$): δ 7.75 (d, J = 7.1 Hz, 1H), 7.65−7.59 (m, 4H), 7.45−7.40 (m, 2H), 7.40−7.34 (m, 4H), 4.38−3.92 (m, 1H), 2.59−2.19 (m, 1H), 2.13−1.40 (m, 6H), 1.22−1.10 (m, 9H), 1.08−0.98 (m, 9H).

*N-(1-((1R,5S)-3-((tert-Butyldiphenylsilyl)oxy)bicyclo[3.1.0]hexan-6-yl)propyl)-2-methylpropane-2-sulfinamide (Step d, **76Et**).* To a cooled −78 °C solution of *N*-((*E*)-((1*R*,5*S*)-3-((*tert*-butyldiphenylsilyl)oxy)bicyclo[3.1.0]hexan-6-yl)methylene)-2-methylpropane-2-sulfinamide **75** (8 g, 17 mmol) in THF (64 mL) was added EtMgBr (23 mL of 3 M solution in diethylether, 68 mmol). The resulting mixture was stirred at −78 °C for ∼5 min, removed from the cooling bath, and allowed to warm to RT overnight. The reaction was cooled in ice and quenched with saturated NH_4Cl (150 mL) and stirred for 1 h. The mixture was diluted with DCM (200 mL) and the organic layer was separated. The aqueous layer was extracted with DCM. The organic layers were combined, washed with saturated NaCl, dried over $MgSO_4$, filtered, and concentrated to give **76Et** (7.8 g, 16 mmol), which was used directly in the next step. MS (ES^+) $C_{29}H_{43}NO_2SSi$ calculated 497; found 498$[M + H]^+$. ^1H NMR (600 MHz, $CDCl_3$): δ 7.66−7.58 (m, 4H), 7.45−7.39 (m, 2H), 7.39−7.32 (m, 4H), 4.35−3.85 (m, 1H), 3.21−2.49 (m, 1H), 2.40−0.78 (m, 31H).

(1R,5S)-6-(1-Aminopropyl)bicyclo[3.1.0]hexan-3-ol (Step f). To a solution of *N*-(1-((1*R*,5*S*)-3-((*tert*-butyldiphenylsilyl)oxy)bicyclo-[3.1.0]hexan-6-yl)propyl)-2-methylpropane-2-sulfinamide (3.2 g, 6.4 mmol) in MeOH (50 mL) cooled in an ice bath was added HCl in MeOH [prepared immediately before use by the addition of AcCl (18.3 mL, 257 mmol) into MeOH (25 mL) cooled in an ice bath and stirred for 5 min]. The reaction was removed from the ice bath and stirred at RT overnight. The reaction was concentrated and the residual solvent was azeotroped with ACN and toluene (3×) to give the title compound, HCl salt, off white solid, and used as is immediately. MS (ES^+) $C_9H_{17}NO$ calculated 155; found 156 $[M + H]^+$.

*4-Chloro-N-(1-((1R,3r,5S,6r)-3-hydroxybicyclo[3.1.0]hexan-6-yl)-propyl)benzamide (Step g, **77Et**).* The crude (1*R*,5*S*)-6-(1-aminopropyl)bicyclo[3.1.0]hexan-3-ol hydrochloride was diluted with DCM (50.0 mL) and to this were added DIEA (5.6 mL, 32 mmol), HOBT (1.6 g, 9.6 mmol), 4-chlorobenzoic acid (1.1 g, 7.1 mmol), and EDC (1.4 g, 7.1 mmol). The reaction was stirred at RT for 4 days. The reaction was diluted with DCM and washed with NaOH (0.25 M), citric acid (0.25 M), water, and brine. The aqueous washes were extracted with DCM once. The organic layers were combined, dried over Na_2SO_4, filtered, concentrated, and purified by flash chromatography [0−50% of EtOAc/IPA (8:2) in hexanes] to give **77Et**, as the first eluting diastereomer, (776 mg, 2.6 mmol, 4% yield) white solid. MS (ES^+) $C_{16}H_{20}ClNO_2$ calculated 293; found 294 $[M + H]^+$. ^1H NMR (500 MHz, CD_3OD): δ 7.79 (d, J = 8.6 Hz, 2H), 7.46 (d, J = 8.5 Hz, 2H), 4.32−4.27 (m, 1H), 3.29−3.25 (m, 1H), 2.12−1.97 (m, 2H), 1.80−1.58 (m, 4H), 1.36−1.24 (m, 2H), 1.24−1.20 (m, 1H), 0.96 (t, J = 7.4 Hz, 3H).

*4-Chloro-N-(1-((1R,3r,5S,6r)-3-(quinolin-4-yloxy)bicyclo[3.1.0]-hexan-6-yl)propyl)benzamide (Step h, **21**).* To a solution of 4-chloro-*N*-(1-((1*R*,3*r*,5*S*,6*r*)-3-hydroxybicyclo[3.1.0]hexan-6-yl)propyl)-benzamide **77Et** (49 mg, 0.17 mmol) in DMSO (0.34 mL) under nitrogen was added sodium hydride (60% in mineral oil, 15 mg, 0.38 mmol) and the mixture was stirred at RT for 30 min until gas evolution ceased. To the resulting yellow mixture was added 4-bromoquinoline (43 mg, 0.21 mmol), and the reaction was stirred at 80 °C overnight. To the mixture was added 2 drops of a saturated NH_4Cl. The mixture was filtered (0.2 μM Whatman syringe filter), rinsed with DMSO (3 × 0.3 mL), and the filtrate was purified by mass-triggered preparative HPLC (mobile phase: A = 0.1% TFA/H_2O, B = 0.1% TFA/MeCN; gradient: B = 20−50%; 12 min; column: C18) to give **21** as a glassy yellow solid (55 mg, 62%). MS (ES^+) $C_{25}H_{25}ClN_2O_2$ calculated 420; found, 421 $[M + H]^+$. ^1H NMR (600 MHz, $CDCl_3$): δ 8.95 (d, J = 6.42 Hz, 1H), 8.48 (d, J = 7.93 Hz, 1H), 8.41 (d, J = 8.69 Hz, 1H), 8.16−8.11 (m, 1H), 8.10−8.05 (m, 1H), 7.92 (ddd, J = 8.40, 7.08, 1.13 Hz, 1H), 7.80−7.75 (m, 2H), 7.48−7.43 (m, 2H), 7.40 (d, J = 6.80 Hz, 1H), 5.49 (t, J = 6.61 Hz, 1H), 3.45−3.37 (m, 1H), 2.60−2.48 (m, 2H), 2.31−2.21 (m, 2H), 1.82−1.73 (m, 1H), 1.73−1.65 (m, 1H), 1.63−1.58 (m, 1H), 1.55 (td, J = 5.85, 3.40 Hz, 1H), 1.27 (dt, J = 9.06, 3.21 Hz, 1H), 0.97 (t, J = 7.36 Hz, 3H).

*4-Chloro-N-(1-((1R,3s,5S,6r)-3-(quinolin-4-yloxy)bicyclo[3.1.0]-hexan-6-yl) propyl)benzamide (**22**). 4-Chloro-N-(1-((1R,3s,5S,6r)-3-hydroxybicyclo[3.1.0]hexan-6-yl)propyl)benzamide (Step g, **78Et**).* From the flash chromatography purification of step g as described above for compound **77Et**, the title compound **78Et** was isolated as the second eluting diastereomer (0.21 g, 0.71 mmol, 11% yield) as a white solid. MS (ES^+) $C_{16}H_{20}ClNO_2$ calculated 293; found 294 $[M + H]^+$. ^1H NMR (500 MHz, CD_3OD): δ 7.78 (d, J = 8.6 Hz, 2H), 7.46 (d, J = 8.6 Hz, 2H), 3.95−3.87 (m, 1H), 3.26−3.18 (m, 1H), 2.09 (ddd, J = 24.4, 12.6, 7.1 Hz, 2H), 1.75−1.55 (m, 4H), 1.35−1.23 (m, 2H), 0.94 (t, J = 7.4 Hz, 3H), 0.71 (dt, J = 9.3, 3.2 Hz, 1H).

*4-Chloro-N-(1-((1R,3s,5S,6r)-3-(quinolin-4-yloxy)bicyclo[3.1.0]-hexan-6-yl)propyl)benzamide (Step h, **22**).* To a solution of 4-chloro-*N*-(1-((1*R*,3*s*,5*S*,6*r*)-3-hydroxybicyclo[3.1.0]hexan-6-yl)propyl)-benzamide **78Et** (27 mg, 0.084 mmol) in DMSO (0.17 mL) under nitrogen was added sodium hydride (60% in mineral oil, 8.1 mg, 0.20 mmol) and the mixture was stirred at RT for 30 min. To the resulting yellow mixture was added 4-bromoquinoline (25 mg, 0.12 mmol), and the resulting mixture was stirred at 80 °C overnight. To the mixture was added two drops of a saturated NH_4Cl. The mixture was filtered (0.2 μM Whatman syringe filter), rinsed with DMSO (3 × 0.3 mL), and the filtrate was purified by mass-triggered preparative HPLC (mobile phase: A = 0.1% TFA/H_2O, B = 0.1% TFA/MeCN; gradient: B = 20−50%; 12 min; column: C18) to give **22** (32.9 mg, 73%). HRMS (ES^+) $C_{25}H_{25}ClN_2O_2$ calculated 421.1677 $[M + H]^+$; found 421.1671 $[M + H]^+$. ^1H NMR (600 MHz, CD_3OD): δ 8.94 (d, J = 6.80 Hz, 1H), 8.45 (d, J = 7.93 Hz, 1H), 8.34 (d, J = 8.69 Hz, 1H), 8.14−8.09 (m, 1H), 8.08−8.04 (m, 1H), 7.88 (ddd, J = 8.21, 6.89, 1.13 Hz, 1H), 7.84−7.79 (m, 2H), 7.50−7.47 (m, 2H), 7.46 (d, J = 6.80 Hz, 1H), 5.17 (quin, J = 6.89 Hz, 1H), 3.41 (qd, J = 8.62, 5.85 Hz, 1H), 2.61−2.65 (m, 1H), 2.56 (dd, J = 13.41, 6.99 Hz, 1H), 2.28−2.18 (m, 2H), 1.83−1.75 (m, 1H), 1.75−1.67 (m, 1H), 1.64 (td, J = 6.04, 3.40 Hz, 1H), 1.56 (td, J = 6.04, 3.40 Hz, 1H), 1.00 (t, J = 7.37 Hz, 3H), 0.90 (dt, J = 8.69, 3.40 Hz, 1H).

*4-Chloro-N-((R)-1-((1R,3S,5S,6r)-3-(5,6-difluoro-1H-benzo[d]-imidazole-1-yl)bicyclo[3.1.0]hexan-6-yl)propyl)benzamide (**62**). (S)-N-((E)-((1R,5S,6r)-3-((tert-Butyldiphenylsilyl)oxy)bicyclo[3.1.0]-hexan-6-yl)methylene)-2-methylpropane-2-sulfinamide (Step c, **75(S)**).* (1*R*,5*S*,6*r*)-3-((*tert*-Butyldiphenylsilyl)oxy)bicyclo[3.1.0]-hexane-6-carbaldehyde **74** (26.5 g, 72.7 mmol) was dissolved in DCM (73 mL) and (*S*)-2-methylpropane-2-sulfinamide (17.6 g, 145 mmol) along with copper(II) sulfate (11.6 g, 72.7 mmol) were added.

https://doi.org/10.1021/acs.jmedchem.1c00679
J. Med. Chem. XXXX, XXX, XXX−XXX

The solution was stirred at RT overnight. The solution was filtered through Celite, concentrated, and purified by flash chromatography (5−20% EtOAc in hexanes) to give **75(S)** (29 g, 63 mmol, 86% yield), and $C_{27}H_{37}NO_2SSi$ calculated 467; found 468 $[M + H]^+$. ^1H NMR (500 MHz, DMSO-d_6): δ 7.62−7.52 (m, 4H), 7.50−7.37 (m, 7H), 4.35 (t, J = 6.2 Hz, 1H), 2.10−1.98 (m, 2H), 1.97−1.90 (m, 2H), 1.88−1.55 (m, 3H), 1.10 (s, 9H), 1.02 (s, 9H).

*(S)-N-((1R)-1-((1R,5S)-3-((tert-Butyldiphenylsilyl)oxy)bicyclo-[3.1.0]hexan-6-yl)propyl)-2-methylpropane-2-sulfinamide (Step d, **76Et(R)**).* To a cooled −78 °C solution of (*S*,*E*)-*N*-(((1*R*,5*S*)-3-((*tert*-butyldiphenylsilyl)oxy)bicyclo[3.1.0]hexan-6-yl)methylene)-2-methylpropane-2-sulfinamide **75(S)** (29.6 g, 63.2 mmol) in THF (126 mL) was added ethylmagnesium bromide (31.6 mL, 95 mmol). The resulting mixture was stirred at −78 °C for ∼5 min, removed from the bath, and allowed to warm to RT overnight. The reaction was slowly poured into a mixture of ice and saturated NH_4Cl (150 mL) and stirred for until the ice melted. The mixture was diluted with EtOAc (400 mL) and the product extracted into the organic layer. The aqueous layer was extracted with EtOAc and the organic layers were combined, washed with saturated NaCl, dried over $MgSO_4$, filtered, and concentrated to give **76Et(R)** (32 g, 65 mmol, 103% yield) as a clear very viscous oil/semisolid/gum. MS (ES^+) $C_{29}H_{43}NO_2SSi$ calculated 497; found 498 $[M + H]^+$. ^1H NMR (600 MHz, DMSO): δ 7.65−7.52 (m, 4H), 7.51−7.34 (m, 6H), 4.91−4.73 (m, 1H), 4.33−4.22 (m, 1H), 2.40 (dt, J = 11.2, 5.6 Hz, 1H), 1.94−1.83 (m, 2H), 1.78−1.67 (m, 2H), 1.66−1.39 (m, 2H), 1.37−1.17 (m, 2H), 1.16−1.04 (m, 9H), 1.02−0.89 (m, 12H), 0.85−0.76 (m, 1H).

*4-Chloro-N-((R)-1-((1R,3R,5S,6r)-3-hydroxybicyclo[3.1.0]hexan-6-yl)propyl)benzamide (Step f and g, **77Et(R)**).* To a cooled 0 °C solution of (*S*)-*N*-((1*R*)-1-((1*R*,5*S*)-3-((*tert*-butyldiphenylsilyl)oxy)-bicyclo[3.1.0]hexan-6-yl)propyl)-2-methylpropane-2-sulfinamide **76Et(R)** (32 g, 65 mmol) in MeOH (200 mL) was added HCl (4 M in MeOH, 4 equiv) freshly prepared by the slow addition of acetyl chloride (18.4 mL, 260 mmol) to MeOH (70 mL) at 0 °C, stirred for 15 min, and then transferred using a syringe, and the resulting mixture was stirred at 0 °C for 10 min, ice bath removed, and kept at RT for 3 h. The reaction was cooled in an ice bath, slowly basified with DIEA (57 mL, 320 mmol), concentrated, and dried under house vacuum overnight. The reaction was resuspended in DMF (200 mL), DIEA (23 mL, 130 mmol) and 2,5-dioxopyrrolidin-1-yl 4-chlorobenzoate (17 g, 68 mmol) were added, and the reaction was stirred at RT overnight. The reaction was diluted with EtOAc (500 mL) and washed with 0.25 M NaOH (400 mL), 0.25 M HCl (400 mL), water (300 mL), and brine (200 mL). The aqueous layers were extracted with EtOAc (1 × 500, 1 × 200 mL), the organic layers were combined, dried over $MgSO_4$, filtered, and concentrated to give the crude product as a yellow solid, 35 g. The crude (a mixture of the TBDPS intermediate and the desired alcohol) was dissolved in THF (25 mL), cooled in an ice bath, and TBAF (1 M in THF, 70 mL, 70 mmol) was added dropwise. The reaction was stirred at 0 °C for 5 min then at RT overnight. The reaction was concentrated, diluted in THF (10 mL), and more TBAF (30 mL) was added. The reaction was heated at 40 °C overnight. The reaction was poured into ice water and extracted with EtOAc (3 × 200 mL). The organic layers were washed with brine, combined, dried over $MgSO_4$, filtered, and concentrated to give the crude desired product as a yellow semi solid. The material was diluted with toluene (100 mL), heated to reflux, and allowed to cool to RT overnight. The solid was filtered off, washed with toluene (3 × 10 mL), hexanes (3 × 20 mL), and dried over house vacuum to give a mixture of cis alcohol (**78Et(R)**) to trans alcohol (**77Et(R)**) ∼ 10:1 as a white solid (2.7 g). The filtrate was concentrated to give a yellow semisolid (30.5 g) that was dissolved in DCM/MeOH, supported on silica gel and purified by flash chromatography in two batches [either 10−70% or 10−60% of a solution of EtOAc/IPA (8:2) in hexanes] to give **77Et(R)** as the first eluting chiral diastereomer (9.6 g, 33 mmol, 50% yield) as a white solid. MS (ES^+) $C_{16}H_{20}ClNO_2$ calculated 293; found 294 $[M + H]^+$. ^1H NMR (500 MHz, DMSO): δ 8.34 (d, J = 8.7 Hz, 1H), 7.89 (d, J = 8.7 Hz, 2H), 7.52 (d, J = 8.6 Hz, 2H), 4.42 (d, J = 2.8 Hz, 1H), 4.17 (td, J = 6.4, 2.6 Hz, 1H), 3.28−3.19 (m, 1H), 1.97−1.84 (m, 2H), 1.67−1.52 (m, 4H), 1.27 (dt, J = 9.1, 3.2 Hz, 1H), 1.23−1.11 (m, 2H), 0.87 (t, J = 7.4 Hz, 3H).

2,5-Dioxopyrrolidin-1-yl 4-Chlorobenzoate. To a 500 mL round bottom flask were added 4-chlorobenzoic acid (50 g, 319 mmol), bis(2,5-dioxopyrrolidin-1-yl) carbonate (90 g, 351 mmol), DMAP (0.975 g, 7.98 mmol), and then DMF (319 mL). The resulting mixture was stirred at 40 °C overnight. The reaction mixture was poured into ice water (∼500 mL water, ∼200 mL of ice) and the resulting mixture was stirred until the ice melted. The white solid was filtered off, washed with water, 0.25 M HCl (100 mL), 0.25 M NaOH (100 mL), water, hexanes, ethyl ether, hexanes, dried over house vacuum for 1 h, and dried in a lyophilizer to give (73 g, 288 mmol, 90% yield) as a white solid. MS (ES^+) $C_{11}H_8ClNO_4$ calculated 253; found 139 $[M - NHS]^+$. ^1H NMR (600 MHz, DMSO): δ 8.11 (d, J = 8.1 Hz, 2H), 7.75 (d, J = 8.1 Hz, 2H), 2.90 (s, 4H).

*(1R,3R,5S,6r)-6-((R)-1-(4-Chlorobenzamido)propyl)bicyclo[3.1.0]-hexan-3-yl Methanesulfonate (Step i, **79Et(R)**).* To a solution of 4-chloro-*N*-((*R*)-1-((1*R*,3*r*,5*S*,6*r*)-3-hydroxybicyclo[3.1.0]hexan-6-yl)-propyl)benzamide **77Et(R)** (9.6 g, 33 mmol) in DCM (100 mL) cooled in an ice bath were added TEA (9.1 mL, 65 mmol) and Ms-Cl (3.8 mL, 49 mmol, dropwise) and the resulting mixture was stirred in the ice bath for 5 min then at RT for 2 h. The reaction was cooled in an ice bath diluted with DCM and quenched with 1 M HCl. The reaction was mixed, separated, and the aqueous layer extracted with EtOAc twice. The organic layers were washed with water and saturated NaCl, combined, dried over Na_2SO_4, filtered, and concentrated to give **79EtR** (13 g, 35 mmol, 108% yield) as a clear semisolid. MS (ES^+) $C_{17}H_{22}ClNO_4S$ calculated 371; found 372 $[M + H]^+$. ^1H NMR (300 MHz, DMSO-d_6): δ 8.39 (d, J = 8.6 Hz, 1H), 7.89 (d, J = 8.8 Hz, 2H), 7.53 (d, J = 8.8 Hz, 2H), 5.13 (t, J = 6.5 Hz, 1H), 3.34−3.23 (m, 1H), 3.12 (s, 3H), 2.32−2.14 (m, 2H), 2.04−1.85 (m, 2H), 1.74−1.51 (m, 2H), 1.38−1.26 (m, 2H), 1.01−0.93 (m, 1H), 0.88 (t, J = 7.4 Hz, 3H).

*4-Chloro-N-((R)-1-((1R,3S,5S,6r)-3-(5,6-difluoro-1H-benzo[d]-imidazole-1-yl)bicyclo[3.1.0]hexan-6-yl)propyl)benzamide (Step j, **62**, IACS-9779).* To a suspension of (1*R*,3*R*,5*S*,6*r*)-6-((*R*)-1-(4-chlorobenzamido)propyl)bicyclo[3.1.0]hexan-3-yl methanesulfonate **79Et(R)** (12.1 g, 32.5 mmol) in dioxane (100 mL) were added 5,6-difluoro-1*H*-benzo[*d*]imidazole (12.5 g, 81 mmol) and cesium carbonate (26.5 g, 81 mmol) and the resulting mixture was stirred at 65 °C for 1 day. The reaction was concentrated, diluted with DMF (100 mL), and heated at 65 °C for 4.5 h. The reaction was poured into ice water, stirred, and warmed to RT. The mixture was diluted with EtOAc and the desired product was extracted into the organic phase. The aqueous layer was extracted twice with EtOAc. The organic layers were washed with brine, combined, dried over $MgSO_4$, filtered, and concentrated to give a yellow semisolid (30 g). The crude was supported on silica gel and purified twice in two batches. The first flash chromatography purifications were with increasing concentrations of a solution of EtOAc/IPA (8:2) or EtOAc/IPA/MeOH/NH_4OH (80:20:2:2) in hexanes (5−50%) and the second was with increasing concentrations of a solution of DCM/MeOH/NH_4OH (90:10:1) in DCM (5−50%). The first batch was crystallized from EtOH to give 4.4 g of the desired product as a white solid. The impure chromatography fractions from both batches were combined with the filtrate from the first batch crystallization, purified by flash chromatography, and combined with the pure material from the second batch to produce 5.7 g of the desired product. The combined total of **62** was 9.4 g (22 mmol, 67% yield). The title compound **62** (IACS-9779) was also synthesized by WuXi Apptec, 288 Fute Zhong Road, Waigaoqiao Free Trade Zone, Shanghai 200131, China, EW10144-31-P1. HRMS (ES^+) $C_{23}H_{22}ClF_2N_3O$ calculated 430.1492 $[M + H]^+$; found 430.1488 $[M + H]^+$. ^1H NMR (600 MHz, DMSO): δ 8.43 (s, 1H), 8.32 (d, J = 8.6 Hz, 1H), 7.90 (d, J = 8.3 Hz, 2H), 7.84 (dd, J = 10.9, 7.3 Hz, 1H), 7.69 (dd, J = 11.2, 7.4 Hz, 1H), 7.55 (d, J = 8.4 Hz, 2H), 4.65−4.55 (m, 1H), 3.47−3.37 (m, 1H), 2.38−2.31 (m, 1H), 2.29−2.12 (m, 3H), 1.72−1.61 (m, J = 6.8 Hz, 2H), 1.52−1.35 (m, 2H), 1.14 (dt, J = 7.3, 3.4 Hz, 1H), 0.92 (t, J = 7.4 Hz, 3H).

Compounds 84 and 85. *(1R)-1-((1R,5S)-3-((tert-Butyldiphenylsilyl)oxy)bicyclo[3.1.0]hexan-6-yl)propan-1-amine (**83Et(R)**).* To a cooled (0 °C) solution of (*S*)-*N*-((1*R*)-1-((1*R*,5*S*)-3-((*tert*-butyldiphenylsilyl)oxy)bicyclo[3.1.0]hexan-6-yl)propyl)-2-methylpropane-2-sulfinamide **76Et(R)** (13.56 g, 27.2 mmol) in

https://doi.org/10.1021/acs.jmedchem.1c00679
J. Med. Chem. XXXX, XXX, XXX−XXX

methanol (272 mL) was added HCl (4 M in dioxane, 34.0 mL, 136 mmol) dropwise. The solution was stirred at RT for 2 h. The solution was cooled to 0 °C and Hunig's base (23.79 mL, 136 mmol) was added to quench. The solution was concentrated under pressure, taken up in EtOAc, washed with water, and the organics were collected, dried, and concentrated under pressure to the title compound **83Et(R)** (9.52 g, 24.18 mmol, 89% yield) and used directly as crude in the next step. MS (ES^+) $C_{25}H_{35}NOSi$ calculated 393; found 377 in m/z $[M\text{-}NH_2]^+$.

*(2R)-N-((1R)-1-((1R,5S,6r)-3-((tert-Butyldiphenylsilyl)oxy)bicyclo-[3.1.0]hexan-6-yl)propyl)-3,3,3-trifluoro-2-methoxy-2-phenylpropanamide (**84**).* To a solution of (1*R*)-1-((1*R*,5*S*,6*r*)-3-((*tert*-butyldiphenylsilyl)oxy)bicyclo[3.1.0]hexan-6-yl)propan-1-amine **83Et(R)** (5 mg, 0.013 mmol) in DCM (127 μL) were added (*S*)-3,3,3-trifluoro-2-methoxy-2-phenylpropanoyl chloride (3.53 mg, 0.014 mmol) and Hunig's base (3.33 μL, 0.019 mmol) and the resulting mixture was stirred at 25 °C for 15 min. The mixture was diluted with DCM (3 mL), H_2O (2 mL) was added, and the layers were separated. The aqueous phase was extracted with DCM (3 × 3 mL), the combined organic layers were washed with saturated NaCl, dried over Na_2SO_4, filtered, and concentrated under reduced pressure. The title compound **84** was used without further purification. MS (ES^+) $C_{35}H_{42}F_3NO_3Si$ calculated 609; found 610 in m/z $[M + H]^+$. ^1H NMR (600 MHz, DMSO-d_6): δ 7.65−7.63 (m, 5H), 7.51−7.49 (m, 10H), 4.26 (t, J = 6.3 Hz, 1H), 3.72 (s, 3H), 3.16−3.12 (m, 1H), 1.91−1.83 (m, 2H), 1.67−1.65 (m, 3H), 1.59−1.57 (m, 2H), 1.46 (dt, J = 9.1, 3.2 Hz, 1H), 1.25−1.22 (m, 1H), 1.19−1.18 (m, 1H), 0.99 (s, 9H), 0.73 (t, J = 7.4 Hz, 3H).

*(2S)-N-((1R)-1-((1R,5S,6r)-3-((tert-Butyldiphenylsilyl)oxy)bicyclo-[3.1.0]hexan-6-yl)propyl)-3,3,3-trifluoro-2-methoxy-2-phenylpropanamide (**85**).* To a solution of (1*R*)-1-((1*R*,5*S*,6*r*)-3-((*tert*-butyldiphenylsilyl)oxy)bicyclo[3.1.0]hexan-6-yl)propan-1-amine **83Et(R)** (5 mg, 0.013 mmol) in DCM (127 μL) were added (*R*)-3,3,3-trifluoro-2-methoxy-2-phenylpropanoyl chloride (3.53 mg, 0.014 mmol) and Hunig's base (3.33 μL, 0.019 mmol) and the resulting mixture was stirred at 25 °C for 15 min. The mixture was diluted with DCM (3 mL), H_2O (2 mL) was added, and the layers were separated. The aqueous phase was extracted with DCM (3 × 3 mL), the combined organic layers were washed with saturated NaCl, dried over Na_2SO_4, filtered, and concentrated under reduced pressure. The title compound **85** was used without further purification. MS (ES^+) $C_{35}H_{42}F_3NO_3Si$ calculated 609; found 610 in m/z $[M + H]^+$. ^1H NMR (600 MHz, DMSO-d_6): δ 8.22 (d, J = 8.8 Hz, 1H), 7.64−7.62 (m, 5H), 7.52−7.48 (m, 10H), 4.25 (t, J = 6.3 Hz, 1H), 3.72 (s, 3H), 3.63−3.57 (m, 1H), 3.15−3.08 (m, 2H), 1.91−1.81 (m, 2H), 1.66−1.62 (m, 3H), 1.57 (dd, J = 14.2, 6.7 Hz, 1H), 1.14−1.11 (m, 1H), 0.94 (s, 9H), 0.88 (t, J = 7.3 Hz, 3H).

*N-(4-Chlorophenyl)-2-((1R,3s,5S,6r)-3-(5,6-difluoro-1H-benzo[d]-imidazole-1-yl)bicyclo[3.1.0]hexan-6-yl)propanamide (**70**). (1R,5S)-3-((tert-Butyldiphenylsilyl)oxy)bicyclo[3.1.0]hexane-6-carbaldehyde, (**74ml**, Mother Liquor).* (1*R*,3*s*,5*S*,6*r*)-3-((*tert*-butyldiphenylsilyl)oxy)bicyclo[3.1.0]hexane-6-carbaldehyde, the cis isomer, can be crystalized from crude aldehyde. The crude aldehyde mixture of diastereomers (450 g) was heated to 50 °C with stirring (~30 min) in hexanes (700 mL) to give an orange solution (total volume 1300 mL). The solution was concentrated under reduced pressure until crystallization began. The mixture was then allowed to cool to RT over 8 h, and then cooled to 4 °C for 3 days. The mixture was filtered and the resulting solid was washed with hexanes to give a white crystalline solid, predominantly the cis isomer (218.6 g), which may be recrystallized from warm methanol. ^1H NMR (500 MHz, $CDCl_3$): δ 8.92 (d, J = 5.2 Hz, 1H), 7.66−7.58 (m, 4H), 7.46−7.41 (m, 2H), 7.40−7.35 (m, 4H), 3.95−3.83 (m, 1H), 2.10−1.99 (m, 2H), 1.97−1.87 (m, 4H), 1.34 (dt, J = 5.2, 2.5 Hz, 1H), 1.03 (s, 9H). The mother liquor (**ml**) was concentrated to give the title compound **74ml** as an orange oil (230.6 g), and used as is in the next step. The NMR mixture of diastereomers (not a complete integration): ^1H NMR (500 MHz, $CDCl_3$): δ 9.26 (d, J = 4.7 Hz, 0.46H), 9.04 (d, J = 6.3 Hz, 0.21H), 8.92 (d, J = 5.3 Hz, 0.17H), 7.69−7.57 (m, 4H), 7.48−7.33 (m, 6H), 4.44−4.37 (m, 0.23H), 4.36−4.31 (m, 0.55H), 3.94−3.86 (m, 0.19H), 2.49 (dt, J = 4.9, 2.5 Hz, 0.51H), 2.27−2.14 (m, 0.88H), 2.09−1.88 (m, 4.53H), 1.57 (td, J = 8.0, 6.1 Hz, 0.23H), 1.34 (dt, J = 5.2, 2.5 Hz, 0.2H), 1.11−0.97 (m, 9H).

*1-((1R,3r,5S,6r)-3-((tert-Butyldiphenylsilyl)oxy)bicyclo[3.1.0]-hexan-6-yl)ethanol (**86p**, Step p).* To a cooled 0 °C solution of (1*R*,3*r*,5*S*,6*r*)-3-((*tert*-butyldiphenylsilyl)oxy)bicyclo[3.1.0]hexane-6-carbaldehyde **74ml** (100 g, 274 mmol) in THF (300 mL) was added methylmagnesium bromide (110 mL, 329 mmol). The resulting mixture was stirred at 0 °C for 3 h, saturated NH_4Cl (20 mL) was added slowly at 0 °C, and the layers were separated. The aqueous phase was extracted with EtOAc (3 × 50 mL), the combined organic layers were washed with brine, dried over Na_2SO_4, filtered, and concentrated under reduced pressure. The title product **86p**, as a yellow oil, was used without further purification. MS (ES^+) $C_{24}H_{32}O_2Si$ calculated 380; found 363 $[M - OH]^+$.

*1-((1R,3r,5S,6r)-3-((tert-Butyldiphenylsilyl)oxy)bicyclo[3.1.0]-hexan-6-yl)ethanone (**86**, Step q).* To a cooled 0 °C solution of **86p** (104 g, 273 mmol) in DCM (wet) (364 mL) was added DMP (139 g, 328 mmol) portion wise. The resulting mixture was stirred at 25 °C for 3 h. The reaction mixture was cooled to 0 °C, saturated $NaHCO_3$ (20 mL) was added slowly, an equal volume of $Na_2S_2O_3$ was also added, the mixture was allowed to stir for 30 min, and the layers were separated. The aqueous phase was extracted with DCM (3 × 50 mL), the combined organic layers were washed with brine, dried over Na_2SO_4, filtered, and concentrated under reduced pressure. The residue was purified via a silica gel plug eluting with DCM to give the title compound **86** (83 g, 80%) as a pale orange liquid, and was used without further purification. MS (ES^+) $C_{24}H_{30}O_2Si$ calculated 378; found 379 $[M + H]^+$.

*tert-Butyl(((1R,3r,5S,6r)-6-((E)-1-methoxyprop-1-en-2-yl)bicyclo-[3.1.0]hexan-3-yl)oxy)diphenylsilane (**87**, Step r).* To a −13 °C solution of (methoxymethyl)triphenylphosphonium chloride (5.23 g, 15.3 mmol) in THF (21.8 mL) was added LHMDS (14.8 mL, 14.8 mmol) and the resulting mixture was stirred at 2−5 °C for 1 h. A solution of **86** (3.3 g, 8.72 mmol) in THF (7.3 mL) was added dropwise over 30 min and the reaction was stirred at 25 °C for 12 h. 1 M HCl (5 mL) was added, and the layers were separated. The aqueous phase was extracted with EtOAc (3 × 20 mL), the combined organic layers were washed with brine, dried over Na_2SO_4, filtered, and concentrated under reduced pressure. The residue was purified via silica gel chromatography (5−20% EtOAc in hexanes) to give the title compound **87** (1.96 g, 4.82 mmol, 55.3% yield) as a colorless liquid. MS (ES^+) $C_{26}H_{34}O_2Si$ calculated 406; found 407 $[M + H]^+$. ^1H NMR (600 MHz, DMSO): δ 7.60−7.55 (m, 4H), 7.48−7.41 (m, 6H), 5.93−5.72 (m, 1H), 4.37−3.88 (m, 1H), 3.52−3.36 (m, 3H), 1.98−1.88 (m, 2H), 1.82−1.65 (m, 2H), 1.46−1.10 (m, 5H), 1.05−0.65 (m, 10H).

*2-((1R,3r,5S,6r)-3-((tert-Butyldiphenylsilyl)oxy)bicyclo[3.1.0]-hexan-6-yl)propanal (**88s**, Step s).* To a solution of **87** (7.5 g, 18.4 mmol) in dioxane (52.7 mL) were added PPTS (5.10 g, 20.3 mmol) and water (8.8 mL) and the resulting mixture was stirred at 70 °C for 12 h. The volatiles were removed under reduced pressure. The reaction mixture was diluted with EtOAc (30 mL) and washed with H_2O (2 × 50 mL). The layers were separated, and the organic layer was washed with brine (2 × 50 mL), dried over Na_2SO_4, filtered, and concentrated under reduced pressure to give the title compound **88s** as a pale yellow oil, and was used without further purification.

*2-((1R,3r,5S,6r)-3-((tert-Butyldiphenylsilyl)oxy)bicyclo[3.1.0]-hexan-6-yl)propanoic Acid (**88**, Step t).* To a cooled 0 °C solution of **88s** (7.24 g, 18.44 mmol) in *t*BuOH (138 mL) and 2-methyl-2-butene (39.1 mL, 369 mmol) was added dropwise as freshly prepared solution of sodium chlorite (3.34 g, 36.9 mmol) and potassium dihydrogenphosphate (5.02 g, 36.9 mmol) in water (46.1 mL). The resulting mixture was stirred at 0 °C for 2 h, then allowed to warm to 25 °C with vigorous stirring for 12 h. Brine (150 mL) was added, and the layers were separated. The aqueous phase was extracted with DCM (3 × 75 mL), the combined organic layers were dried over Na_2SO_4, filtered, and concentrated under reduced pressure. The residue was purified via silica gel chromatography (0−5% MeOH in DCM) to give the title compound **88** (6.7 g, 16.4 mmol, 89% yield) as a colorless liquid. MS (ES^-) $C_{25}H_{32}O_3Si$ calculated 408; found 407 $[M - H]^-$. ^1H NMR (600 MHz, DMSO): δ 11.94 (s, 1H), 7.65−7.60 (m, 2H), 7.59−7.52 (m,

https://doi.org/10.1021/acs.jmedchem.1c00679
J. Med. Chem. XXXX, XXX, XXX−XXX

4H), 7.49−7.35 (m, 4H), 4.30−3.88 (m, 1H), 1.97−1.36 (m, 4H), 1.31−1.16 (m, 1H), 1.17−1.07 (m, 7H), 1.06−0.90 (m, 7H), 0.89−0.80 (m, 1H).

*2-((1R,5S,6r)-3-((tert-Butyldiphenylsilyl)oxy)bicyclo[3.1.0]hexan-6-yl)-N-(4-chlorophenyl)propanamide (**89/90u**, Step u).* To a solution of **88** (800 mg, 1.95 mmol) and pyridine (0.47 mL, 5.87 mmol) in EtOAc (20 mL) was added T3P (2,4,6-tripropyl-1,3,5,2,4,6-trioxatriphosphinane 2,4,6-trioxide, 50% in EtOAc, 2.9 mL, 2.9 mmol) and the resulting mixture was stirred at RT for 0.5 h. To this mixture, 4-chloroaniline (275 mg, 2.15 mmol) was added and the mixture was stirred at RT for 12 h. The mixture was quenched with 10% Na_2CO_3 (30 mL) and extracted with EtOAc (2 × 50 mL). Combined organics were washed with brine (2 × 30 mL), dried over $MgSO_4$, filtered, and concentrated to give the crude product. The residue was purified via silica gel chromatography (2−20% EtOAc in hexanes) to give the title compound **88**/**90u** (735 mg, 1.42 mmol, 72% yield) as a white solid. MS (ES^+) $C_{31}H_{36}ClNO_2Si$ calculated 518; found 519 $[M + H]^+$. The product was used without further purification.

*N-(4-Chlorophenyl)-2-((1R,3r,5S,6r)-3-hydroxybicyclo[3.1.0]hexan-6-yl)propanamide (**89**) and N-(4-Chlorophenyl)-2-((1R,3s,5S,6r)-3-hydroxybicyclo[3.1.0]hexan-6-yl)propanamide (**90**, Step v).* To a solution of **88**/**90u** (1.6 g, 3.1 mmol) in THF (2 mL) was added a solution of TBAF in THF (1 M, 10.0 mL, 10.0 mmol) and the resulting mixture was stirred at 50 °C for 24 h. The reaction mixture was diluted with EtOAc (50 mL), 5% HCl (15 mL) was added, and the layers were separated. The aqueous phase was extracted with EtOAc (3 × 10 mL), the combined organic layers were washed with water (20 mL), followed by brine (20 mL), dried over $MgSO_4$, filtered, and concentrated under reduced pressure. The residue was purified via silica gel chromatography (10−80% EtOAc in hexane) to give the title compound **89** as the first eluting diastereomer (220 mg, 0.786 mmol, 25.5% yield) as a clear oil. MS (ES^+) $C_{15}H_{18}ClNO_2$ calculated 279; found 280 $[M + H]^+$. ^1H NMR (500 MHz, $CDCl_3$): δ 7.66 (s, 1H), 7.55−7.49 (m, 2H), 7.32−7.27 (m, 2H), 4.44 (t, J = 6.4 Hz, 1H), 2.23−2.13 (m, 2H), 1.80−1.75 (m, 2H), 1.70−1.65 (m, 1H), 1.45−1.20 (m, 7H). The title compound **90** was obtained as the second diastereomer. MS (ES^+) $C_{15}H_{18}ClNO_2$ calculated 279; found 280 $[M + H]^+$. ^1H NMR (500 MHz, DMSO): δ 9.80 (s, 1H), 7.63 (d, J = 8.9 Hz, 2H), 7.34 (d, J = 8.8 Hz, 2H), 4.49 (d, J = 5.6 Hz, 1H), 3.82−3.73 (m, 1H), 2.01−1.84 (m, 2H), 1.69−1.61 (m, 1H), 1.58−1.44 (m, 2H), 1.25−1.20 (m, 1H), 1.10 (d, J = 6.8 Hz, 3H), 1.06−1.00 (m, 1H), 0.68−0.63 (m, 1H).

*(1R,3r,5S,6r)-6-(1-((4-Chlorophenyl)amino)-1-oxopropan-2-yl)-bicyclo[3.1.0]hexan-3-yl Methanesulfonate (**70i**, Step i).* To a solution of **89** (215 mg, 0.77 mmol) in DCM (5 mL) were added Ms-Cl (0.12 mL, 1.54 mmol) and TEA (0.32 mL, 2.3 mmol) and the resulting mixture was stirred at 0 °C for 2 h. The reaction mixture was diluted with DCM (20 mL), water (10 mL) was added, and the layers were separated. The aqueous phase was extracted with DCM (3 × 10 mL), the combined organic layers were washed with 5% HCl (2 × 10 mL), followed by brine (1 × 10 mL), dried over $MgSO_4$, filtered, and concentrated under reduced pressure. The residue was purified via silica gel chromatography (20−80% EtOAc in hexane) to give the title compound **70i** (242 mg, 0.676 mmol, 88% yield) as a clear oil. MS (ES^+) $C_{16}H_{20}ClNO_4S$ calculated 357; found 358 $[M + H]^+$. ^1H NMR (500 MHz, $CDCl_3$): δ 7.55−7.49 (m, 2H), 7.32−7.27 (m, 2H), 5.21 (t, J = 6.4 Hz, 1H), 2.99 (s, 3H), 2.35−2.15 (m, 4H), 1.81−1.71 (m, 1H), 1.48−1.40 (m, 1H), 1.39−1.35 (m, 1H), 1.31 (d, J = 7.0 Hz, 3H), 1.16−1.12 (m, 1H).

N-(4-Chlorophenyl)-2-((1R,3s,5S,6r)-3-(5,6-difluoro-1H-benzo[d]-imidazol-1-yl)bicyclo[3.1.0]hexan-6-yl)propanamide (70), IACS-70099 (Step j). To a solution of **70i** in 1,4-dioxane (5 mL) were added cesium carbonate and 5,6-difluoro-1*H*-benzo[*d*]imidazole and the resulting mixture was stirred at 65 °C for 12 h. The reaction mixture was diluted with EtOAc (15 mL), water (10 mL) was added, and the layers were separated. The aqueous phase was extracted with EtOAc (3 × 10 mL), the combined organic layers were washed with brine, dried over $MgSO_4$, filtered, and concentrated under reduced pressure. The residue was purified via silica gel chromatography (5−15% 2-propanol in DCM) to give *N*-(4-chlorophenyl)-2-((1*R*,3*s*,5*S*,6*r*)-3-(5,6-difluoro-1*H*-benzo[*d*]imidazol-1-yl)bicyclo[3.1.0]hexan-6-yl)propanamide (155 mg, 0.373 mmol, 58.0% yield) as a light yellow oil). This was then triturated with ether−hexane (10 mL) to give 70 mg of the white solid of the desired material. NMR data and LC−MS confirmed the identity of the compound. Rest of the mother liquor was then concentrated, and the residue was purified by reverse-phase preparative HPLC (mobile phase: A = 0.1% NH_4OH/H_2O, B = 0.1% NH_4OH/MeCN; gradient: B = 10−100%; 12 min) to give the title compound racemic **70** (25 mg) as a white solid. MS (ES^+) $C_{22}H_{20}ClF_2N_3O$ calculated 415; found 416 $[M + H]^+$. ^1H NMR (600 MHz, DMSO-d_6): δ 9.90 (s, 1H), 8.43 (s, 1H), 7.89 (dd, J = 11.0, 7.3 Hz, 1H), 7.73−7.60 (m, 3H), 7.42−7.31 (m, 2H), 4.73−4.59 (m, 1H), 2.33 (dd, J = 12.4, 7.6 Hz, 1H), 2.27−2.12 (m, 3H), 1.86−1.77 (m, 1H), 1.57−1.50 (m, 1H), 1.33 (q, J = 6.7, 5.0 Hz, 1H), 1.21−1.19 (m, 4H). The racemic solid was purified by SFC (Averica Discovery Services, 50 D'Angelo Drive Suite 6 Marlborough MA 01752, AV17301-E1) to give the title compound **70**. The title compound **70** was also synthesized by WuXi Apptec, 288 Fute Zhong Road, Waigaoqiao Free Trade Zone, Shanghai 200131, China, EW-10232-17-P1; with similar SFC conditions described for **71**, **IACS-70465**.

*N-(4-Chlorophenyl)-2-((1R,3s,5S,6r)-3-((6-fluoroquinolin-4-yl)-oxy)bicyclo[3.1.0]hexan-6-yl)propanamide (**71**), IACS-70465 (Step w).* To a cooled 0 °C suspension of NaH (14.30 mg, 0.357 mmol) in DMF (1787 μL) was added **90** (50 mg, 0.179 mmol). The resulting mixture was stirred at 0 °C for 30 min then at 25 °C for an additional 15 min. The solution was cooled to 0 °C and 4-bromo-6-fluoroquinoline (52.5 mg, 0.232 mmol) was added and the resulting mixture was stirred at 25 °C for 3 h. Saturated NH_4Cl (2 mL) was added, and the layers were separated. The aqueous phase was extracted with DCM (3 × 5 mL), the combined organic layers were washed with saturated NaCl, dried over Na_2SO_4, filtered, and concentrated under reduced pressure. The residue was purified via silica gel chromatography (0−20% MeOH in DCM with 2% TEA) to give the title compound racemic **71** (58 mg, 0.137 mmol, 76% yield) as an off-white solid. MS (ES^+) $C_{24}H_{22}ClFN_2O_2$ calculated 424; found 425 $[M + H]^+$. ^1H NMR (600 MHz, DMSO-d_6): δ ppm 0.83−0.93 (m, 1H), 1.15−1.24 (m, 3H), 1.30−1.51 (m, 2H), 1.68−1.79 (m, 1H), 1.99−2.13 (m, 2H), 2.39−2.46 (m, 1H), 2.51−2.58 (m, 1H), 5.13−5.25 (m, 1H), 7.31−7.40 (m, 2H), 7.44−7.52 (m, 1H), 7.63−7.72 (m, 2H), 7.85−7.93 (m, 1H), 7.94−8.01 (m, 1H), 8.08−8.20 (m, 1H), 8.89−9.05 (m, 1H), 9.86−9.99 (m, 1H). The racemic solid was purified by SFC (Averica Discovery Services, 50 D'Angelo Drive Suite 6 Marlborough MA 01752, AV18044-E2) to give the title compound **71**. The title compound **71** was also synthesized by WuXi Apptec, 288 Fute Zhong Road, Waigaoqiao Free Trade Zone, Shanghai 200131, China, EW118833-13, and separated by SFC (column: DAICEL CHIRALCEL OJ (250 mm × 30 mm, 10 μm); mobile phase: [0.1% NH_4OH EtOH]; B %: 35−35%, 3−20 min). Compound, **71**, **IACS-70465** (41.44 g, 96.55 mmol, 23.70% yield, 99% purity) was obtained as a white solid. ^1H NMR (400 MHz, DMSO-d_6): δ 9.87 (s, 1H), 8.66 (d, J = 5.1 Hz, 1H), 8.00 (dd, J = 5.5, 9.0 Hz, 1H), 7.80−7.56 (m, 4H), 7.36 (d, J = 8.4 Hz, 2H), 7.11 (d, J = 5.1 Hz, 1H), 4.89 (quin, J = 7.0 Hz, 1H), 2.41 (br dd, J = 7.2, 12.9 Hz, 1H), 1.97 (dq, J = 5.9, 12.8 Hz, 2H), 1.85−1.73 (m, 1H), 1.51 (br s, 1H), 1.31 (br s, 1H), 1.19 (d, J = 6.6 Hz, 3H), 0.93−0.84 (m, 1H).

IDO1 Enzyme Assay. Inhibition of recombinant human His-tagged IDO1 enzyme (R&D Systems, catalog # 6030-AO) was assessed by measuring the conversion of Trp to NFK using a RFMS system (Agilent Technologies). IDO1 enzyme (1 nM) was incubated in the absence or presence of various concentrations of compounds in assay buffer (40 mM Tris, pH 7.0, 15 μM Tween-20, containing 5 mM sodium ascorbate, 5 μM methylene blue, and 0.5 μM catalase) in a 384-well plate. After 10 min at RT, Trp (6 μM) was added to a final volume of 60 μL per well, and the reaction plate was incubated at RT for 1 h. Reactions were quenched by addition of 30 μL 0.24% formic acid containing 15 μM deuterated Trp-*d5* as an internal standard. Samples were analyzed via RFMS to quantify NFK (AUC of the total ion count, TIC) and Trp (AUC of TIC). A C18 cartridge was used with mobile phases of 0.1% formic acid and 80% ACN/0.1% formic acid under isocratic conditions. Dose−response curves were analyzed using IC_{50} regression curve fitting (GeneData Screener). Curves were plotted as

https://doi.org/10.1021/acs.jmedchem.1c00679
J. Med. Chem. XXXX, XXX, XXX−XXX

percent of control and normalized by high controls without inhibitor (100%), and low controls without substrate (0%).

Human IDO1 Cell Assay. The human HeLa cervix carcinoma cell line was obtained from the American Type Culture Collection (ATCC) and maintained in Dulbecco's modified Eagle medium (DMEM) media containing 10% fetal bovine serum (FBS). Cells (7000/well) were seeded onto a 384-well plate in 50 μL of media and incubated at 37 °C, 5% CO_2 overnight. Cell media were aspirated, fresh media containing 10 ng/mL human IFNγ (R&D Systems) were added, and cells were incubated in the absence or presence of various concentrations of compounds (final 0.5% DMSO) for 24 h at 37 °C, 5% CO_2. Aliquots of the cell conditioned media were removed from the cell plate, and mixed with an equal volume of 200 mM $ZnSO_4$ to precipitate media containing protein. Two volumes of acetonitrile were added by mixing, and the samples were then centrifuged at 2250*g* for 20 min at 4 °C. Aliquots of the supernatant were diluted 1:10 in 0.1% formic acid containing 3 μM of deuterated Trp-*d*5 as an internal standard. Samples were analyzed via RFMS to quantify NFK (AUC of TIC) and Trp (AUC of TIC). A C18 cartridge was used with mobile phases of 0.1% formic acid and 80% ACN/0.1% formic acid under isocratic conditions. Dose−response curves were analyzed using IC_{50} regression curve fitting (GeneData Screener). Curves were plotted as percent of control and normalized by high controls without inhibitor (100%), and low controls (0%) containing 1 μM of a potent cell-permeable IDO1 inhibitor (epacadostat). Cell viability was also assessed using the Cell Titer Glo Kit (Promega) following manufacturer's recommendations.

Mouse IDO1 Cell Assay. The murine PANC02 pancreatic ductal adenocarcinoma cell line was routinely maintained in DMEM media containing 10% FBS. Cells (3000/well) were seeded onto a 384-well plate in 50 μL of media and incubated at 37 °C, 5% CO_2 overnight. Cell media were aspirated, fresh media containing 30 ng/mL mouse IFNγ (Gibco Life Technologies, cat# PMC4031) were added, and cells were incubated in the absence or presence of various concentrations of compounds (final 0.5% DMSO) for 48 h at 37 °C, 5% CO_2. Aliquots of the cell conditioned media were removed from the cell plate, and mixed with an equal volume of 200 mM $ZnSO_4$ to precipitate media containing protein. Two volumes of acetonitrile were added by mixing, and samples were then centrifuged at 2250G for 20 min at 4 °C. Aliquots of the supernatant were diluted 1:10 in 0.1% formic acid containing 3 μM of deuterated Trp-*d*5 as an internal standard. Samples were analyzed via RFMS to quantify NFK (AUC of TIC) and Trp (AUC of TIC). A C18 cartridge was used with mobile phases of 0.1% formic acid and 80% ACN/0.1% formic acid under isocratic conditions. Dose−response curves were analyzed using IC_{50} regression curve fitting (GeneData Screener). Curves were plotted as percent of control and normalized by high controls without inhibitor (100%), and low controls (0%) containing 1 μM of a potent cell permeable IDO1 inhibitor epacadostat. Cell viability was also assessed using the Cell Titer Glo Kit (Promega) following manufacturer's recommendations.

TDO Cell Assay. The human A-172 glioblastoma cell line was obtained from the American Type Culture Collection (ATCC) and maintained in DMEM media containing 10% FBS. Cells (7000/well) were seeded onto a 384-well plate in 50 μL of media and incubated at 37 °C, 5% CO_2 overnight. Cell media were aspirated, fresh media containing 1 mM Trp were added, and cells were incubated in the absence or presence of various concentrations of compounds (final 0.5% DMSO) for 16 h at 37 °C, 5% CO_2. Aliquots of the cell-conditioned media were removed from the cell plate, and mixed with an equal volume of 200 mM $ZnSO_4$ to precipitate media containing protein. Two volumes of acetonitrile were added by mixing, and samples were then centrifuged at 2250*g* for 20 min at 4 °C. Aliquots of the supernatant were diluted 1:10 in 0.1% formic acid containing 3 μM of deuterated Trp-*d*5 as an internal standard. Samples were analyzed via RFMS to quantify NFK (AUC of TIC) and Trp (AUC of TIC). A C18 cartridge was used with mobile phases of 0.1% formic acid and 80% ACN/0.1% formic acid under isocratic conditions. Dose−response curves were analyzed using IC_{50} regression curve fitting (GeneData Screener). Curves were plotted as percent of control and normalized by high controls without inhibitor (100%), and low controls (0%) containing 1 μM of a potent cell permeable IDO1 inhibitor (epacadostat). Cell viability was also assessed using the Cell Titer Glo Kit (Promega) following manufacturer's recommendations.

Recombinant Human His-Tagged IDO1 Production. Human IDO1 was expressed in *Escherichia coli* BL21 (DE3) in Luria Bertani media supplemented with 100 μg mL^{-1} carbenicillin. For protein batches, where high levels of heme incorporation were desired, 1.5 mM δ-aminolevulinic acid was also added to the growth media but this supplement was not included for low-heme IDO1 protein preparations. Once the *E. coli* culture reached an optical density of 0.7, the temperature was reduced to 18 °C and recombinant protein expression was induced with 0.5 mM IPTG. After overnight incubation, the *E. coli* cells were harvested by centrifugation and the cell pellet was lyzed in 50 mM HEPES, 500 mM NaCl, and 2 mM TCEP at pH 8.0. The cell lysate was clarified by centrifugation at 20,000 rpm at 4 °C for 1 h and purified by Ni affinity chromatography using 50 mM HEPES, 500 mM NaCl, 500 mM imidazole, and 2 mM TCEP at pH 8.0 as the elution buffer. The IDO1 protein was further purified by size exclusion chromatography using an S200 column pre-equilibrated in 25 MES and 150 mM KCl at pH 6.5. The ratio of the 406 and 280 nm absorbance peaks for the protein was used to determine the heme content, based on the 406:280 ratio of 2.75:1 for 100% heme-bound holoenzyme, as previously described.[70] Low levels of heme incorporation contained <5% heme content and high levels contained 75%.

Cell Lysate Preparation and IDO1 Activity. The HeLa cell line (ATCC, CCL-2) was cultured in DMEM media containing 10% FBS. HEK293-TetR (GenTarget, SC005-Puro, and GenTarget) were transduced with hIDO1-inducible lentiviral particles (GenTarget, LVP302) following the manufacturer's protocol, and a bulk stable-inducible HEK293-TetR-IDO1 cell line was generated after selection in DMEM media containing 10% FBS, puromycin (1 μg/mL), and blasticidin (10 μg/mL). Expression of endogeneous human IDO1 in HeLa cells was induced after 10 ng/ml of IFN-γ treatment, and recombinant human IDO1 in HEK293-TetR-IDO1 cells was induced after 1 μg/ml of doxycycline. Expression of IDO1 protein was confirmed via western-blot analysis using a mouse monoclonal antibody against human IDO1 protein (anti-IDO1 [4D2] and Abcam ab55305). Antibody specificity against human IDO1 was confirmed via western-blot analysis of purified human IDO1 protein. HSP90 expression was assessed via western-blot using anti-HSP90 (Millipore), Figure S1.

HeLa or HEK293-TetR-IDO1 cells were induced with IFN-γ or doxycycline in the absence or presence of IDO1 inhibitors at 37 °C, 0.5% CO_2 for a period of 24 h. Cells were extensively washed with phosphate buffered saline, and cell lysates were prepared by harvesting the cells using the CelLytic-M solution (Sigma-Aldrich, C2978) containing 1× Halt Protease inhibitor cocktail (ThermoFisher, 78429). Cell lysates were diluted in assay buffer (40 mM Tris, pH 7.0, and 15 μM Tween-20) to yield 20−30% enzyme turnover for further studies. Reconstitution of IDO1 apoenzyme to active holoenzyme was achieved by adding increasing concentration of hemin to cell lysates. First, 3 mM hemin (Sigma-Aldrich, 51280) stock solution was prepared in 300 mM triethylamine, and then further diluted in assay buffer as required. Hemin and/or inhibitor were titrated in assay buffer, then combined with either the cell lysate or purified recombinant human His-tagged IDO1 protein for the enzymatic assay.

IDO1 enzymatic activity was assessed by measuring the conversion of Trp to NFK using RFMS. Cell lysates or purified IDO1 enzyme (1 nM) were incubated in the absence or presence of various concentrations of compounds in assay buffer (40 mM Tris, pH 7.0, 15 μM Tween-20, containing 5 mM sodium ascorbate, 5 μM methylene blue, and 0.5 μM catalase) in a 384-well plate. After 10 min at RT, Trp (6 μM) was added to a final volume of 60 μL per well, and the reaction plate was incubated at RT for 1 h. Reactions were quenched by addition of 30 μL 0.24% formic acid containing 15 μM deuterated-Trp-*d*5 as an internal standard, and then sampled on a RFMS instrument using a C18 cartridge, using 80% acetonitrile with 0.1% formic acid for elution. Parent and product ions were monitored for NFK, deuterated Trp, KYN, and Trp. AUC of the TIC of each the compound was integrated using Agilent Mass Hunter software. AUC values for NFK were normalized to deuterated-Trp AUC values and graphed using GraphPad Prism.

https://doi.org/10.1021/acs.jmedchem.1c00679
J. Med. Chem. XXXX, XXX, XXX−XXX

Whole Blood Assay. Fresh peripheral blood was collected with 2 h of collection from Bloodworks Northwest (all donors with signed informed consents). The blood was aliquoted (200 μL per well into a 96-well round bottom plate). Serial dilutions of the test compounds were performed initially in DMSO and then in culture medium so that the final DMSO concentration per well becomes 0.1%. Solvent control cultures also contained 0.1% DMSO. The test compounds ($n = 4$) were added at 12 concentrations to the blood, 15 min prior to the addition of LPS (25 μg/mL) and IFNγ (100 ng/mL). Four replicates were initiated for each concentration of each test compound. The blood was incubated for 24 h at 37 °C and 5% CO_2. Samples were spun, the plasma removed, and stored at −80 °C until sample analysis via LCMS (described at the PK/PD methodology).

DSF Assay. Equal volumes of apo-IDO, DMSO or inhibitor, and Sypro Orange (ThermoFisher) were mixed in assay buffer (40 mM Tris, pH 7.0 with 15 μM Tween-20) to achieve final concentrations of 4 μM of enzyme, 0.5% DMSO, and 50 μM of compound, and plates containing the mixture were covered with an optical adhesive film cover (Applied Biosystems), centrifuged at 1000 rpm for 1 min, and incubated for 10 min at 25 °C. Plates were subsequently loaded into a QuantStudio6 real-time PCR instrument (Applied Biosystems), initially incubated at 25 °C for 2 min and thereafter subjected to a temperature gradient from 25 to 99 °C (~2 °C/10 min) in a step and hold mode with 0.4 °C temperature increments. Fluorescence emission at 586 was monitored and recorded. Protein Thermal Shift software (Applied Biosystems) was used to calculate the first derivative melting temperature.

Animals and Xenograft Models for PK and In Vivo Studies. All PK and in vivo experiments were conducted in accordance with the animal welfare procedures of the Institutional Animal Care and Use Committee (IACUC).

General Formulation Protocol. Preparation of IV dosing solution in 20% DMSO + 60% PEG400 + 20% water at 0.06 mg/mL: To a 10 mM stock solution of compound (0.06 mL) in a clear vial was added DMSO (0.54 mL). The solution was vortexed for 2 min and PEG400 (1.8 mL) was added. The mixture was vortexed for 2 min, water (0.6 mL) was added, and the solution was vortexed for additional 2 min. Preparation of po dosing solution in 0.5% methyl cellulose (MC) in water at 1 mg/mL: to compound (1) (4.1 mg) in a clean tube was added 0.5% MC in water (4.1 mL). The mixture was vortexed for 2 min, sonicated for 20 min, stirred for 30 min, and homogenized with ULTRA-TURPAX at 4500 rpm for 5 min.

In Vivo Animal Studies. Protocol number 00000884-RN02 was approved by The University of Texas MD Anderson Cancer Center Institutional Animal Care and Use Committee (IACUC), and adhered to the National Institutes of Health (NIH) guidelines. All mice were housed in state-of-the-art Association for the Assessment and Accreditation for Laboratory Animal Care (AAALAC)-accredited animal research facilities. All animals were maintained under the supervision and care of the veterinarians associated with the Animal Facilities, who oversee a comprehensive and well-executed health surveillance program. Female C57BL/6 mice (strain code: 000664, purchased from Jackson Lab) aged 6−12 weeks and weighing approximately 20−25 g were used for PANC02 studies. Female Balb/c mice (strain code: 028, purchased from Charles River) aged 6−12 weeks and weighing approximately 20−25 g were used for CT26 studies. Female NSG mice (strain code: 005557, purchased from Jackson Lab) aged 6−12 weeks and weighing approximately 20−25 g were used for SKOV3 studies. Animal health was monitored daily by observation and sentinel animal blood sample analysis. Animal experiments were conducted in accordance with the Guideline of IACUC, MDACC. Mice were fed animal diet 5053 from LabDiet ad libitum. PANC02, CT26, or SKOV3 cells were scaled up and then harvested on the day of cell inoculation. For PANC02, each mouse received 5.0×10^5 cells in 0.2 mL PBS. For CT26, each mouse received 2.0×10^5 cells in 0.2 mL PBS. For SKOV3, cells were diluted 1:1 with Matrigel just before implantation, and each mouse received 2.5×10^6 cells in 0.2 mL. Cells were implanted subcutaneously in the right flank. PANC02, CT26, or SKOV3 tumors were monitored by caliper before randomly sorting and dividing into several groups ($n = 5$−10 mice per group) based on the study design and requirements. Treatment was started from day 14 to 36 days postimplantation, depending on mouse models and requirements of the tumor size. Vehicle controls or IDO inhibitors were given orally using a sterile 1 mL syringe and a 18-gauge gavage needle using formulations as described above.

Pharmacokinetics. The PK study was performed at ChemPartner (No. 5 Building, 998 Halei Road, Zhangjiang Hi-Tech Park, Pudong New Area, Shanghai, China. www.chempartner.com).

Mice. Female mice (CD1 strain, purchased from Shanghai JH Laboratory Animal Co. LTD) weighing 20−30 g were used for this study. Food and water were made available to all animals ad libitum. The test article was dosed via tail vein and oral gavage, respectively. Blood samples were collected from animals by retro-orbital bleeding into test tubes containing K2EDTA predose and at 0.083, 0.25, 0.5, 1, 2, 4, 8, and 24 h postdose (three animals per time point with three time points collected per animal) into tubes containing the anticoagulant K_2EDTA. Plasma was separated from the blood by centrifugation at 4 °C and stored at −70 °C until analysis. The test article concentrations in plasma were quantified using a liquid chromatography with the tandem mass spectrometry (LC−MS/MS) method.

Rat. Male rats (SD strain, purchased from Shanghai JH Laboratory Animal Co. LTD) weighing 200−300 g were used for this study. Animals were fasted overnight and fed 4 h postdose. Water was made available ad libitum for all animals. The test article was dosed via dorsal foot vein and via oral gavage, respectively. Blood samples were collected via tail vein from all animals at predose and at 0.083, 0.25, 0.5, 1, 2, 4, 8, and 24 h postdose into tubes containing the anticoagulant K_2EDTA. Plasma was separated from the blood by centrifugation at 4 °C and stored at −70 °C until analysis. The test article concentrations in plasma were quantified using the LC−MS/MS method.

Dog. Male Beagle dogs (purchased from Beijing Marshall Biotechnology Co., Ltd) weighing 7−10 kg were used for this study. Animals were fasted overnight and fed 4 h postdose. The test article was administered to dogs via the cephalic vein or via oral gavage. Blood samples were collected via the saphenous vein or cephalic vein from all animals at predose and 0.083, 0.25, 0.5, 1, 2, 4, 8, and 24 h postdose into tubes containing the anticoagulant K_2EDTA. Plasma was separated from the blood by centrifugation at 4 °C and stored at −70 °C until analysis. The test article concentrations in plasma were quantified using the LC−MS/MS method.

Monkey. Male Cynomolgus monkeys (purchased from Hainan Jingang Biotech. Co., Ltd) weighing 3−5 kg were used for this study. Animals were fasted overnight and fed 4 h postdose. The test article was administered to monkeys via the cephalic vein or via nasal gavage. Blood samples were collected via the saphenous vein or cephalic vein from all animals at predose and 0.083, 0.25, 0.5, 1, 2, 4, 8, and 24 h postdose into tubes containing the anticoagulant K_2EDTA. Plasma was separated from the blood by centrifugation at 4 °C and stored at −70 °C until analysis. The test article concentration in plasma was quantified using the LC−MS/MS method.

Sample Collection for PK/PD Analysis. Tumor and plasma were harvested at the desired time point after the last dose. Blood was obtained via the retro-orbital sinus into a Vacutainer K2 EDTA tube to a volume of 250 μL. The Vacutainer vials were centrifuged for 10 min as 2000*g* without braking. The supernatant (plasma) was carefully aspirated into a microcentrifuge tube and placed onto dry ice prior to storage at −80 °C. Tumor samples from the right flank were obtained and cut into several (at least 5 or 6) approximately 100 mg pieces of comparable size with a scalpel. These pieces are immediately placed into a labeled cryovial and snap frozen in liquid nitrogen prior to storage at −80 °C. KYN and Trp were purchased from Sigma-Aldrich. L-Kynurenine-*d6* (KYN-*d6*) and L-tryptophan-*d5* (Trp-*d5*) were purchased from Cambridge Isotope Laboratories. DMSO were purchased from Sigma-Aldrich. Acetonitrile, methanol, isopropanol, water, and formic acid (all LC−MS grade) were obtained from Fisher Chemicals (Fair Lawn, NJ, USA). Blank human plasma samples from healthy donors were purchased from Bioreclamation IVT (Baltimore, MD, USA).

Stock Solutions, Standards, and Quality Controls. The analyte reference standard (KYN and TRP) stock solutions were prepared at

https://doi.org/10.1021/acs.jmedchem.1c00679
J. Med. Chem. XXXX, XXX, XXX−XXX

1.00 mg/mL in water. Working solutions were obtained by diluting stock solutions to 100 μL/mL. KYN-*d6* and Trp-*d5* internal standard solutions were also prepared in water. Calibration standards and QC samples of KYN and TRP were prepared in acetonitrile in the range from 1 to 200 ng/mL. Calibration standards and QC samples of IACS compounds were prepared in the range from 1 to 1000 ng/mL by spiking work solutions to blank mouse plasma.

Liquid Chromtography. Quantitative analysis was performed using a Shimadzu Nexera X2 LC system consisting of a binary pump, a column oven, a DAD detector, and an autosampler with a 10 μL injection loop autosampler. The autosampler temperature was set at 4 °C. Chromatographic separation was carried out on a Supelco Ascentis Express RP-Amide column (30 × 2.1 mm, 2.7 μm) for KYN and TRP and on a Supelco Ascentis Express C18 column (20 × 2.1 mm, 2.7 μm) for IACS compounds. The column temperature was maintained at 40 °C. For the analysis of KYN and TRP, mobile phase A was 0.1 acetic acid in water and mobile phase B was 0.1% acetic acid in acetonitrile. The mobile phase was delivered in a gradient mode: 80% B (0−1 min), 80−10% B (1−3 min), 10% B (3−5 min), 10−80% B (5−5.3 min), and 80% B (5.3−10 min). The column temperature was 40 °C, and the flow rate was 0.5 mL/min. For the analysis of IACS compounds, mobile phase A was 0.1 acetic acid in water and mobile phase B was 0.1% acetic acid in acetonitrile. The mobile phase was delivered in a gradient: 5% B (0−0.3 min), 5−95% (0.3−1.3 min), 95% (1.31−1.60 min), and 5% (1.61−2.00 min). Wash solvent 1 was 50% methanol in water and wash solvent 2 was 0.2% formic acid in a mixture of acetonitrile, methanol, isopropanol, and water (50:50:50:50, v/v/v/v).

Mass Spectrometry. Eluents from column were monitored using an AB Sciex 5500 triple quadrupole mass spectrometer with an ESI source. A mass spectrometer was operated in the positive ion mode and its operation parameters were optimized to maximize its sensitivity by a direct infusion of analytes at 10 ng/mL in an acetonitrile/water (1:2, v/v): ion spray voltage of 5500 V, CAD 8, curtain gas 35, Gas1 35, Gas2 50, and source temperature 400 °C. The MS data were first acquired by a Sciex software Analyst version 1.6.2 and then processed using Sciex software MultiQuant version 3.0.2. KYN, TRP, and IACS compounds were detected in MRM mode and their corresponding mass spectrometry parameters reported. PK parameters were estimated using Phoenix WinNonlin 8.3 software.

Sample Preparation. For the analysis of KYN and TRP in plasma samples—an aliquot of 25 μL of standards, QC samples, and clinical human plasma samples was manually transferred to a well of a 1 mL 96-DW plate. Two hundred microliters of acetonitrile that was chilled at 4 °C were added to wells using a liquid−liquid handling robot, Biomek FX^P Automation Workstation. After vortexing for 10 min, samples were centrifuged at 4000 rpm and 4 °C for 10 min. One hundred microliters of supernatant were diluted with 200 μL of acetonitrile/water (1:1) containing 250 ng/mL KYN-d6 and 250 ng/mL TRP-5. After vortexing for 5 min, samples were centrifuged at 4000 rpm and 4 °C for 5 min. An aliquot of 2 μL was injected into the LC system for separation and analysis. For the analysis of IACS compounds in plasma samples: an aliquot of 25 μL of standards, QC samples, and clinical human plasma samples were manually transferred to a well of a 1 mL 96-DW plate. Two hundred microliters of acetonitrile containing IACS-5318 at 5 ng/mL as the internal standard that was chilled at 4 °C were added to wells using a liquid−liquid handling robot, Biomek FX^P Automation Workstation. After vortexing for 10 min, samples were centrifuged at 4000 rpm and 4 °C for 10 min. One hundred microliters of supernatant were diluted with 200 μL of water. After vortexing for 5 min, samples were centrifuged at 4000 rpm and 4 °C for 5 min. An aliquot of 2 μL was injected into the LC system for separation and analysis. For analysis of tumor tissue samples, tumor tissue samples were homogenized using OminiBEAD Ruptor24 coupled with Omini BR CRYO to make homogenates at 100 mg(tissue)/mL in MeOH/H_2O (8:2). The volume (μL) of this solvent added to the vial containing tumor tissue was [(1000 × weight (mg)/100) − weight (mg)] assuming that the density of the tissue was 1.0. After homogenization, homogenates were centrifuged at 15,000 rpm and 4 °C for 15 min. An aliquot of 100 μL of the supernatant was diluted with 100 μL of ACN/H_2O (1:1) containing 250 ng/mL Trp-*d5* and 250 ng/mL KYN-*d6* as IS, vortexed for 15 s, and centrifuged at 15,000 rpm and 4 °C for 5 min before injection for the analysis of KYN and TRP. For the analysis of IACS compounds, 50 μL of the supernatant was diluted with 150 μL of acetonitrile containing an internal standard at 5 ng/mL. The injection volume was 2 μL.

■ ASSOCIATED CONTENT

Supporting Information

The Supporting Information is available free of charge at https://pubs.acs.org/doi/10.1021/acs.jmedchem.1c00679.

Preparation of compounds 18−20, 23−61, and 63−69; full western blot; procedures for microsomal stability; CYP inhibition; plasma protein binding; hERG assays; X-ray crystallography; sequence alignment of the binding site of IDO1; representative HeLa cellular assay and viability curves for **22** and **62**; and LCMS traces for **17**, **17R**, **21**, **22**, **24**, **31**, **34**, **38**, **56**, **57**, **58**, **59**, and **62** (IACS-9779), **63**, **64**, **65**, and **70** (IACS-70099), **71** (IACS-70465), and **72** (PDF)

Molecular formula strings (CSV)

■ AUTHOR INFORMATION

Corresponding Author

Matthew M. Hamilton − *IACS (Institute for Applied Cancer Science), University of Texas, MD Anderson Cancer Center, Houston, Texas 77054, United States;* orcid.org/0000-0002-1703-1685; Email: mmhamilton@mdanderson.org

Authors

Faika Mseeh − *IACS (Institute for Applied Cancer Science), University of Texas, MD Anderson Cancer Center, Houston, Texas 77054, United States*

Timothy J. McAfoos − *IACS (Institute for Applied Cancer Science), University of Texas, MD Anderson Cancer Center, Houston, Texas 77054, United States*

Paul G. Leonard − *IACS (Institute for Applied Cancer Science), University of Texas, MD Anderson Cancer Center, Houston, Texas 77054, United States*

Naphtali J. Reyna − *IACS (Institute for Applied Cancer Science), University of Texas, MD Anderson Cancer Center, Houston, Texas 77054, United States*

Angela L. Harris − *TRACTION (Translational Research to Advance Therapeutics and Innovation in Oncology), University of Texas, MD Anderson Cancer Center, Houston, Texas 77054, United States*

Alan Xu − *IACS (Institute for Applied Cancer Science), University of Texas, MD Anderson Cancer Center, Houston, Texas 77054, United States*

Michelle Han − *IACS (Institute for Applied Cancer Science), University of Texas, MD Anderson Cancer Center, Houston, Texas 77054, United States*

Michael J. Soth − *IACS (Institute for Applied Cancer Science), University of Texas, MD Anderson Cancer Center, Houston, Texas 77054, United States;* orcid.org/0000-0002-2649-5537

Barbara Czako − *IACS (Institute for Applied Cancer Science), University of Texas, MD Anderson Cancer Center, Houston, Texas 77054, United States;* orcid.org/0000-0002-3357-7514

Jay P. Theroff − *IACS (Institute for Applied Cancer Science), University of Texas, MD Anderson Cancer Center, Houston, Texas 77054, United States*

https://doi.org/10.1021/acs.jmedchem.1c00679
J. Med. Chem. XXXX, XXX, XXX−XXX

Pijus K. Mandal − *IACS (Institute for Applied Cancer Science), University of Texas, MD Anderson Cancer Center, Houston, Texas 77054, United States*
Jason P. Burke − *IACS (Institute for Applied Cancer Science), University of Texas, MD Anderson Cancer Center, Houston, Texas 77054, United States*
Brett Virgin-Downey − *IACS (Institute for Applied Cancer Science), University of Texas, MD Anderson Cancer Center, Houston, Texas 77054, United States*
Alessia Petrocchi − *IACS (Institute for Applied Cancer Science), University of Texas, MD Anderson Cancer Center, Houston, Texas 77054, United States*
Dana Pfaffinger − *IACS (Institute for Applied Cancer Science), University of Texas, MD Anderson Cancer Center, Houston, Texas 77054, United States*
Norma E. Rogers − *IACS (Institute for Applied Cancer Science), University of Texas, MD Anderson Cancer Center, Houston, Texas 77054, United States*
Connor A. Parker − *IACS (Institute for Applied Cancer Science), University of Texas, MD Anderson Cancer Center, Houston, Texas 77054, United States*
Simon S. Yu − *IACS (Institute for Applied Cancer Science), University of Texas, MD Anderson Cancer Center, Houston, Texas 77054, United States*
Yongying Jiang − *IACS (Institute for Applied Cancer Science), University of Texas, MD Anderson Cancer Center, Houston, Texas 77054, United States*
Stephan Krapp − *Proteros Biostructures GmbH, D-82152 Martinsried, Germany*
Alfred Lammens − *Proteros Biostructures GmbH, D-82152 Martinsried, Germany*
Graham Trevitt − *XenoGesis Ltd, Nottingham, Nottinghamshire NG1 1GF, U.K.*
Martin R. Tremblay − *Tesaro Inc., Waltham, Massachusetts 02451, United States*
Keith Mikule − *Tesaro Inc., Waltham, Massachusetts 02451, United States*
Keith Wilcoxen − *Tesaro Inc., Waltham, Massachusetts 02451, United States*
Jason B. Cross − *IACS (Institute for Applied Cancer Science), University of Texas, MD Anderson Cancer Center, Houston, Texas 77054, United States*
Philip Jones − *IACS (Institute for Applied Cancer Science), University of Texas, MD Anderson Cancer Center, Houston, Texas 77054, United States*
Joseph R. Marszalek − *TRACTION (Translational Research to Advance Therapeutics and Innovation in Oncology), University of Texas, MD Anderson Cancer Center, Houston, Texas 77054, United States*
Richard T. Lewis − *IACS (Institute for Applied Cancer Science), University of Texas, MD Anderson Cancer Center, Houston, Texas 77054, United States*

Complete contact information is available at: https://pubs.acs.org/10.1021/acs.jmedchem.1c00679

Author Contributions

This manuscript was written through contributions of all authors. All authors have given approval to the final version of the manuscript.

Notes

The authors declare no competing financial interest.

Authors will release the atomic coordinates and experimental data upon article publication.

■ ACKNOWLEDGMENTS

This work was supported by Tesaro Inc. and the University of Texas MD Anderson Cancer Center. The authors would like to thank Fernando Alvarez for proof reading and editing assistance and Dr. Maria Emilia Di Francesco for helpful discussion and suggestions.

■ ABBREVIATIONS

ACN, acetonitrile; AhR, aryl hydrocarbon receptor; ATCC, American Type Culture Collection, supplier of authenticated cells lines and microorganisms; AUC, area under the curve; BID, twice a day (bis in die); BMS, Bristol Myers Squibb; ClCOMTPA, α-methoxy-α-trifluoromethylphenylacetyl chloride; Cl_{int}, intrinsic clearance; clog *P*, calculated log of partition coefficient; C_{max}, maximum measured concentration; C_{min}, minimal effective concentration; CT26, mouse colorectal carcinoma cell line; C_u, unbound concentration; CYP, cytochrome P450; CYP2C9, 2C9 isoform of CYP; CYP3A4, 3A4 isoform of CYP; DAD, diode-array detection; DCM, dichloromethane; DIEA, *N*,*N*-diisopropylethylamine, Hunig's base; Dibal-H, diisobutylaluminum hydride; DMAP, 4-dimethylaminopyridine; DMEM, Dulbecco's modified Eagle medium; DMF, dimethyl formamide; DMSO, dimethyl sulfoxide; DTNAB, di-*tert*-butyl azodicarboxylate; ECG, electrocardiogram; FBS, fetal bovine serum; FP, fluorescence polarization hERG assay; GAS, IFN-γ-activated site; HATU, hexafluorophosphate azabenzotriazole tetramethyl uronium; HEK 293, human embryonic kidney cell line; HeLa cells, HEPES, 4-(2-hydroxyethyl)-1-piperazineethanesulfonic acid buffer; IC_{50}, inhibitory concentration at 50%; immortalized cell line derived from Henrietta Lacks; hERG, human Ether-à-go-go-Related Gene potassium ion channel; hIDO1, human indoleamine 2,3-dioxygenase 1; HOBT, 1-hydroxybenzotriazole; hPPB, human plasma protein binding; IDO1, indoleamine 2,3-dioxygenase 1; IFNγ, interferon-γ; ISREs, interferon-stimulated response elements; IVIVE, in vitro−in vivo extrapolation; KO*t*Bu, potassium *t*-butoxide; KYN, l-kynurenine; LAH, lithium aluminum hydride; LCMS, liquid chromatography mass spectrometry; LPS, lipopolysaccharides endotoxin molecules; MES, 2-(*N*-morpholino)-ethanesulfonic acid buffer; MDCK, Madin Darby canine kidney cell; MDR1, gene that encodes for efflux protein P-glycoprotein (P-gp); mpk, mg per kg; MP, manual patch clamp hERG assay; MS, mass spectrometry; MsCl, mesyl chloride; NFK, *N*-formylkynurenine; NOD, nonobese diabetic strain of mice; NSG, NOD SCID gamma mice; PANCO2, mouse pancreatic nonmetastatic cancer cell line; P_{app}, apparent permeability coefficient; PBS, phosphate-buffered saline buffer solution; PCR, polymerase chain reaction; PD, pharmacodynamics; PD1, programmed cell death protein 1; PDL1, programmed death-ligand 1; PK, pharmacokinetics; po, per os (oral administration); polymer-TPP, triphenylphosphine polymer-bound, Sigma-Aldrich 366455; QD, once a day (quaque); QP, Q-patch hERG assay; SAR, structure activity relationship; SCID, severe combined immunodeficiency; SFC, supercritical fluid chromatography; SKOV3, human-derived ovarian cancer cell line; S_NAr, nucleophilic aromatic substitution; SOC3, suppressor of cytokine signaling 3; SRC, nonreceptor tyrosine kinases; T cell, lymphocytes developed in the thymus gland; TBDPS-Cl,

https://doi.org/10.1021/acs.jmedchem.1c00679
J. Med. Chem. XXXX, XXX, XXX−XXX

tert-butyl(chloro)diphenylsilane; TDO, tryptophan 2,3-dioxygenase; Tdp, torsades de pointes; TE, target engagement; THF, tetrahydrofuran; TI, therapeutic index; TIC, total ion count; TILs, tumor-infiltrating lymphocytes; TLC, thin layer chromatography; Treg cells, regulatory T cells; Trp, l-tryptophan; V_{dss}, volume of distribution at the steady state

REFERENCES

(1) Freewan, M.; Rees, M. D.; Plaza, T. S.; Glaros, E.; Lim, Y. J.; Wang, X. S.; Yeung, A. W.; Witting, P. K.; Terentis, A. C.; Thomas, S. R. Human Indoleamine 2,3-Dioxygenase Is A Catalyst Of Physiological Heme Peroxidase Reactions. *J. Biol. Chem.* **2013**, *288*, 1548−1567.

(2) Brochez, L.; Chevolet, I.; Kruse, V. The Rationale Of Indoleamine 2,3-Dioxygenase Inhibition For Cancer Therapy. *Eur. J. Canc.* **2017**, *76*, 167−182.

(3) Giannone, G.; Ghisoni, E.; Genta, S.; Scotto, G.; Tuninetti, V.; Turinetto, M.; Valabrega, G. Immuno-Metabolism And Microenvironment In Cancer: Key Players For Immunotherapy. *Int. J. Mol. Sci.* **2020**, *21*, 4414.

(4) Austin, C. J. D.; Rendina, L. M. Targeting Key Dioxygenases In Tryptophan−Kynurenine Metabolism For Immunomodulation And Cancer Chemotherapy. *Drug Discovery Today* **2015**, *20*, 609−617.

(5) Théate, I.; van Baren, N.; Pilotte, L.; Moulin, P.; Larrieu, P.; Renauld, J.-C.; Hervé, C.; Gutierrez-Roelens, I.; Marbaix, E.; Sempoux, C.; Van den Eynde, B. J. Extensive Profiling Of The Expression Of The Indoleamine 2,3-Dioxygenase 1 Protein In Normal And Tumoral Human Tissues. Cancer Immunology Research 2014, 3 (2), 161-172. *Cancer Immunol. Res.* **2015**, *3*, 161−172.

(6) Roszik, J.; Tanese, K.; Ekmekcioglu, S. Editorial: Targeting Metabolism In Cancer Immunotherapy. *Front. Immunol.* **2018**, *9*.2029 DOI: 10.3389/fimmu.2018.02029

(7) Yu, J.; Sun, J.; Wang, S. E.; Li, H.; Cao, S.; Cong, Y.; Liu, J.; Ren, X. Upregulated Expression Of Indoleamine 2, 3-Dioxygenase In Primary Breast Cancer Correlates With Increase Of Infiltrated Regulatory T Cellsin Situand Lymph Node Metastasis. *Clin. Dev. Immunol.* **2011**, *2011*, 1−10.

(8) Ino, K.; Yamamoto, E.; Shibata, K.; Kajiyama, H.; Yoshida, N.; Terauchi, M.; Nawa, A.; Nagasaka, T.; Takikawa, O.; Kikkawa, F. Inverse Correlation Between Tumoral Indoleamine 2,3-Dioxygenase Expression And Tumor-Infiltrating Lymphocytes In Endometrial Cancer: Its Association With Disease Progression And Survival. *Clin. Cancer Res.* **2008**, *14*, 2310−2317.

(9) Galli, F.; Aguilera, J.; Palermo, B.; Markovic, S.; Nisticò, P.; Signore, A. Relevance Of Immune Cell And Tumor Microenvironment Imaging In The New Era Of Immunotherapy. *J. Exp. Clin. Canc. Res.* **2020**, 39.89 DOI: 10.1186/s13046-020-01586-y

(10) Zhai, L.; Ladomersky, E.; Lenzen, A.; Nguyen, B.; Patel, R.; Lauing, K. L.; Wu, M.; Wainwright, D. A. IDO1 In Cancer: A Gemini Of Immune Checkpoints. *Cell. Mol. Immunol.* **2018**, *15*, 447−457.

(11) Peng, Y.-H.; Ueng, S.-H.; Tseng, C.-T.; Hung, M.-S.; Song, J.-S.; Wu, J.-S.; Liao, F.-Y.; Fan, Y.-S.; Wu, M.-H.; Hsiao, W.-C.; Hsueh, C.-C.; Lin, S.-Y.; Cheng, C.-Y.; Tu, C.-H.; Lee, L.-C.; Cheng, M.-F.; Shia, K.-S.; Shih, C.; Wu, S.-Y. Important Hydrogen Bond Networks In Indoleamine 2,3-Dioxygenase 1 (IDO1) Inhibitor Design Revealed By Crystal Structures Of Imidazoleisoindole Derivatives With IDO1. *J. Med. Chem.* **2016**, *59*, 282−293.

(12) Yue, E. W.; Douty, B.; Wayland, B.; Bower, M.; Liu, X.; Leffet, L.; Wang, Q.; Bowman, K. J.; Hansbury, M. J.; Liu, C.; Wei, M.; Li, Y.; Wynn, R.; Burn, T. C.; Koblish, H. K.; Fridman, J. S.; Metcalf, B.; Scherle, P. A.; Combs, A. P. Discovery Of Potent Competitive Inhibitors Of Indoleamine 2,3-Dioxygenase With In Vivo Pharmacodynamic Activity and Efficacy In A Mouse Melanoma Model. *J. Med. Chem.* **2009**, *52*, 7364−7367.

(13) Crosignani, S.; Bingham, P.; Bottemanne, P.; Cannelle, H.; Cauwenberghs, S.; Cordonnier, M.; Dalvie, D.; Deroose, F.; Feng, J. L.; Gomes, B.; Greasley, S.; Kaiser, S. E.; Kraus, M.; Négrerie, M.; Maegley, K.; Miller, N.; Murray, B. W.; Schneider, M.; Soloweij, J.; Stewart, A. E.; Tumang, J.; Torti, V. R.; Van Den Eynde, B.; Wythes, M. Discovery Of A Novel And Selective Indoleamine 2,3-Dioxygenase (IDO-1) Inhibitor 3-(5-Fluoro-1H-Indol-3-Yl)Pyrrolidine-2,5-Dione (EOS200271/PF-06840003) And Its Characterization As A Potential Clinical Candidate. *J. Med. Chem.* **2017**, *60*, 9617−9629.

(14) Beck, H.; Carlos, J.; Osipov, M.; Powers, J.; Reilly, M.; Shunatona, H.; Walker, J.; Zibinsky, M.; Balog, J.; Williams, D.; Guo, W. Immunoregulatory agents. WO 2016073738 A2, May 12, 2016.

(15) Beck, H.; Carlos, J.; Osiprov, J.; Powers, J.; Reilly, M.; Shunatona, H.; Walker, J.; Zibrinsky, M.; Balog, J.; Williams, D.; Markwalder, J.; Cherney, E.; Shan, W.; Huang, A. Immunoregulatory agents. WO 2016073770 A1, May 12, 2016.

(16) Yao, Y.; Liang, H.; Fang, X.; Zhang, S.; Xing, Z.; Shi, L.; Kuang, C.; Seliger, B.; Yang, Q. What Is The Prospect Of Indoleamine 2,3-Dioxygenase 1 Inhibition In Cancer? Extrapolation From The Past. *J. Exp. Clin. Canc. Res.* **2021**, *40*, 60.

(17) Feng, X.; Liao, D.; Liu, D.; Ping, A.; Li, Z.; Bian, J. Development Of Indoleamine 2,3-Dioxygenase 1 Inhibitors For Cancer Therapy And Beyond: A Recent Perspective. *J. Med. Chem.* **2020**, *63*, 15115−15139.

(18) Beatty, G. L.; O'Dwyer, P. J.; Clark, J.; Shi, J. G.; Bowman, K. J.; Scherle, P. A.; Newton, R. C.; Schaub, R.; Maleski, J.; Leopold, L.; Gajewski, T. F. First-In-Human Phase I Study Of The Oral Inhibitor Of Indoleamine 2,3-Dioxygenase-1 Epacadostat (INCB024360) In Patients With Advanced Solid Malignancies. *Clin. Cancer Res.* **2017**, *23*, 3269−3276.

(19) Long, G. V.; Dummer, R.; Hamid, O.; Gajewski, T. F.; Caglevic, C.; Dalle, S.; Arance, A.; Carlino, M. S.; Grob, J.-J.; Kim, T. M.; Demidov, L.; Robert, C.; Larkin, J.; Anderson, J. R.; Maleski, J.; Jones, M.; Diede, S. J.; Mitchell, T. C. Epacadostat Plus Pembrolizumab Versus Placebo Plus Pembrolizumab In Patients With Unresectable Or Metastatic Melanoma (ECHO-301/KEYNOTE-252): A Phase 3, Randomised, Double-Blind Study. *Lancet Oncol.* **2019**, *20*, 1083−1097.

(20) Nayak, A.; Hao, Z.; Sadek, R.; Dobbins, R.; Marshall, L.; Vahanian, N.; Ramsey, J.; Kennedy, E.; Mautino, M.; Link, C.; Lin, R.; Royer-Joo, S.; Morrissey, K.; Mahrus, S.; McCall, B.; Pirzkall, A.; Munn, D.; Janik, J.; Khleif, S. 346 Phase 1A Study Of The Safety, Pharmacokinetics, And Pharmacodynamics Of GDC-0919 In Patients With Recurrent/Advanced Solid Tumors. *Eur. J. Canc.* **2015**, *51*, S69.

(21) Nelp, M. T.; Kates, P. A.; Hunt, J. T.; Newitt, J. A.; Balog, A.; Maley, D.; Zhu, X.; Abell, L.; Allentoff, A.; Borzilleri, R.; Lewis, H. A.; Lin, Z.; Seitz, S. P.; Yan, C.; Groves, J. T. Immune-Modulating Enzyme Indoleamine 2,3-Dioxygenase Is Effectively Inhibited By Targeting Its Apo-Form. *Proc. Natl. Acad. Sci. U.S.A.* **2018**, *115*, 3249−3254.

(22) Balog, A.; Lin, T.-a.; Maley, D.; Gullo-Brown, J.; Kandoussi, E. H.; Zeng, J.; Hunt, J. T. Preclinical Characterization Of Linrodostat Mesylate, A Novel, Potent, And Selective Oral Indoleamine 2,3-Dioxygenase 1 Inhibitor. *Mol. Cancer Ther.* **2020**, *20*, 467−476.

(23) Zhu, M. M. T.; Dancsok, A. R.; Nielsen, T. O. Indoleamine Dioxygenase Inhibitors: Clinical Rationale And Current Development. *Curr. Oncol. Rep.* **2019**, *21*.2 DOI: 10.1007/s11912-019-0750-1

(24) Lewis-Ballester, A.; Pham, K. N.; Batabyal, D.; Karkashon, S.; Bonanno, J. B.; Poulos, T. L.; Yeh, S. R. Structural Insights Into Substrate And Inhibitor Binding Sites In Human Indoleamine 2,3-Dioxygenase 1. *Nat. Commun.* **2017**, *8*, 1693.

(25) Röhrig, U. F.; Reynaud, A.; Majjigapu, S. R.; Vogel, P.; Pojer, F.; Zoete, V. Inhibition Mechanisms Of Indoleamine 2,3-Dioxygenase 1 (IDO1). *J. Med. Chem.* **2019**, *62*, 8784−8795.

(26) Pham, K. N.; Yeh, S.-R. Mapping The Binding Trajectory Of A Suicide Inhibitor In Human Indoleamine 2,3-Dioxygenase 1. *J. Am. Chem. Soc.* **2018**, *140*, 14538−14541.

(27) Serafini, M.; Torre, E.; Aprile, S.; Grosso, E. D.; Gesù, A.; Griglio, A.; Colombo, G.; Travelli, C.; Paiella, S.; Adamo, A.; Orecchini, E.; Coletti, A.; Pallotta, M. T.; Ugel, S.; Massarotti, A.; Pirali, T.; Fallarini, S. Discovery Of Highly Potent Benzimidazole Derivatives As Indoleamine 2,3-Dioxygenase-1 (IDO1) Inhibitors: From Structure-Based Virtual Screening To In Vivo Pharmacodynamic Activity. *J. Med. Chem.* **2020**, *63*, 3047−3065.

(28) Peng, Y.-H.; Liao, F.-Y.; Tseng, C.-T.; Kuppusamy, R.; Li, A.-S.; Chen, C.-H.; Fan, Y.-S.; Wang, S.-Y.; Wu, M.-H.; Hsueh, C.-C.; Chang, J.-Y.; Lee, L.-C.; Shih, C.; Shia, K.-S.; Yeh, T.-K.; Hung, M.-S.; Kuo, C.-

https://doi.org/10.1021/acs.jmedchem.1c00679
J. Med. Chem. XXXX, XXX, XXX−XXX

C.; Song, J.-S.; Wu, S.-Y.; Ueng, S.-H. Unique Sulfur−Aromatic Interactions Contribute To The Binding Of Potent Imidazothiazole Indoleamine 2,3-Dioxygenase Inhibitors. *J. Med. Chem.* **2020**, *63*, 1642−1659.
(29) Song, X.; Sun, P.; Wang, J.; Guo, W.; Wang, Y.; Meng, L.-h.; Liu, H. Design, Synthesis, And Biological Evaluation Of 1,2,5-Oxadiazole-3-Carboximidamide Derivatives As Novel Indoleamine-2,3-Dioxygenase 1 Inhibitors. *Eur. J. Med. Chem.* **2020**, *189*, 112059.
(30) Cowley, P.; McGowan, M.; Brown, T.; Han, Y.; Liu, K.; Pu, Q.; Wise, A.; Zhang, H.; Zhou, H. Novel substituted imidazopyridine compounds as inhibitors of indoleamine 2,3-dioxygenase and/or tryptophan-2,3-dioxygenase. WO 2017189386 A1, Nov 2, 2017.
(31) Lewis, R.; Jones, P.; Petrocchi, A.; Reyna, N.; Hamilton, M.; Cross, J.; Tremblay, M.; Leonard, P. Compounds. WO 2018136887 A1, July 26, 2018.
(32) Cherney, E. C.; Zhang, L.; Nara, S.; Zhu, X.; Gullo-Brown, J.; Maley, D.; Lin, T.-A.; Hunt, J. T.; Huang, C.; Yang, Z.; Darienzo, C.; Discenza, L.; Ranasinghe, A.; Grubb, M.; Ziemba, T.; Traeger, S. C.; Li, X.; Johnston, K.; Kopcho, L.; Fereshteh, M.; Foster, K.; Stefanski, K.; Fargnoli, J.; Swanson, J.; Brown, J.; Delpy, D.; Seitz, S. P.; Borzilleri, R.; Vite, G.; Balog, A. Discovery And Preclinical Evaluation Of BMS-986242, A Potent, Selective Inhibitor Of Indoleamine-2,3-Dioxygenase 1. *ACS Med. Chem. Lett.* **2021**, *12*, 288−294.
(33) Zhang, L.; Cherney, E. C.; Zhu, X.; Lin, T.-a.; Gullo-Brown, J.; Maley, D.; Johnston-Allegretto, K.; Kopcho, L.; Fereshteh, M.; Huang, C.; Li, X.; Traeger, S. C.; Dhar, G.; Anandam, A.; Mahankali, S.; Padmanabhan, S.; Rajanna, P.; Murali, V.; Mariappan, T.; Borzilleri, R.; Vite, G.; Hunt, J. T.; Balog, A. Discovery Of Imidazopyridines As Potent Inhibitors Of Indoleamine 2,3-Dioxygenase 1 For Cancer Immunotherapy. *ACS Med. Chem. Lett.* **2021**, *12*, 494−501.
(34) Pu, Q.; Zhang, H.; Guo, L.; Cheng, M.; Doty, A. C.; Ferguson, H.; Fradera, X.; Lesburg, C. A.; McGowan, M. A.; Miller, J. R.; Geda, P.; Song, X.; Otte, K.; Sciammetta, N.; Solban, N.; Yu, W.; Sloman, D. L.; Zhou, H.; Lammens, A.; Neumann, L.; Bennett, D. J.; Pasternak, A.; Han, Y. Discovery Of Potent And Orally Available Bicyclo[1.1.1]-Pentane-Derived Indoleamine-2,3-Dioxygenase 1 (IDO1) Inhibitors. *ACS Med. Chem. Lett.* **2020**, *11*, 1548−1554.
(35) White, C.; McGowan, M. A.; Zhou, H.; Sciammetta, N.; Fradera, X.; Lim, J.; Joshi, E. M.; Andrews, C.; Nickbarg, E. B.; Cowley, P.; Trewick, S.; Augustin, M.; von Köenig, K.; Lesburg, C. A.; Otte, K.; Knemeyer, I.; Woo, H.; Yu, W.; Cheng, M.; Spacciapoli, P.; Geda, P.; Song, X.; Smotrov, N.; Curran, P.; Heo, M. R.; Abeywickrema, P.; Miller, J. R.; Bennett, D. J.; Han, Y. Strategic Incorporation Of Polarity In Heme-Displacing Inhibitors Of Indoleamine-2,3-Dioxygenase-1 (IDO1). *ACS Med. Chem. Lett.* **2020**, *11*, 550−557.
(36) Dorsey, F. C.; Benhadji, K.; Sams, L.; Young, D.; Schindler, J.; Huss, K.; Nikolayev, A.; Carpenito, C.; Clawson, D.; Jones, B.; Faber, A.; Thomas, J.; Haney, S.; Zhao, G.; McMillen, W.; Smeal, T.; Sall, D.; Kalos, M.; Geeganage, S.; Henry, J. Identification And Characterization Of The IDO1 Inhibitor LY3381916. Proceedings of the American Association for Cancer Research Annual Meeting 2018; 2018 Apr 14-18; Chicago, IL. Philadelphia (PA) AACR. *Cancer Res.* **2018**, *78*, 5245.
(37) Li, D.; Deng, Y.; Achab, A.; Bharathan, I.; Hopkins, B. A.; Yu, W.; Zhang, H.; Sanyal, S.; Pu, Q.; Zhou, H.; Liu, K.; Lim, J.; Fradera, X.; Lesburg, C. A.; Lammens, A.; Martinot, T. A.; Cohen, R. D.; Doty, A. C.; Ferguson, H.; Nickbarg, E. B.; Cheng, M.; Spacciapoli, P.; Geda, P.; Song, X.; Smotrov, N.; Abeywickrema, P.; Andrews, C.; Chamberlin, C.; Mabrouk, O.; Curran, P.; Richards, M.; Saradjian, P.; Miller, J. R.; Knemeyer, I.; Otte, K. M.; Vincent, S.; Sciammetta, N.; Pasternak, A.; Bennett, D. J.; Han, Y. Carbamate And N-Pyrimidine Mitigate Amide Hydrolysis: Structure-Based Drug Design Of Tetrahydroquinoline IDO1 Inhibitors. *ACS Med. Chem. Lett.* **2021**, *12*, 389−396.
(38) Kinzel, O.; Steeneck, C.; Anderhub, S.; Hornberger, M.; Pinto, S.; Morschhaeuser, B.; Albers, M.; Sonnek, C.; Wang, Y.; Mallinger, A.; Czekańska, M.; Hoffmann, T. Discovery Of Highly Potent Heme-Displacing IDO1 Inhibitors Based On A Spirofused Bicyclic Scaffold. *Bioorg. Med. Chem. Lett.* **2021**, *33*, 127738.
(39) ClinicalTrials.gov/ct2/show/NCT03351231 (accessed March 21, 2021).
(40) Hutchinson, S. E.; Leveridge, M. V.; Heathcote, M. L.; Francis, P.; Williams, L.; Gee, M.; Munoz-Muriedas, J.; Leavens, B.; Shillings, A.; Jones, E.; Homes, P.; Baddeley, S.; Chung, C.-w.; Bridges, A.; Argyrou, A. Enabling Lead Discovery For Histone Lysine Demethylases By High-Throughput Rapidfire Mass Spectrometry. *J. Biomol. Screen* **2011**, *17*, 39−48.
(41) Marquez, V. E.; Choi, Y.; Comin, M. J.; Russ, P.; George, C.; Huleihel, M.; Ben-Kasus, T.; Agbaria, R. Understanding How The Herpes Thymidine Kinase Orchestrates Optimal Sugar And Nucleobase Conformations To Accommodate Its Substrate At The Active Site: A Chemical Approach. *J. Am. Chem. Soc.* **2005**, *127*, 15145−15150.
(42) Li, J.; Lowary, T. L. Synthesis Of Bicyclo[3.1.0]Hexane Derivatives As Conformationally Restricted Analogues Of B-Arabinofuranosyl And A-Galactofuranosyl Rings. *Org. Lett.* **2008**, *10*, 881−884.
(43) Colombo, C.; Pinto, B. M.; Bernardi, A.; Bennet, A. J. Synthesis And Evaluation Of Influenza A Viral Neuraminidase Candidate Inhibitors Based On A Bicyclo[3.1.0]Hexane Scaffold. *Org. Biomol. Chem.* **2016**, *14*, 6539−6553.
(44) Bentzien, J.; Hickey, E. R.; Kemper, R. A.; Brewer, M. L.; Dyekjær, J. D.; East, S. P.; Whittaker, M. An In Silico Method For Predicting Ames Activities Of Primary Aromatic Amines By Calculating The Stabilities Of Nitrenium Ions. *J. Chem. Inf. Model.* **2010**, *50*, 274−297.
(45) Shamovsky, I.; Ripa, L.; Börjesson, L.; Mee, C.; Nordén, B.; Hansen, P.; Hasselgren, C.; O'Donovan, M.; Sjö, P. Explanation For Main Features Of Structure−Genotoxicity Relationships Of Aromatic Amines By Theoretical Studies Of Their Activation Pathways In CYP1A2. *J. Am. Chem. Soc.* **2011**, *133*, 16168−16185.
(46) Teasdale, A.; Elder, D.; Chang, S.-J.; Wang, S.; Thompson, R.; Benz, N.; Sanchez Flores, I. H. Risk Assessment Of Genotoxic Impurities In New Chemical Entities: Strategies To Demonstrate Control. *Org. Process Res. Dev.* **2013**, *17*, 221−230.
(47) Teffera, Y.; Berry, L. M.; Brake, R. L.; Lewis, R. T.; Saffran, D. C.; Moore, E.; Liu, J.; Zhao, Z. Impact Of Hydrolysis-Mediated Clearance On The Pharmacokinetics Of Novel Anaplastic Lymphoma Kinase Inhibitors. *Drug Metab. Dispos.* **2013**, *41*, 238−247.
(48) Compound **21**: permeability MDCK-MDR1 cell line assay (P_{app} × 10^{-6} cm/s, wt A−B/B−A, ratio; MDR1 A−B/B−A, ratio) 5.53/5.61, 1.02; 3.70/2.07, 0.56. Compound **22**: mouse plasma stability, 12.8 h. permeability (P_{app} × 10^{-6} cm/s, wt A−B/B−A, ratio; MDR1 A−B/B−A, ratio) 3.63/1.73, 0.48; 1.86/1.40, 0.75.
(49) Yeung, A. W. S.; Terentis, A. C.; King, N. J. C.; Thomas, S. R. Role Of Indoleamine 2,3-Dioxygenase In Health And Disease. *Clin. Sci.* **2015**, *129*, 601−672.
(50) Badawy, A. A.-B. Kynurenine Pathway Of Tryptophan Metabolism: Regulatory And Functional Aspects. *Int. J. Tryptophan Res.* **2017**, *10*, 117864691769193.
(51) Robinson, C. M.; Shirey, K. A.; Carlin, J. M. Synergistic Transcriptional Activation Of Indoleamine Dioxygenase By IFN-Γ And Tumor Necrosis Factor-A. *J. Interferon Cytokine Res.* **2003**, *23*, 413−421.
(52) Thomas, S. R.; Salahifar, H.; Mashima, R.; Hunt, N. H.; Richardson, D. R.; Stocker, R. Antioxidants Inhibit Indoleamine 2,3-Dioxygenase In IFN-Γ-Activated Human Macrophages: Posttranslational Regulation By Pyrrolidine Dithiocarbamate. *J. Immunol.* **2001**, *166*, 6332−6340.
(53) Orabona, C.; Pallotta, M. T.; Volpi, C.; Fallarino, F.; Vacca, C.; Bianchi, R.; Belladonna, M. L.; Fioretti, M. C.; Grohmann, U.; Puccetti, P. SOCS3 Drives Proteasomal Degradation Of Indoleamine 2,3-Dioxygenase (IDO) And Antagonizes IDO-Dependent Tolerogenesis. *Proc. Natl. Acad. Sci. U.S.A.* **2008**, *105*, 20828−20833.
(54) Poncelet, L.; Ait-Belkacem, R.; Marillier, R.; Gomes, B.; Stauber, J. Target Exposure and Pharmacodynamics Study Of The Indoleamine 2,3-Dioxygenase-1 (IDO-1) Inhibitor Epacadostat In The CT26 Mouse Tumor Model. *J. Pharm. Biomed. Anal.* **2019**, *170*, 220−227.
(55) Fu, X.; Yang, Y.; Xie, J.; Pan, X.; Yang, X.; Du, Z.; Hao, E. Subcutaneous Inoculation Position Affects The Immune Environment

https://doi.org/10.1021/acs.jmedchem.1c00679
J. Med. Chem. XXXX, XXX, XXX−XXX

In CT26 Carcinomas. *Biochem. Biophys. Res. Commun.* **2019**, *512*, 244−249.
(56) Tuntland, T.; Ethell, B.; Kosaka, T.; Blasco, F.; Zang, R. X.; Jain, M.; Gould, T.; Hoffmaster, K. Implementation Of Pharmacokinetic And Pharmacodynamic Strategies In Early Research Phases Of Drug Discovery And Development At Novartis Institute Of Biomedical Research. *Front. Pharmacol.* **2014**, *5*.174 DOI: 10.3389/fphar.2014.00174
(57) Jamieson, C.; Moir, E. M.; Rankovic, Z.; Wishart, G. Medicinal Chemistry Of Herg Optimizations: Highlights And Hang-Ups. *J. Med. Chem.* **2006**, *49*, 5029−5046.
(58) Redfern, W.; Carlsson, L.; Davis, A.; Lynch, W.; Mackenzie, I.; Palethorpe, S.; Siegl, P.; Strang, I.; Sullivan, A.; Wallis, R. Relationships Between Preclinical Cardiac Electrophysiology, Clinical QT Interval Prolongation And Torsade De Pointes For A Broad Range Of Drugs: Evidence For A Provisional Safety Margin In Drug Development. *Cardiovasc. Res.* **2003**, *58*, 32−45.
(59) Wan, H.; Selvaggio, G.; Pearlstein, R. A. Toward In Vivo-Relevant Herg Safety Assessment And Mitigation Strategies Based On Relationships Between Non-Equilibrium Blocker Binding, Three-Dimensional Channel-Blocker Interactions, Dynamic Occupancy, Dynamic Exposure, And Cellular Arrhythmia. *PloS One* **2020**, *15*, No. e0234946.
(60) Kongsamut, S.; Kang, J.; Chen, X.-L.; Roehr, J.; Rampe, D. A Comparison Of The Receptor Binding And HERG Channel Affinities For A Series Of Antipsychotic Drugs. *Eur. J. Pharmacol.* **2002**, *450*, 37−41.
(61) Walsh, S. P.; Shahripour, A.; Tang, H.; de Jesus, R. K.; Teumelsan, N.; Zhu, Y.; Frie, J.; Priest, B. T.; Swensen, A. M.; Alonso-Galicia, M.; Felix, J. P.; Brochu, R. M.; Bailey, T.; Thomas-Fowlkes, B.; Zhou, X.; Pai, L.-Y.; Hampton, C.; Hernandez, M.; Owens, K.; Ehrhart, J.; Roy, S.; Kaczorowski, G. J.; Yang, L.; Garcia, M. L.; Pasternak, A. Differentiation Of ROMK Potency From Herg Potency In The Phenacetyl Piperazine Series Through Heterocycle Incorporation. *Bioorg. Med. Chem. Lett.* **2016**, *26*, 2339−2343.
(62) Murphy, J. Pre-Clinical Murine Models: Syngeneic Models For Immuno-Oncology. *MOJ Immunol.* **2015**, *2*()00052 . DOI: 10.15406/moji.2015.02.00052
(63) Saito, R.; Kobayashi, T.; Kashima, S.; Matsumoto, K.; Ogawa, O. Faithful Preclinical Mouse Models For Better Translation To Bedside In The Field Of Immuno-Oncology. *Int. J. Clin. Oncol.* **2019**, *25*, 831−841.
(64) Lewis, R.; Hamilton, M.; Jones, P.; Petrocchi, A.; Reyna, N.; McAfoos, T.; Cross, J.; Soth, M. Compounds useful as inhibitors of indoleamine 2,3-dioxygenase and/or tryptophan dioxygenase. WO 2020018670 A1, Janurary 23, 2020.
(65) Sonpavde, G.; Necchi, A.; Gupta, S.; Steinberg, G. D.; Gschwend, J. E.; Van Der Heijden, M. S.; Garzon, N.; Ibrahim, M.; Raybold, B.; Liaw, D.; Rutstein, M.; Galsky, M. D. ENERGIZE: A Phase III Study Of Neoadjuvant Chemotherapy Alone Or With Nivolumab With/Without Linrodostat Mesylate For Muscle-Invasive Bladder Cancer. *Future Oncol.* **2020**, *16*, 4359−4368.
(66) Lyssikatos, J. P.; Liu, W.; Siu, M.; Estrada, A.; Patel, S.; Liang, G.; Huestis, M.; Chen, K. Pyrazole derivatives and uses thereof as inhibitors of dlk. WO 2015091889 A1, June 25, 2015.
(67) Hanan, E.; Chan, B.; Estrada, A.; Shore, D.; Lyssikatos, J. Mild And General One-Pot Reduction And Cyclization Of Aromatic And Heteroaromatic 2-Nitroamines To Bicyclic 2H-Imidazoles. *Synlett* **2010**, *2010*, 2759−2764.
(68) Ellman, J. A.; Owens, T. D.; Tang, T. P. N-Tert-Butanesulfinyl Imines: Versatile Intermediates For The Asymmetric Synthesis Of Amines. *Acc. Chem. Res.* **2002**, *35*, 984−995.
(69) Hoye, T. R.; Jeffrey, C. S.; Shao, F. Mosher Ester Analysis For The Determination Of Absolute Configuration Of Stereogenic (Chiral) Carbinol Carbons. *Nat. Protoc.* **2007**, *2*, 2451−2458.
(70) Shimizu, T.; Nomiyama, S.; Hirata, F.; Hayaishi, O. Indoleamine 2,3-Dioxygenase. Purification And Some Properties. *J. Biol. Chem.* **1978**, *253*, 4700−4706.

https://doi.org/10.1021/acs.jmedchem.1c00679
J. Med. Chem. XXXX, XXX, XXX−XXX